Space-Air-Ground FSO Transmission System Design for Reliable and Very-High-Throughput Satellite Communications

by

Ramy Mahmoud Samy Zaghloul
B.Sc., Military Technical College, 2008
M.Sc., Military Technical College, 2018

A Dissertation Submitted in Partial Fulfillment of the
Requirements for the Degree of

DOCTOR OF PHILOSOPHY

in the Department of Electrical and Computer Engineering

© Ramy Mahmoud Samy Zaghloul, 2023
University of Victoria

All rights reserved. This dissertation may not be reproduced in whole or in part, by photocopying or other means, without the permission of the author.

Space-Air-Ground FSO Transmission System Design for Reliable and Very-High-Throughput Satellite Communications

by

Ramy Mahmoud Samy Zaghloul
B.Sc., Military Technical College, 2008
M.Sc., Military Technical College, 2018

Supervisory Committee

Dr. Hong-Chuan Yang, Supervisor
(Department of Electrical and Computer Engineering)

Dr. Tao Lu, Departmental Member
(Department of Electrical and Computer Engineering)

Dr. Jianping Pan, Outside Member
(Department of Computer Science)

ABSTRACT

Recent advances demonstrate satellite communications (SatComs) as a potent enabler for future Terabits/s wireless networks and bridging the digital divide. Existing SatCom systems, however, are mostly dependent on radio frequency (RF) with limited available bandwidth, which is the main bottleneck for further data rate increases. Free-space optical (FSO) communications, with huge license-free bandwidth, have emerged as a candidate alternative. Despite their ability to deliver high-throughput transmissions, FSO communications are weather-dependent and susceptible to atmospheric turbulence effects. Therefore, improving the FSO-link usability is crucial for better exploring its higher transmission rate. The goal of this research is to develop effective FSO-based SatCom solutions that can achieve very high throughput while enjoying high reliability and, as such, provide trustworthy support for future global connectivity.

In this thesis, we adopt novel space-air-ground (SAG) FSO transmission approaches in the design of advanced SatCom systems for next-generation wireless networks. We first propose a reliable Terabits satellite feeder link solution. In particular, we propose a new SAG-FSO network with a strategically deployed high-altitude platform (HAP) relay to successfully remedy the atmospheric turbulence effects. We show that such a design can substantially mitigate the effects of atmospheric turbulence. Then, we integrate the proposed SAG-FSO network and hybrid single-hop (SH) FSO/RF transmission to create a SatCom feeder link with significantly improved performance and reliability. The numerical results show that the integrated transmission system achieves about 10 dB performance gain over existing solutions for both downlink and uplink scenarios. To mitigate weather effects and increase the reliability of SAG-FSO networks even further, we propose to combine SAG-FSO transmission with site diversity.

With the recent technological advancements in solar cells and batteries, HAP-based relays can operate continuously for several months. A SatCom system with

multiple HAP relays can enable a much more flexible design than a conventional one with multiple ground station sites. More precisely, we consider switching-based HAP relays with a hybrid SAG-FSO/RF transmission for SatCom. Our proposed system switches between HAPs based on the ground-HAP channel quality, as there are more atmospheric turbulence and weather effects. Meanwhile, the ground-HAP links corresponding to different HAP relays may experience correlated atmospheric turbulence. The obtained results illustrate that, despite the correlation adversely affecting performance, the transmission system still maintains a considerable gain over hybrid FSO/RF and single HAP systems.

To increase the transmission rate for end users in a particular hot-spot area with higher traffic demand while maintaining ubiquitous coverage, we propose parallel RF and FSO transmissions to explore their complementary properties in beamwidth and bandwidth. In particular, RF transmissions serve the users over a large geographical area, while the FSO link is employed to increase the throughput to a particular hot-spot area with higher capacity demand through an access point. Independent data streams are adaptively sent over both links to satisfy capacity and availability requirements. Such a transmission strategy can effectively provide a high-speed connection to a centralized location. In addition, it can maintain ubiquitous coverage for numerous Internet-of-Things devices dispersed over a large geographical area via an RF link.

We adopt the analytical system performance evaluation approach and develop efficient analytical expressions for important performance metrics for the proposed SatCom systems. Selected numerical examples and their discussions provide useful insights for engineering applications.

Contents

List of Figures

List of Tables

List of Abbreviations

AP	Access Point
ASEP	Average Symbol Error Probability
AWGN	Additive White Gaussian Noise
BER	Bite Error Rate
CSI	Channel State Information
CDF	Cumulative Distribution Function
DRL	Deep Reinforcement Learning
FSO	Free Space Optical
HAPs	High-Altitude Platforms
HD	Heterodyne Detection
ITU	International Telecommunication Union
IM/DD	Intensity Modulation and Direct Detection
GEO	Geosynchronous Equatorial Orbit
G-G	Gamma-Gamma
LEO	Low Earth Orbit
MEO	Medium Earth Orbit
MRC	Maximal Ratio Combining
MISO	Multiple Input Single Output
NTNs	Non-Terrestrial Networks
OP	Outage Probability
PDF	Probability Density Function
PSK	Phase Shift Keying
QoS	Quality-of-Service

RF	Radio Frequency
SAG	Space-Air-Ground
SIMO	Single Input Multiple Output
SIM	Subcarrier Intensity Modulation
SNR	Signal-to-Noise Ratio
UAV	Unmanned Aerial Vehicle

ACKNOWLEDGEMENTS

In the name of Allah, the Most Gracious and the Most Merciful

Alhamdulillah, all praises belongs to Allah the merciful for his blessing and guidance. He gave me the strength to reach what I desire. I would like to thank:

Dr. Hong-Chuan Yang, for his enthusiasm, guidance, advice, encouragement, and support during my work under his supervision. It would not possible to finish my research without his valuable help of constructive comments and suggestions during all stages of my PhD study.

Dr. Tao Lu and Dr. Jianping Pan, for their willingness to serve on my supervisory committee. I really appreciate their valuable time and constructive comments on my thesis.

Also, I would like to thank:

Dr. Anas Chaaban from University of British Columbia for serving as my external examiner. It is my great honor to have such an expert on my committee.

Dr. Mohamed-Slim Alouini from King Abdullah University of Science and Technology for sparing his precious time and constructive comments, which helped improve the quality of my work.

Finally, I would like to thank:

my parents, my lovely wife Manar, and my sons Ahmed and Adam, for their patience, understanding, support, love, and continuing encouragement over all these years.

PREFACE

This thesis is based on the publications listed below.

1. **R. Samy**, H.-C. Yang, T. Rakia, and M.-S. Alouini, "Parallel FSO and RF transmissions for high-throughput remote access with satellite communications," in *IEEE Transactions on Aerospace and Electronic Systems*, early access, Sep. 2023.

2. **R. Samy**, H.-C. Yang, T. Rakia, and M.-S. Alouini, "Hybrid SAG-FSO/SH-FSO/RF transmission for next-generation satellite communication systems," in *IEEE Transactions on Vehicular Technology*, early access, May 2023.

3. **R. Samy**, H. -C. Yang, T. Rakia and M. -S. Alouini, "Reliable terabits feeder link for very high-throughput satellite systems with SAG-FSO transmission," in *IEEE Wireless Communications*, early access, Apr. 2023.

4. **R. Samy**, H. -C. Yang, T. Rakia and M. -S. Alouini, "Space-Air-Ground FSO networks for high-throughput satellite Ccommunications," in *IEEE Communications Magazine*, vol. 61, no. 3, pp. 82-87, Mar. 2023.

5. **R. Samy**, H. -C. Yang, T. Rakia and M. -S. Alouini, "Ergodic capacity analysis of satellite communication systems With SAG-FSO/SH-FSO/RF transmission," *in IEEE Photonics Journal*, vol. 14, no. 5, pp. 1-9, Art no. 7347909, Oct. 2022.

6. **R. Samy**, H. -C. Yang, T. Rakia and M. -S. Alouini, "Symbol error rate analysis of satellite communication systems with SAG-FSO/SH-FSO/RF transmission," in GLOBECOM 2022 - 2022 IEEE Global Communications Conference, Rio de Janeiro, Brazil, 2022, pp. 431-436.

Chapter 1

Introduction and Motivation

1.1 Background

While taken for granted by many living in fully developed communities, Internet connectivity remains unavailable or unaffordable in many regions of the world. Prohibitive setup costs have created a digital divide that isolates a substantial portion of the world's population, approximately 2.7 billion people, from the connected world [1]. Next-generation wireless networks should open up new avenues for connectivity and contribute to the reduction of the digital divide. Indeed, the growing demand has motivated the development of non-terrestrial networks (NTNs) to efficiently deliver broadband services and connect remote communities [2–4]. NTNs can help improve coverage and service quality, particularly in areas where traditional terrestrial networks may have blind spots [5–7].

1.1.1 Non-terrestrial Networks

Satellite communication (SatCom) is an attractive way to complement and support terrestrial networks because of their unique capability of global coverage [8–10]. Several companies have developed satellite constellations to cover underserved com-

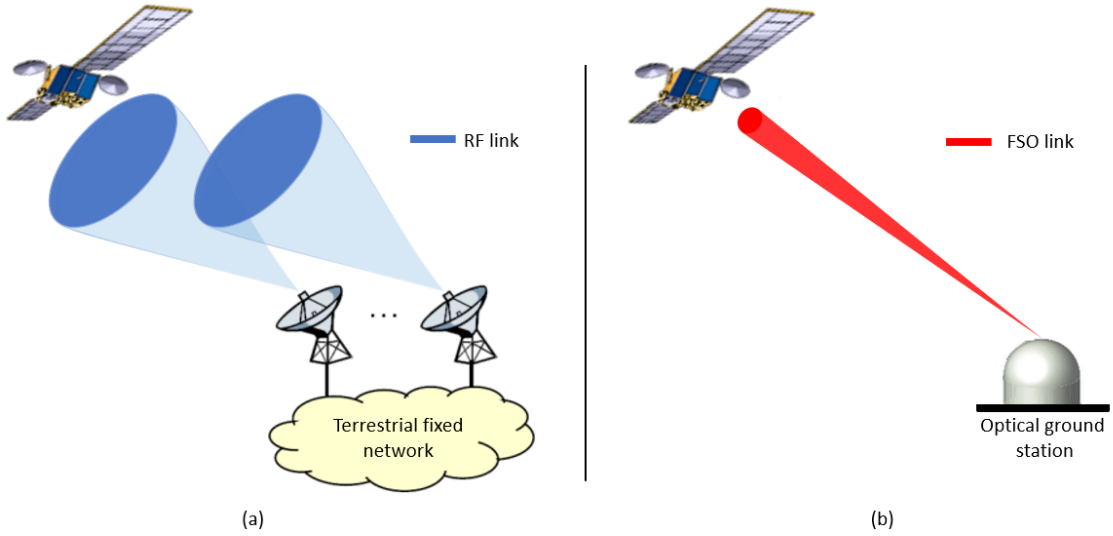

Figure 1.1: High-throughput SatCom feeder link: (a) RF-based solution; (b) Optical-based solution

munities and provide broadband Internet access around the world [11–13]. In low-earth orbits (LEO), SpaceX had launched over 4700 Starlink satellites as of July 2023; OneWeb had a 634-satellite constellation as of May 2023; Telesat plans to launch a global service with 298 satellites in 2025. Moreover, high-throughput SatCom systems in geostationary-earth orbits (GEO) are also planned to improve the user experience for broadband services, such as Ka-Sat with a throughput of 70 Gigabits/s, ViaSat-1 with 140 Gigabits/s, ViaSat-2 with 350 Gigabits/s, and ViaSat-3 with a throughput of up to 1 Terabits/s by the end of 2023. They serve as significant initial steps towards the advent of the "Internet from Space" [14].

Existing SatCom systems are mainly based on licensed radio frequency (RF) bands, e.g., the Ku-band (12-18 GHz), the Ka-band (27-40 GHz), and the Q/V band (40-50 GHz) and use multiple RF beams to communicate with separate ground stations (GSs), as demonstrated in Figure 1.1(a) [15]. The number of GSs is primarily determined by the targeted traffic and the capacity of a GS. The RF bandwidth limitation remains one of the key challenges for high-throughput transmission. RF-based solution typically requires about 50 GSs to achieve 1 Terabits/s throughput,

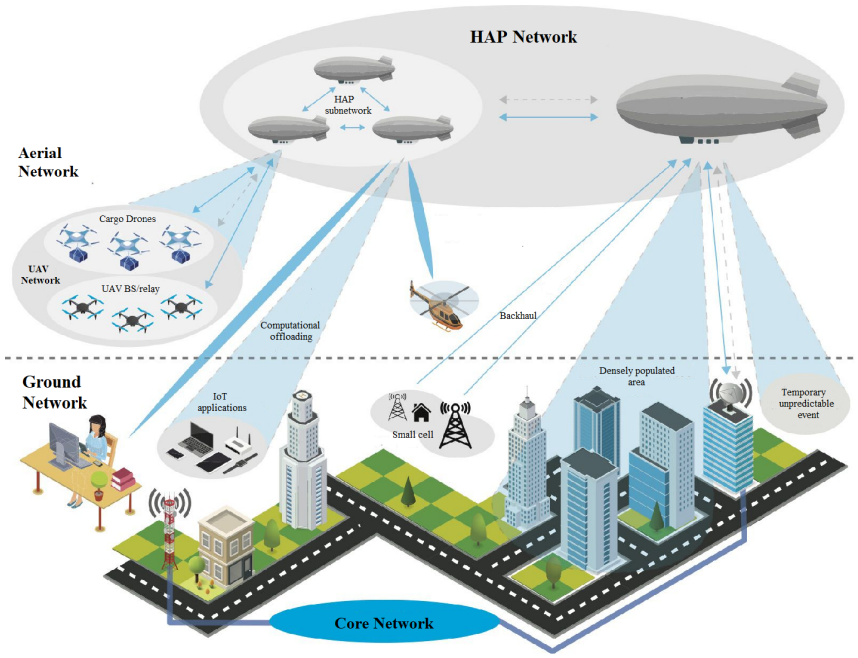

Figure 1.2: Representation of HAP-based networks [20].

which entails very high complexity and cost [16]. Furthermore, the service cost of satellite communications is still too high for the general public in remote communities and developing countries. High-altitude platforms (HAPs) are also being explored as a way of extending the coverage of terrestrial networks and providing wireless connectivity to unserved or underserved communities [17–19]. A network of floating balloons that serve as mobile base stations with adjustable locations is used to provide Internet access, as shown in Figure 1.2 [20]. For example, Project Loon provided Internet access to Kenya's rural millions and Puerto Rico in 2017 after Hurricane Maria damaged the island's communications infrastructure. Despite these successful use cases, Project Loon was shut down in 2021 due to over-cost concerns. RF spectrum scarcity remains a big challenge to delivering affordable high data-rate transmissions through HAPs. So, to reduce the cost per transmitted bit to a similar level as terrestrial networks, it is essential to increase the capacity of NTNs to Terabits/s in a cost-effective manner.

1.1.2 Free-space Optical Communications

To address the RF spectrum scarcity problem, one possible solution is to tap into the much wider optical spectrum and harness the great potential of optical transmission technology. Free-space optical (FSO) exploits an unlicensed spectrum with a larger operational bandwidth. A single FSO feeder link can replace a large number of RF feeder links, as shown in Figure 1.1(b), with reduced cost and complexity. The German Aerospace Center (DLR) proved the practicality of using FSO communications in a GEO-equivalent turbulent channel in May 2018, setting a world record of 13.16 Terabits/s as a part of the Terabit-throughput optical satellite system technology (THRUST) program [21]. Recently, the National Aeronautics and Space Administration (NASA) plans to establish a 200 Gigabits/s optical link from a nanosatellite in LEO to the ground as a part of the Terabyte Infrared Delivery (TBIRD) program [22]. Besides the huge available bandwidth, FSO communications enjoy several additional advantages, such as immunity to interference, decreased size (≈ 0.1 of RF), and lower power consumption (≈ 0.5 of RF) [23]. Therefore, FSO-based SatCom systems are the ideal solution to lower the cost per transmitted bit and provide affordable high-speed Internet access anywhere on the globe.

1.2 Problem Statement and Motivation

Despite the many advantages of FSO-based transmission, optical signals are affected by a wide range of factors when propagating through the atmosphere. Particles in the atmosphere absorb and/or scatter optical waves. The particle-wave interaction causes attenuation due to fog, rain, snow, and clouds [23]. On a clear day, optical attenuation is about 0.2 dB/km, but when there are dense clouds, it could reach 300 dB/km. Moreover, high levels of air pollution (smoke, dust, and smog) and humidity in urban regions reduce FSO link visibility. FSO transmissions also suffer from atmospheric turbulence, which is generated when aerosol particles experience wind

and solar heating. Turbulent inhomogeneities lead to the formation of turbulent cells (eddies) of varying temperatures. Such a phenomenon creates fluctuations in the refractive index along the signal path and, in turn, causes the random variation of the phase and amplitude of the received optical signal [24]. Furthermore, FSO transmissions are vulnerable to pointing errors because of the misalignment between the transmitter and the receiver and the beam-wandering effects [25]. Beam wandering occurs when the optical beam diameter is smaller than the eddy size. So, the uplink transmission to satellites is especially prone to beam-wandering effects. The optical beam encounters turbulence near the transmitter and is deflected from its original path.

A possible way to solidify the FSO approach for SatCom is to explore the complementary nature of RF transmission [26]. Specifically, FSO and RF links are vulnerable to non-overlapping weather conditions that are highly unlikely to occur simultaneously. Rain and fog are the most common causes of link unavailability for RF and FSO transmission, respectively [27]. Besides, RF transmissions are less sensitive to pointing error effects due to their wider beamwidth that may extend to hundreds of kilometers. The resulting hybrid FSO/RF SatCom enjoys the benefits of both links while avoiding weather-dependent effects. Different implementation strategies were proposed in this regard, such as hard switching and diversity combining [28, 29]. Meanwhile, because of the scarcity of the RF spectrum, the RF link can only deliver a data rate of a few hundred Megabits/s. Thus, combining with or switching back to the RF link will reduce the overall system transmission rate. To better explore the Terabits/s transmission rate of FSO links, there is a pressing need to increase FSO-link usability.

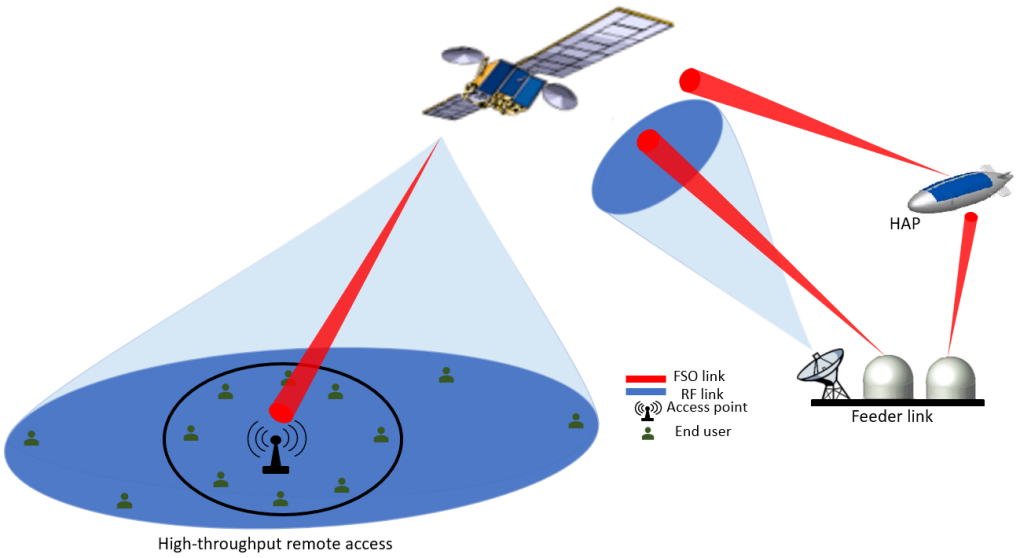

Figure 1.3: Proposed high-throughput SatCom solutions.

1.3 Research Overview

The goal of this research is to develop promising, very high-throughput SatCom solutions that can efficiently and effectively support broadband global connectivity and help bridge the digital divide. To reach this goal, there are many technical challenges to be addressed. We need to devise transmission solutions that can alleviate FSO channel impairments, such as beam-wandering-induced pointing errors, beam scintillation, and weather-dependent effects, which are inevitable and inherent issues in FSO communications. Besides, we need to increase the usability of the FSO link in order to maximize the benefits of its higher transmission rate. Furthermore, despite the FSO link's potential to provide high-throughput transmission, it can only cover a small region due to its narrow beamwidth. The FSO beamwidth at the ground station can range from tens of meters to a few kilometers, depending on the satellite altitude and zenith angle. It is expected that SatCom systems should serve a group of users simultaneously over a wide geographical area. SatCom systems should also deliver a high-speed connection to support broadband access in a certain hot-demand area.

To effectively overcome these technical challenges, we propose innovative approaches to SatCom system design, as shown in Figure 1.3, that can achieve high transmission rates and ubiquitous coverage while enjoying high reliability at reduced cost and complexity. First, efficient satellite feeder link designs are proposed to explore the Terabits/s throughput of FSO transmissions while maintaining high reliability. Newly suggested space-air-ground (SAG) networks are utilized to successfully mitigate atmospheric impairments. In addition, hybrid FSO/RF is adopted to address weather-dependent effects. Next, parallel RF and FSO transmissions are considered for end users to best explore their complementary properties in bandwidth and beamwidth. The goal is to develop a SatCom system that can satisfy the demand for ubiquitous coverage while boosting throughput in a certain high-demand area. The proposed system is ideal for providing coverage to a remote community where a traditional terrestrial solution is prohibitively expensive. Such a strategy will also be useful for flexible SatCom system design with multiple ground station sites.

In general, there are two approaches to evaluating the performance of SatCom systems. One approach is to conduct experiments, which are typically costly and time-consuming. On the other hand, analytical system performance evaluation can be a possible alternative, and the obtained numerical results can be efficiently used at the beginning stage of system design. In this work, we will focus on the efficient analytical performance evaluation of the proposed SatCom systems, which provides useful insights for engineering applications.

1.4 Thesis Contributions

The contribution of the thesis can be summarized as follows:

We propose a low-zenith-angle HAP relay deployment strategy to alleviate atmospheric turbulence effects and increase the FSO's usability for SatCom systems.

Then we present a novel SAG network that integrates the suggested SAG-FSO and hybrid FSO/RF transmissions to create a satellite feeder link with significantly improved performance and reliability. End-to-end outage probability (OP), average symbol error rate (ASEP), and ergodic capacity performance are analyzed over Gamma-Gamma (G-G) fading for FSO links in the presence of beam wandering, atmospheric turbulence, weather attenuation, pointing errors, free-space loss, and beam divergence loss and Rician fading for the RF link for both uplink and downlink scenarios. We also derive the optimum switching thresholds for the FSO links, which minimize the overall system ASEP.

We propose to combine the suggested SAG-FSO transmission with site diversity to mitigate weather effects and increase the reliability of SAG-FSO networks. To achieve a similar diversity benefit with reduced cost and lower complexity, we also propose switching-based HAP relays with a hybrid SAG-FSO/RF transmission system. The proposed solution switches between HAPs depending on the ground-HAP channel quality. Meanwhile, the ground-HAP links corresponding to different HAP relays may experience correlated atmospheric turbulence. To quantify the effect of correlated atmospheric turbulence, we derived a novel, unified analytical expression of the ASEP for both intensity modulation and direct detection (IM/DD) and heterodyne detection (HD) detection schemes over G-G fading. The ASEP analysis reveals that changing the correlation coefficient value doesn't affect the transmission system's diversity gain but degrades the ASEP performance. However, the transmission system still maintains a considerable gain over hybrid FSO/RF and SAG-FSO/RF transmission systems.

We present a parallel FSO and RF transmission system for SatCom to increase throughput to a hot-spot area while preserving ubiquitous coverage. We derive a novel, unified analytical expression of sum capacity outage probability for both IM/DD and HD schemes under Rician and G-G fading models for RF and FSO transmissions, respectively. Additionally, to acquire meaningful insights for en-

gineering applications, we derive a simplified asymptotic expression for the sum capacity outage probability and calculate the diversity gain. We also study the impact of the power allocation on the outage probability of parallel transmission and demonstrate that the optimal ratio varies with the weather condition.

1.5 Thesis Organization

This thesis consists of five chapters. A summary of the remaining chapters and their contributions is presented as follows:

Chapter 2 presents and analyzes a novel transmission system for a reliable SatCom feeder link. To successfully remedy the atmospheric turbulence effects, we propose a new SAG-FSO network with a strategically deployed HAP relay. We show that such a design can substantially mitigate the effects of atmospheric turbulence. Then, we integrate the proposed SAG-FSO network and conventional hybrid single-hop (SH)-FSO/RF transmission to improve overall system reliability and performance even further. Integrating SAG-FSO and SH-FSO transmissions into a single system can remarkably decrease the frequency of switching to a low-throughput RF link, maximally benefiting from the higher transmission rate of FSO communications while enjoying high reliability. We perform a thorough analysis of the resulting SAG-FSO/SH-FSO/RF transmission system. Furthermore, we consider the optimal design of switching thresholds.

In Chapter 3, taking advantage of the SAG-FSO design's excellent performance, we combine site diversity with SAG-FSO transmission to mitigate both atmospheric and weather effects. HAP-based FSO relay hovering directly above a ground station can successfully mitigate atmospheric turbulence impacts, while site diversity is an effective solution for addressing weather effects. Remotely distributed ground stations have a higher probability of experiencing uncorrelated weather conditions. Meanwhile, site diversity typically entails high costs due to the required terrestrial

infrastructure. To achieve a similar diversity benefit with reduced cost and complexity, we propose a SAG-FSO network with multiple HAP relays. We investigate the performance of the proposed transmission system with multiple HAP relays under a correlated atmospheric turbulence channel model. We analytically derive exact and asymptotic ASEP expressions. We also investigate the overall system diversity gain.

Chapter 4 introduces parallel FSO and RF transmissions for high-throughput remote access. In particular, RF transmissions serve the users over a large geographical area, while the FSO link is employed to increase the throughput to a particular hot-spot area with higher capacity demand through an access point. Independent data streams are adaptively sent over both links to satisfy capacity and availability requirements. The ground users can achieve high data transmission over the mixed FSO-RF link through the access point when inside its coverage. However, users have to rely on a direct RF link to the satellite when they are outside the coverage area of the access point. To highlight the significant potential of the proposed SatCom system, we derive a novel analytical expression of the sum capacity outage probability for the transmission to the access point.

Finally, we summarize the thesis in Chapter 5 and suggest some future research directions related to this thesis.

Chapter 2

Hybrid SAG-FSO/SH-FSO/RF Transmission for Next-Generation Satellite Communication Systems

In this chapter, we present a novel transmission scheme for a reliable SatCom feeder link, called hybrid SAG-FSO/SH-FSO/RF transmission. We propose a new SAG-FSO network with a strategically deployed HAP relay that can effectively mitigate the atmospheric turbulence effects. In addition, unlike typical hybrid FSO/RF solutions [26–34], which use a bandwidth-limited RF link as the only backup for FSO-based SatCom, our proposed system uses SH-FSO link as an additional backup, which can improve system performance and reliability even further. Note that, despite the SH-FSO's vulnerability to atmospheric turbulence, it can still support a much higher data rate than RF transmission. We perform a thorough performance analysis of the resulting integrated transmission system. The exact analytical expressions are derived and validated by Monte-Carlo simulations.

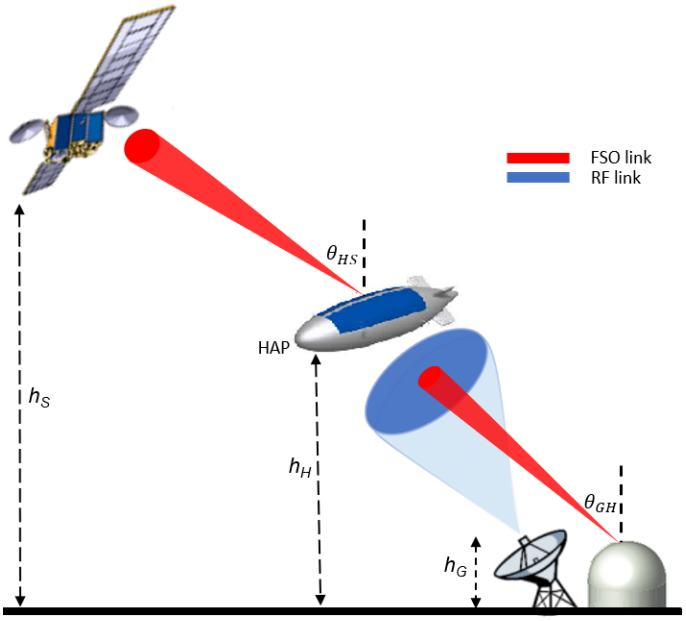

Figure 2.1: SAG network with hybrid FSO/RF transmission in previous work.

2.1 Related Work

Recently, a HAP-based relay deployed between a satellite (SAT) and a ground station has been adopted as an effective way to alleviate FSO channel impairments and increase the FSO link reliability [35]. Such a HAP-based relay creates a SAG network for SatCom systems. Because of the stratosphere's unique properties, where no weather event occurs, HAPs can maintain a quasi-stationary location, allowing for reliable line-of-sight communication between the receiver and transmitter [19]. Therefore, atmospheric turbulence, which is an inevitable and inherent issue in FSO communications, has a reduced impact on FSO transmission through HAP relaying schemes. To improve the performance of the SAG-FSO transmission even further, the RF link is employed to only backup the ground–HAP FSO link, which is more vulnerable to atmospheric effects. A sample design of such hybrid SAG-FSO/RF transmission was first proposed in [31–34] and is shown in Figure 2.1.

The main goal of such a SAG design is to decrease the beam-wandering effects that become more severe as the FSO propagation distance through the atmosphere

increases. With this design, the HAP is deployed in the stratosphere at the same zenith angle as the satellite, effectively dividing the SH-FSO link into shorter hops. According to [31–34], the SAG-FSO/RF transmission achieves a performance gain over traditional SH-FSO/RF transmission in the uplink scenario. However, it only yields a marginal performance improvement over downlink SatCom since the beam-wandering effects are neglected. The ground–HAP FSO link encounters a comparable level of atmospheric turbulence effects as SH-FSO transmission as they share the same zenith angle. While minimizing the beam-wandering impacts, the SAG transmission in [31–34] was unable to successfully mitigate the atmospheric turbulence effects on FSO communication. Furthermore, it is sensitive to satellite zenith angle variation and is more suitable for GEO satellites with relatively small and fixed zenith angles.

2.2 Proposed SatCom Feeder Link

In general, FSO communication performance is negatively affected as the propagation distance increases in a strong-turbulence environment. Ideally, we prefer FSO transmission in a low-zenith-angle direction, which is often not possible for direct ground–SAT transmission due to the zenith angle of satellites. For SAG-FSO transmission through the HAP relay, however, we can achieve low-zenith-angle transmission between the ground station and the HAP by strategically deploying the HAP, which is independent of the satellite position and becomes crucial when working with LEO satellites.

To minimize the traveling distance of the optical signal in a high-attenuation region, we propose a low-zenith-angle HAP deployment strategy, where HAP hovers directly above a ground station, as shown in Figure 2.2. Hence, beam wandering and atmospheric turbulence effects experienced by the ground–HAP hop can be successfully reduced [36, 37]. On the other hand, such HAP deployment results in a

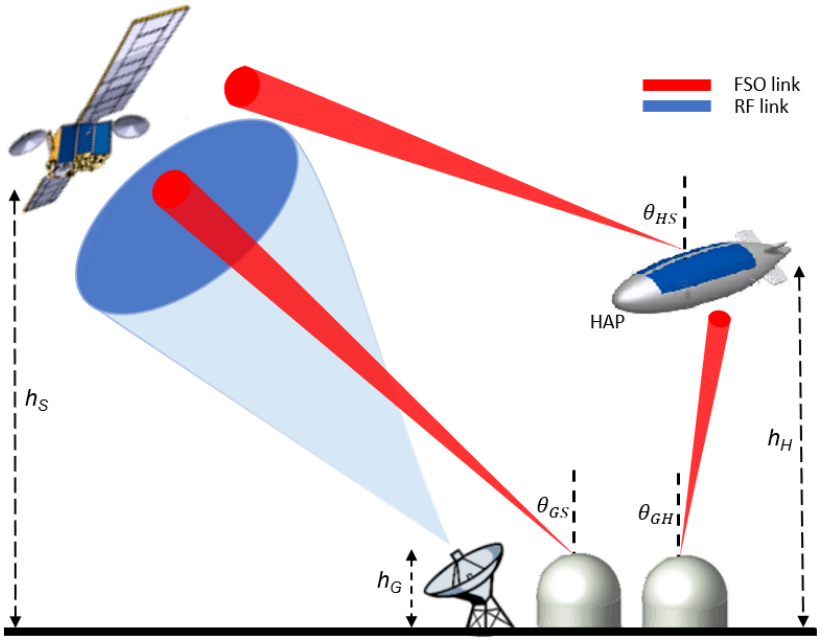

Figure 2.2: SatCom feeder link with SAG-FSO/SH-FSO/RF transmission.

slightly longer propagation distance over the HAP–SAT hop by about 3%, assuming an 80° satellite zenith angle (the worst-case scenario). Apart from propagation distance, optical signal power loss primarily depends on the atmospheric attenuation caused by aerosols. As the concentration of aerosols is negligible at high altitudes, the power loss is insignificant over the HAP-SAT hop [38]. Furthermore, the FSO transmission over the HAP-SAT hop experiences a weak turbulence effect and enjoys high reliability [39]. Therefore, the performance of such a SAG-FSO design is insensitive to the variation of satellite zenith angle as long as optical transceivers are tracking each other accurately [36]. As such, it can work well for both LEO and GEO satellites with arbitrary zenith angles. Moreover, LEO satellites may benefit even more from the SAG-FSO design. The communication session of LEO satellites with a given ground station lasts roughly 45 minutes per day on average [40]. The SAG-FSO link can start satellite acquisition significantly earlier, thanks to the HAP relay, positioned roughly 20 km above the ground station, increasing the duration of each session and the downlink data volume.

Such a SAG-FSO design with a strategically deployed HAP can be integrated with hybrid SH-FSO/RF to create a high-throughput and reliable feeder link for SatCom systems, as shown in Figure 2.2 [36]. The proposed feeder link will only restore the RF transmission if both the SH-FSO and SAG-FSO transmissions are unacceptable. Integrating SH-FSO and SAG-FSO links into a single SatCom system can remarkably minimize the switching frequency to the bandwidth-limited RF link while maintaining high-rate and reliable FSO transmission.

2.3 System and Channel Models

Here, we consider an integrated transmission system, where the ground station can communicate with the SAT through FSO or RF channels, as illustrated in Figure 2.2. We prioritize the FSO transmission through the HAP and use it whenever its link quality is acceptable, i.e., it satisfies a target quality-of-service (QoS) requirement [37]. If the SAG-FSO link is no longer acceptable, the system will first check the SH-FSO transmission before restoring the RF transmission. We use the hard-switching scheme due to its practical relevance. The SH-FSO transmission serves as an additional backup to increase the system's reliability during unfavorable channel conditions. Even though the SH-FSO transmission is more susceptible to atmospheric turbulence effects, it can transmit at a significantly higher data rate than the RF link [41]. We prefer a direct RF link to the satellite to minimize HAP's power consumption and hardware complexity, as HAP is a resource-limited system. Note that the FSO links may undergo correlated fading effects if the distance between FSO transmitters is less than the coherence diameter of the atmosphere [42]. For uncorrelated fading, the current system configuration requires a distance of approximately 20 cm [42, eq. (8)].

2.3.1 Signalling Model

In this work, we apply FSO transmission over the HAP-SAT (HS), ground-HAP (GH), and ground-SAT (GS) hops. For the ground-HAP hop, the baseband signal received at the HAP is given by [31, eq. (2)]

$$y_{\text{GH}}[k] = \left(\eta_{\text{GH}}\ P_{\text{GH}}\ G_{\text{GH}}\ I_{\text{GH}}\right)^{\frac{b}{2}}\ x[k] + n_{\text{GH}}[k], \tag{2.1}$$

where $x[k]$ is the transmitted signal, b depends on the detection scheme used ($b = 2$ for IM/DD scheme and $b = 1$ for HD scheme), η_{GH} indicates the optical-to-electrical conversion efficiency of the receiver (Rx) at the relay, P_{GH} is the transmit (Tx) power over the ground–HAP link, $x[k]$ denotes the modulated symbol, and $n_{\text{GH}}[k]$ denotes the additive white Gaussian noise (AWGN) with $\mathbb{E}\{n_{\text{GH}}[k]n^*_{\text{GH}}[k]\}= \sigma^2_{n_{\text{GH}}}$ [43]. The gain of the ground–HAP link, G_{GH}, equals $\frac{G^{tx}_f\ G^{rx}_f}{FL_{\text{GH}}}$, where G^{tx}_f, G^{rx}_f, and FL_{GH} are the Tx gain, Rx gain, and the free-space loss, respectively. Here, the free-space loss is defined as $\frac{4\pi L_{\text{GH}}}{\lambda_f}$, where λ_f indicates the optical wavelength and $L_{\text{GH}} = (h_{\text{H}} - h_{\text{G}})\sec(\theta_{\text{GH}})$ denotes the slant range, where h_{G}, h_{H}, and θ_{GH} are the aperture height of the ground station, HAP altitude, and HAP zenith angle, respectively. Besides, the aggregated channel irradiance, I_{GH}, can be expressed as [31]

$$I_{\text{GH}} = I^l_{\text{GH}}\ I^a_{\text{GH}}\ I^p_{\text{GH}} \tag{2.2}$$

where I^l_{GH} is the attenuation factor, I^a_{GH} is the atmospheric turbulence, and I^p_{GH} represents the pointing errors. The attenuation factor I^l_{GH} primarily depends on beam divergence loss and atmospheric attenuation due to FSO weather-dependent effects, which is given by [30, eq. (4)]

$$I^l_{\text{GH}} = \frac{\pi D^2_{\text{H}}}{4(\phi_G\ L_{\text{GH}})^2}\ I^w_{\text{GH}}, \tag{2.3}$$

where ϕ_{G}, D_{H}, and I^{w}_{GH} denote the Tx beam divergence angle, Rx aperture diameter at the relay, and the weather-dependent attenuation factor, respectively. Following the Beer-Lambert law, the FSO weather-dependent attenuation can be expressed as $I^{w}_{\text{GH}} = \exp(-\varphi_f \, d_w)$ [23], where φ_f is the attenuation coefficient (in dB/km) due to fog or clouds between the ground station and HAP, and d_w indicates the distance over which the weather impact takes place, i.e., the thickness of considered clouds [44, Sec. (3)]. Similarly, the signalling model for the direct ground–SAT link can be obtained but omitted for conciseness.

At the HAP-based relay, a decode-and-forward (DF) scheme is used to avoid noise forwarding [31, 33, 45, 46]. The received information is first decoded at the HAP-based relay to obtain $\hat{x}[k]$. Then, $\hat{x}[k]$ is forwarded to the satellite. The received signal at the satellite is described as

$$y_{\text{HS}}[k] = \left(\eta_{\text{HS}} \; P_{\text{HS}} \; G_{\text{HS}} \; I_{\text{HS}}\right)^{\frac{b}{2}} \; \hat{x}[k] + n_{\text{HS}}[k], \tag{2.4}$$

where G_{HS} indicates the gain of the HAP-SAT link and is obtained as G_{GH} above. As HAPs are typically stationed at cloud-free altitudes, the weather attenuation will be almost equal to unity. Consequently, I^{l}_{HS} can be simplified to $\frac{\pi D_{\text{S}}^2}{4\left(\phi_{\text{H}} L_{\text{HS}}\right)^2}$.

For the direct RF link to the satellite, the baseband signal at the receiver is represented by [47, eq. (6)]

$$y_r[k] = \sqrt{P_r} \; \sqrt{G_r} \; h_r \; x[k] + n_r[k], \tag{2.5}$$

where h_r is the fading channel gain that follows the Rician fading model, P_r indicates the transmit power, and $n_r[k]$ denotes the AWGN with $\mathbb{E}\{n_r[k] n_r^*[k]\} = \sigma^2_{n_r}$. The noise variance $\sigma^2_{n_r}$ is given by $\sigma^2_{n_r} = P_n N_r$, where P_n and N_r denote the noise power and the noise figure, respectively. The path gain, G_r, can be expressed as [32, eq.

(10)]

$$G_r = \frac{G_r^{tx}\, G_r^{rx}}{FL_r\; L_A\; L_w}, \tag{2.6}$$

where G_r^{tx} denotes the Tx antenna gain, G_r^{rx} denotes the Rx antenna gain, $FL_r = \left(\frac{4\pi L_{\mathrm{GS}}}{\lambda_r}\right)^2$, $L_{\mathrm{GS}} = (h_{\mathrm{S}} - h_{\mathrm{G}})\sec(\theta_{\mathrm{GS}})$ denotes the slant range to satellite, where h_{G}, h_{S}, and θ_{GS} represent the aperture height of the ground station, the SAT altitude, and the SAT zenith angle, respectively. L_A denotes the gaseous atmosphere loss due to water vapor and oxygen, while the loss due to weather effects is represented by L_w. In [48], the international telecommunication union (ITU) recommends clouds and fog attenuation model for frequencies up to 200 GHz, which is given by

$$L_w = \varphi_r\; d_w, \tag{2.7}$$

where φ_r represents the RF weather-dependent attenuation coefficient (in dB/km).

2.3.2 Channel Model

We assume that FSO transmissions experience G-G fading with pointing errors and weather impairments. The excellent agreement between experimental and theoretical data for various turbulence regimes shows that the G-G distribution is a suitable statistical model for describing optical signal irradiance fluctuations [44,49,50]. The probability density function (pdf) of the irradiances I_{ij}, $ij \in \{\mathrm{GS}, \mathrm{HS}, \mathrm{GH}\}$, can be expressed as [51, eq. (1)]

$$f_{I_{ij}}(I) = \frac{\xi_{ij}^2\; I^{-1}}{\Gamma(\alpha_{ij})\Gamma(\beta_{ij})} G_{1,3}^{3,0}\left(\alpha_{ij}\beta_{ij}\frac{I}{I_{ij}^l}\,\middle|\, \begin{matrix} \xi_{ij}^2 + 1 \\ \xi_{ij}^2, \alpha_{ij}, \beta_{ij} \end{matrix}\right), \tag{2.8}$$

where ξ_{ij} is the pointing error coefficient, $\Gamma(\cdot)$ is the Gamma function [52, eq. (8.310)], G$(\cdot)$ is the Meijer G-function [52, eq. (9.301)], and β_{ij} and α_{ij} are the large-scale and small-scale fading parameters of atmospheric turbulence. Note that

β_{ij} and α_{ij} for SatCom uplink follows [25, eq. (7a, 7b)], and for the downlink [53, eq. (7-10)]. The main difference is the beam-wander-induced pointing error effects.

The instantaneous and average received signal-to-noise ratios (SNRs) can be expressed as [31, eq. (6, 9)]

$$\gamma_{ij,b} = \frac{(\eta_{ij}\ P_{ij}\ G_{ij}\ I_{ij})^b}{\sigma^2_{n_{ij}}}, \tag{2.9}$$

$$\bar{\gamma}_{ij,b} = \frac{(\eta_{ij}\ P_{ij}\ G_{ij}\ k_{ij}\ I^l_{ij})^b}{\sigma^2_{n_{ij}}}, \tag{2.10}$$

respectively, where $k_{ij} = \xi^2_{ij}/(\xi^2_{ij}+1)$. With the application of (2.8), (2.9), and the power transformation of random variables, the unified pdf of the instantaneous SNR for IM/DD and HD is obtained after some algebraic manipulations, as [54, eq. (2)]

$$f_{\gamma_{ij}}(\gamma) = \frac{\xi^2_{ij}\ \gamma^{-1}}{b\ \Gamma(\alpha_{ij})\Gamma(\beta_{ij})} G^{3,0}_{1,3}\left(\alpha_{ij}\beta_{ij}k_{ij}\left(\frac{\gamma}{\mu_{ij,b}}\right)^{\frac{1}{b}}\middle|\begin{matrix}\xi^2_{ij}+1\\ \xi^2_{ij},\alpha_{ij},\beta_{ij}\end{matrix}\right), \tag{2.11}$$

where $\mu_{ij,b}$ represents the average electrical SNR, which is linked to $\bar{\gamma}_{ij,b}$ as

$$\mu_{ij,1} = \bar{\gamma}_{ij,1},$$

and

$$\mu_{ij,2} = \frac{\alpha_{ij}\,\beta_{ij}\,\xi^2_{ij}\,(\xi^2_{ij}+2)}{(\alpha_{ij}+1)(\beta_{ij}+1)(\xi^2_{ij}+1)^2}\ \bar{\gamma}_{ij,2}.$$

With the application of (2.11) and [55, eq. (07.34.21.0084.01)], the cumulative distribution function (cdf) of γ_{ij} is obtained after some algebraic manipulations, as

$$F_{\gamma_{ij}}(\gamma) = \mathcal{X}_{ij}\ G^{3b,\ 1}_{b+1,\ 3b+1}\left(\mathcal{E}_{ij}\ \frac{\gamma}{\mu_{ij,b}}\middle|\begin{matrix}1 & , & \mathcal{B}^1_{ij}\\ \mathcal{B}^2_{ij} & , & 0\end{matrix}\right), \tag{2.12}$$

where $\mathcal{X}_{ij} = \frac{b^{\alpha_{ij}+\beta_{ij}-2}\ \xi^2_{ij}}{(2\pi)^{b-1}\ \Gamma(\alpha_{ij})\Gamma(\beta_{ij})}$, $\mathcal{E}_{ij} = \left(\frac{\alpha_{ij}\beta_{ij}k_{ij}}{b^2}\right)^b$, $\mathcal{B}^1_{ij} = \{\frac{\xi^2_{ij}+1}{b},\ldots,\frac{\xi^2_{ij}+b}{b}\}$ comprises of

b terms, and $\mathcal{B}_{ij}^2 = \{\frac{\xi_{ij}^2}{b}, \ldots, \frac{\xi_{ij}^2+b-1}{b}, \frac{\alpha_{ij}}{b}, \ldots, \frac{\alpha_{ij}+b-1}{b}, \frac{\beta_{ij}}{b}, \ldots, \frac{\beta_{ij}+b-1}{b}\}$ comprises of $3b$ terms.

The instantaneous SNR at the RF receiver is represented by [30, eq. (6)]

$$\gamma_r = \bar{\gamma}_r \; h_r^2, \tag{2.13}$$

where

$$\bar{\gamma}_r = \frac{P_r \; G_r}{\sigma_{n_r}^2} \tag{2.14}$$

represents the average SNR of the RF link [56, eq. (5.34)]. In SatCom, RF transmissions encounter minimal reflection and scattering from the environment. As such, we adopt Rician fading to better describe the RF channel [33, 34]. Using (2.13), [57, eq. (2.15)], and the power transformation of random variables, the pdf of the instantaneous SNR can be described as [57, eq. (2.16)]

$$f_{\gamma_r}(\gamma) = \frac{K+1}{\bar{\gamma}_r} \; \exp\left(-(K+1) \; \frac{\gamma}{\bar{\gamma}_r} - K\right) I_0\left(2 \; \sqrt{K(K+1) \; \frac{\gamma}{\bar{\gamma}_r}}\right), \tag{2.15}$$

where K is the Rician factor. With the application of series expansion to the Bessel function [52, eq. (8.447.1)] and rewriting the exponential function using the Meijer-G function [58, eq. (11)], the pdf in (2.15) can be written as

$$f_{\gamma_r}(\gamma) = \mathcal{H}_1 \; \gamma^u \; G_{0,1}^{1,0}\left(\mathcal{F} \; \gamma \;\middle|\; \begin{matrix} - \\ 0 \end{matrix} \right), \tag{2.16}$$

where $\mathcal{H}_1 = \mathcal{F} \; \exp(-K) \; \sum_{u=0}^{\infty} \frac{(K\mathcal{F})^u}{(u!)^2}$ denotes the summation operation and $\mathcal{F} = \frac{K+1}{\bar{\gamma}_r}$. With the application of [55, eq. (07.34.21.0084.01)], the corresponding cdf is given by

$$F_{\gamma_r}(\gamma) = \mathcal{H}_1 \; \gamma^{u+1} \; G_{1,2}^{1,1}\left(\mathcal{F} \; \gamma \;\middle|\; \begin{matrix} -u \\ 0 \; , -u-1 \end{matrix} \right). \tag{2.17}$$

2.4 Performance Analysis

Now, we analyze the OP, ASEP, and ergodic capacity of the integrated transmission system, taking into account beam wandering, beam divergence, pointing errors, atmospheric turbulence, free-space loss, and weather effects.

2.4.1 Outage Analysis

The OP is defined as the probability that the instantaneous received SNR will fall below a particular γ_{th} threshold. The threshold is chosen to meet a predefined QoS requirement, typically in terms of target SEP. The OP of the proposed SatCom can be written as

$$P_{\text{out}}^{\text{SatCom}} = P_{\text{out}}^{\text{SAG}} \; P_{\text{out}}^{\text{SH}} \; P_{\text{out}}^{\text{RF}} \; , \tag{2.18}$$

where $P_{\text{out}}^{\text{RF}} = F_{\gamma_r}(\gamma_{\text{th}})$ denotes the OP of the direct RF link to the satellite calculated using the cdf of γ_r defined in (2.17). $P_{\text{out}}^{\text{SH}}$ represents the OP of the SH-FSO transmission given by (2.12) with the corresponding $\mu_{\text{GS},b}$, ξ_{GS}, β_{GS}, and α_{GS} values. $P_{\text{out}}^{\text{SAG}}$ represents the OP of the SAG-FSO transmission when the instantaneous SNR of either HAP–SAT or ground–HAP hop falls below the predefined threshold γ_{th}. Hence, $P_{\text{out}}^{\text{SAG}}$ can be calculated as

$$P_{\text{out}}^{\text{SAG}} = 1 - \left(1 - P_{\text{out}}^{\text{HS}}\right)\left(1 - P_{\text{out}}^{\text{GH}}\right), \tag{2.19}$$

where $P_{\text{out}}^{\text{HS}}$ and $P_{\text{out}}^{\text{GH}}$ are the OP of both HAP–SAT and ground–HAP hops, respectively, defined by (2.12) using the corresponding $\mu_{ij,b}$, ξ_{ij}, β_{ij}, and α_{ij} values.

2.4.2 Error Rate Analysis

Assuming M-ary phase-shift keying (MPSK) signalling, the SEP conditioned on the instantaneous SNR can be described as [59, eq. (11)]

$$P(e|\gamma) = \frac{A}{2}\text{erfc}\left(\sqrt{\gamma}\sin\frac{\pi}{M}\right), \tag{2.20}$$

where

$$A = \begin{cases} 1, & M = 2; \\ 2, & M > 2. \end{cases} \tag{2.21}$$

Note that the expression in (2.20) is exact when $M = 2$ and an upper bound when $M > 2$ [57, eq. (8.25)]. With the application of [55, eq. (07.34.03.0619.01)], (2.20) is written as

$$P(e|\gamma) = \frac{A}{2\sqrt{\pi}}\, G_{1,2}^{2,0}\left(\gamma\left(\sin\frac{\pi}{M}\right)^2 \;\middle|\; \begin{matrix} 1 \\ 0\,,\frac{1}{2} \end{matrix}\right). \tag{2.22}$$

Applying the Maclaurin series [52, eq. (3.321)], (2.20) can also be rewritten as

$$P(e|\gamma) = \frac{A}{2} \;-\; \frac{A}{\sqrt{\pi}}\,\mathcal{H}_2\,\gamma^{v+\frac{1}{2}}\,, \tag{2.23}$$

where $\mathcal{H}_2 = \sum_{v=0}^{\infty} \frac{(-1)^v \left(\sin\frac{\pi}{M}\right)^{2v+1}}{v!\;(2v+1)}$.

According to the system operation, the SAG-FSO transmission acts as the main link, while the SH-FSO/RF transmission acts as the backup. Therefore, the overall ASEP of the system is given by

$$\bar{P}_e^{\text{SatCom}} = \bar{P}_e^{\text{SAG}} + \; P_{\text{out}}^{\text{SAG}}\;\bar{P}_e^{\text{SH-h}}, \tag{2.24}$$

where $\bar{P}_e^{\text{SAG}}$ represents the ASEP of the SAG-FSO links with acceptable link quality, i.e., γ_{GH} and γ_{HS} are greater than a predefined threshold γ_{th}, $P_{\text{out}}^{\text{SAG}}$ is calculated in

(2.19), and $\bar{P}_e^{\mathrm{SH-h}}$ denotes the ASEP of the hybrid SH-FSO/RF transmission.

Considering DF relaying scheme, $\bar{P}_e^{\mathrm{SAG}}$ is given by [60, eq. (22)],

$$\bar{P}_e^{\mathrm{SAG}} = \bar{P}_e^{\mathrm{HS}} + \bar{P}_e^{\mathrm{GH}} - \bar{P}_e^{\mathrm{HS}}\, \bar{P}_e^{\mathrm{GH}}, \tag{2.25}$$

where $\bar{P}_e^{\mathrm{HS}}$ and $\bar{P}_e^{\mathrm{GH}}$ denote the ASEP of the HAP–SAT and ground–HAP hops, respectively, when $\gamma_{\mathrm{HS}} \geq \gamma_{\mathrm{th}}$ and $\gamma_{\mathrm{GH}} \geq \gamma_{\mathrm{th}}$. The analytical expression of $\bar{P}_e^{\mathrm{GH}}$ can be derived as

$$\begin{aligned}\bar{P}_e^{\mathrm{GH}} &= \int_{\gamma_{\mathrm{th}}}^{\infty} P(e|\gamma)\; f_{\gamma_{\mathrm{GH}}}(\gamma)\; d\gamma \\ &= \underbrace{\int_0^{\infty} P(e|\gamma)\; f_{\gamma_{\mathrm{GH}}}(\gamma)\; d\gamma}_{I_{e_1}} - \underbrace{\int_0^{\gamma_{\mathrm{th}}} P(e|\gamma)\; f_{\gamma_{\mathrm{GH}}}(\gamma)\; d\gamma}_{I_{e_2}}\,. \end{aligned} \tag{2.26}$$

The expression of $\bar{P}_e^{\mathrm{GH}}$ is now split into two terms, I_{e_1} and I_{e_2}. The analytical expression of I_{e_1} can be calculated using (2.11), (2.22), and [55, eq. (07.34.21.0013.01)] as

$$I_{e_1} = \frac{A\; \mathcal{X}_{\mathrm{GH}}}{2\sqrt{\pi}}\; G_{b+2,\; 3b+1}^{\;3b,\;\; 2}\left(\frac{\mathcal{E}_{\mathrm{GH}}}{\left(\sin\frac{\pi}{M}\right)^2 \mu_{\mathrm{GH},b}} \middle| \begin{matrix} 1, \frac{1}{2}, \mathcal{B}_{\mathrm{GH}}^1 \\ \mathcal{B}_{\mathrm{GH}}^2, 0 \end{matrix} \right). \tag{2.27}$$

After applying (2.23), I_{e_2} is obtained by

$$I_{e_2} = \int_0^{\gamma_{\mathrm{th}}} \frac{A}{2}\; f_{\gamma_{\mathrm{GH}}}(\gamma)\; d\gamma \; - \int_0^{\gamma_{\mathrm{th}}} \frac{A}{\sqrt{\pi}}\; \mathcal{H}_2\; \gamma^{\;v+\frac{1}{2}}\; f_{\gamma_{\mathrm{GH}}}(\gamma)\; d\gamma. \tag{2.28}$$

Using [55, eq. (07.34.21.0084.01)], I_{e_2} can be analytically expressed as

$$I_{e_2} = \mathcal{X}_{\text{GH}} \ \frac{A}{2} \ G_{b+1,\ 3b+1}^{\ 3b,\ 1} \left(\mathcal{E}_{\text{GH}} \ \frac{\gamma_{\text{th}}}{\mu_{\text{GH},b}} \ \middle| \ \begin{matrix} 1 & , & \mathcal{B}_{\text{GH}}^{1} \\ \mathcal{B}_{\text{GH}}^{2} & , & 0 \end{matrix} \right)$$
$$- \mathcal{X}_{\text{GH}} \ \frac{A}{\sqrt{\pi}} \ \mathcal{H}_2 \ \gamma_{\text{th}}^{v+\frac{1}{2}} G_{b+1,\ 3b+1}^{\ 3b,\ 1} \left(\mathcal{E}_{\text{GH}} \ \frac{\gamma_{\text{th}}}{\mu_{\text{GH},b}} \ \middle| \ \begin{matrix} 1-v-\frac{1}{2}, \mathcal{B}_{\text{GH}}^{1} \\ \mathcal{B}_{\text{GH}}^{2}, -v-\frac{1}{2} \end{matrix} \right). \quad (2.29)$$

Similar to (2.26), the analytical expression of $\bar{P}_e^{\text{HS}}$ is obtained, replacing $\mu_{\text{GH},b}$, ξ_{GH}, α_{GH}, and β_{GH} with $\mu_{\text{HS},b}$, ξ_{HS}, α_{HS}, and β_{HS}. Consequently, the ASEP of the FSO transmission through the HAP in (2.25) can be obtained.

The ASEP of the SH-FSO/RF transmission in (2.24) is calculated as [31, eq. (27)]

$$\bar{P}_e^{\text{SH-h}} = \bar{P}_e^{\text{SH}} + \ P_{\text{out}}^{\text{SH}} \ \bar{P}_e^{\text{RF}}, \quad (2.30)$$

where $P_{\text{out}}^{\text{SH}}$ can be calculated using (2.12) with the corresponding parameters $\mu_{\text{GS},b}$, ξ_{GS}, β_{GS}, and α_{GS}, $\bar{P}_e^{\text{SH}}$ denotes the ASEP of the SH-FSO transmission when $\gamma_{\text{GS}} \geq \gamma_{\text{th}}$ and is calculated using (2.27) and (2.29) with the corresponding $\mu_{\text{GS},b}$, ξ_{GS}, β_{GS}, and α_{GS} values, and $\bar{P}_e^{\text{RF}}$ indicates the ASEP of the RF link, which is represented by

$$\bar{P}_e^{\text{RF}} = \int_0^{\infty} P(e|\gamma) \ f_{\gamma_r}(\gamma) \ d\gamma. \quad (2.31)$$

With the application of (2.16) and (2.22), and [55, eq. (07.34.21.0013.01)], $\bar{P}_e^{\text{RF}}$ can be analytically expressed as

$$\bar{P}_e^{\text{RF}} = \frac{A}{2\sqrt{\pi} \left(\sin \frac{\pi}{M}\right)^{2u+2}} \ \mathcal{H}_1 \ G_{2,2}^{1,2} \left(\frac{\mathcal{F}}{\left(\sin \frac{\pi}{M}\right)^2} \ \middle| \ \begin{matrix} -u \ , & -u-\frac{1}{2} \\ 0 \ , & -u-1 \end{matrix} \right). \quad (2.32)$$

2.4.3 Ergodic Capacity Analysis

The ergodic capacity of the integrated SatCom system can be calculated as

$$\bar{C}^{\text{SatCom}} = \bar{C}^{\text{SAG}} \; + \; P_{\text{out}}^{\text{SAG}} \;\; \bar{C}^{\text{SH-h}}, \tag{2.33}$$

where $\bar{C}^{\text{SAG}}$ and $\bar{C}^{\text{SH-h}}$ are the ergodic capacities of SAG-FSO and hybrid SH-FSO/RF links, respectively. Using DF relaying, the end-to-end capacity of the SAG-FSO transmission scheme is given by [61, eq. (16)]

$$\bar{C}^{\text{SAG}} = \min\left\{\bar{C}^{\text{GH}} \;, \;\; \bar{C}^{\text{HS}}\right\}, \tag{2.34}$$

where $\bar{C}^{\text{GH}}$ and $\bar{C}^{\text{HS}}$ denote the capacity of the ground–HAP and HAP–SAT FSO links when their instantaneous SNR is greater than γ_{th}. $\bar{C}^{\text{GH}}$ can be calculated as

$$\begin{aligned}\bar{C}^{\text{GH}} &= \int_{\gamma_{\text{th}}}^{\infty} \text{BW}_f \; \log_2(1+\epsilon\;\gamma) \; f_{\gamma_{\text{GH}}}(\gamma) \; d\gamma \\ &= \underbrace{\frac{\text{BW}_f}{\ln(2)} \int_0^{\infty} \ln(1+\epsilon\;\gamma) \; f_{\gamma_{\text{GH}}}(\gamma) \; d\gamma}_{I_{c_1}} - \underbrace{\frac{\text{BW}_f}{\ln(2)} \int_0^{\gamma_{\text{th}}} \ln(1+\epsilon\;\gamma) \; f_{\gamma_{\text{GH}}}(\gamma) \; d\gamma}_{I_{c_2}},\end{aligned} \tag{2.35}$$

where BW_f is the bandwidth of the FSO link and ϵ is a constant such that $\epsilon = 1$ for HD technique and $\epsilon = e/(2\pi)$ for IM/DD technique. Note that the expression in (2.35) is an exact solution for HD, while it is a lower bound for IM/DD [51]. To evaluate the integral I_{c_1}, we rewrite $\ln(1+\epsilon\gamma)$ into a Meijer G-function using [55, eq. (07.34.03.0456.01)]. The analytical expression of I_{c_1} is obtained after some algebraic manipulations, using (2.11) and [55, eq. (07.34.21.0013.01)] as

$$I_{c_1} = \frac{\text{BW}_f \, \mathcal{X}_{\text{GH}}}{\ln(2)} \; G_{b+2,\; 3b+2}^{\;3b+2,\;\; 1} \left(\frac{\mathcal{E}_{\text{GH}}}{\epsilon \; \mu_{\text{GH},b}} \;\middle|\; \begin{matrix} 0,\; 1 \;,\; \mathcal{B}_{\text{GH}}^1 \\ \mathcal{B}_{\text{GH}}^2 \;,\; 0,\; 0 \end{matrix} \right). \tag{2.36}$$

To evaluate I_{c_2}, $\ln(1+\epsilon\ \gamma)$ is replaced by its Taylor series as [41, eq. (14)]

$$\ln(1+\epsilon\ \gamma) = \ln(1+\epsilon\ a)\ +\ \sum_{m=1}^{\infty} \frac{(-1)^{m+1}\ \epsilon^m}{m\ (1+\epsilon\ a)^m}\ \sum_{n=0}^{m} \binom{m}{n} (-a)^{m-n}\ \gamma^n. \tag{2.37}$$

Now, I_{c_2} can be expressed in the form of $I_{c_2} = I_{c_{21}} + I_{c_{22}}$, as

$$I_{c_{21}} = \frac{\mathrm{BW}_f}{\ln(2)} \int_0^{\gamma_{\mathrm{th}}} \ln(1+\epsilon\ a)\ f_{\gamma_{\mathrm{GH}}}(\gamma)\ d\gamma, \tag{2.38}$$

and,

$$I_{c_{22}} = \frac{\mathrm{BW}_f}{\ln(2)} \int_0^{\gamma_{\mathrm{th}}} \ \sum_{m=1}^{\infty} \frac{(-1)^{m+1}\ \epsilon^m}{m\ (1+\epsilon\ a)^m}\ \sum_{n=0}^{m} \binom{m}{n}\ (-a)^{m-n}\ \gamma^n\ f_{\gamma_{\mathrm{GH}}}(\gamma)\ d\gamma, \tag{2.39}$$

respectively. By using (2.11), (2.38), (2.39), and [55, eq. (07.34.21.0084.01)], the analytical expressions of $I_{c_{21}}$ and $I_{c_{22}}$ are given by

$$I_{c_{21}} = \mathrm{BW}_f\ \log_2(1+\epsilon\ a)\ P_{\mathrm{out}}^{\mathrm{GH}}, \tag{2.40}$$

and

$$I_{c_{22}} = \frac{\mathrm{BW}_f\ \mathcal{X}_{\mathrm{GH}}}{\ln 2} \sum_{m=1}^{\infty} \frac{(-1)^{m+1}\ \epsilon^m}{m(1+\epsilon\ a)^m} \sum_{n=0}^{m} \binom{m}{n} (-a)^{m-n}\ \gamma_{\mathrm{th}}^n \times G_{b+1,\ 3b+1}^{3b,\ 1} \left(\mathcal{E}_{\mathrm{GH}}\ \frac{\gamma_{\mathrm{th}}}{\mu_{\mathrm{GH},b}} \ \middle|\ \begin{matrix} 1-n & , & \mathcal{B}_{\mathrm{GH}}^1 \\ \mathcal{B}_{\mathrm{GH}}^2 & , & -n \end{matrix} \right), \tag{2.41}$$

respectively. Note that a is a constant satisfying the ratio test of [41, eq. (14)]. We set $a = 5.295$ to ensure the convergence of the Taylor series. The expression of $\bar{C}^{\mathrm{HS}}$ can be obtained similar to (2.35), using the corresponding parameters α_{HS}, β_{HS}, ξ_{HS}, and $\mu_{\mathrm{HS},b}$. Then, $\bar{C}^{\mathrm{SAG}}$ in (2.34) can be analytically evaluated.

The ergodic capacity of the hybrid SH-FSO/RF transmission scheme can be

computed as [28, eq. (3)]

$$\bar{C}^{\mathrm{SH-h}} = \bar{C}^{\mathrm{SH}} \; + \; P_{\mathrm{out}}^{\mathrm{SH}} \;\; \bar{C}^{\mathrm{RF}}, \tag{2.42}$$

where $\bar{C}^{\mathrm{SH}}$ indicates the capacity of the SH-FSO when $\gamma_{\mathrm{GS}} \geq \gamma_{\mathrm{th}}$ and can be defined as (2.35) and the corresponding $\mu_{\mathrm{GS},b}$, ξ_{GS}, β_{GS}, and α_{GS} values.

The capacity of the RF link can be expressed as

$$\bar{C}^{\mathrm{RF}} = \frac{\mathrm{BW}_r}{\ln(2)} \int_0^{\infty} \ln(1+\gamma) \; f_{\gamma_r}(\gamma) \; d\gamma, \tag{2.43}$$

where BW_r is the bandwidth of the RF link. We first rewrite $\ln(1+\gamma)$ into a Meijer G-function using [55, eq. (07.34.03.0456.01)]. Then, the corresponding analytical expression is obtained after some algebraic manipulations, using (2.16), [55, eq. (07.34.21.0088.01)], and [52, eq. (9.31.2)] as

$$\bar{C}^{\mathrm{RF}} = \frac{BW_{\mathrm{RF}}}{\ln(2)} \; \exp(-K) \; \sum_{u=0}^{\infty} \frac{K^u}{(u!)^2} \; G_{2,3}^{3,1}\left(\frac{K+1}{\bar{\gamma}_r} \middle| \begin{matrix} 0 \;\; , \;\; 1 \\ 1+u, 0, 0 \end{matrix} \right). \tag{2.44}$$

It is worth noting that the terms in the infinite summations of (2.44) decrease at the rate of $\frac{1}{(u!)^2}$, ensuring their convergence. Also, the derived expressions are applicable for both downlink and uplink scenarios by using the appropriate expressions for α_{ij} and β_{ij}.

2.5 Overall System Diversity Gain

To provide further insights into the behavior of the proposed system, we derive simpler asymptotic expressions [62]. In particular, the Meijer G-function is represented in terms of the summation of much simpler functions (see the Appendix of this chapter for derivation details).

2.5.1 OP Diversity Gain

From (2.57) and (2.58), we can observe that $P_{\text{out},a}^{\text{SAG}} \propto \left(\bar{\gamma}_{ij}\right)^{-\mathcal{D}_{\text{O,SAG}}}$, where the diversity gain with respect to outage $\mathcal{D}_{\text{O,SAG}} = \min(\frac{\xi_{\text{GH}}^2}{b}, \frac{\alpha_{\text{GH}}}{b}, \frac{\beta_{\text{GH}}}{b}, \frac{\xi_{\text{HS}}^2}{b}, \frac{\alpha_{\text{HS}}}{b}, \frac{\beta_{\text{HS}}}{b})$. Since $\xi_{\text{GH}} \ll \xi_{\text{HS}}$, $\alpha_{\text{GH}} \ll \alpha_{\text{HS}}$, and $\beta_{\text{GH}} \ll \beta_{\text{HS}}$, $\mathcal{D}_{\text{O,SAG}} = \min(\frac{\xi_{\text{GH}}^2}{b}, \frac{\alpha_{\text{GH}}}{b}, \frac{\beta_{\text{GH}}}{b})$. For the SH-FSO transmission, the diversity gain with respect to outage is given by $\mathcal{D}_{\text{O,SH}} = \min(\frac{\xi_{\text{GS}}^2}{b}, \frac{\alpha_{\text{GS}}}{b}, \frac{\beta_{\text{GS}}}{b})$. Because the higher-order terms are insignificant, just the first term in (2.59) is considered, $P_{a\text{out}}^{\text{RF}} \propto \left(\bar{\gamma}_r\right)^{-1}$. Thus, the diversity gain of the RF link for outage, $\mathcal{D}_{\text{O,RF}}$, is equal to unity. As a result, the overall system diversity gain in terms of OP is given by

$$\mathcal{D}_{\text{O,SatCom}} = \mathcal{D}_{\text{O,SAG}} \; + \; \mathcal{D}_{\text{O,SH}} \; + \; 1. \tag{2.45}$$

2.5.2 ASEP Diversity Gain

It is observed from the derived expressions in (2.62) and (2.63) that $\bar{P}_{e,a}^{\text{SAG}} \propto \left(\bar{\gamma}_{\text{ij}}\right)^{-\mathcal{D}_{e,\text{SAG}}}$. Thus, the diversity gain with rspect to the ASEP of the FSO transmission through the HAP, $\mathcal{D}_{e,\text{SAG}}$, is equal $\min(\frac{\xi_{\text{GH}}^2}{b}, \frac{\alpha_{\text{GH}}}{b}, \frac{\beta_{\text{GH}}}{b})$. Simalr to the SAG-FSO transmission, the diversity gain of the SH-FSO transmission is also obtained for ASEP as $\mathcal{D}_{e,\text{SH}} = \min(\frac{\xi_{\text{GS}}^2}{b}, \frac{\alpha_{\text{GS}}}{b}, \frac{\beta_{\text{GS}}}{b})$. Taking only the dominant term into account, we can deduce from (2.64) that $\bar{P}_{e,a}^{\text{RF}} \propto \left(\bar{\gamma}_r\right)^{-1}$. Thus, the RF diversity gain for ASEP equals unity. Note that the term with the smallest exponent of average SNR dominates the ASEP. Therefore, the overall system diversity gain for ASEP, considering (2.60), is obtained as

$$\mathcal{D}_{e,\text{SatCom}} = \min\left(\min(\frac{\xi_{\text{GH}}^2}{b}, \frac{\alpha_{\text{GH}}}{b}, \frac{\beta_{\text{GH}}}{b}) \; , \; \min(\frac{\xi_{\text{GH}}^2}{b}, \frac{\alpha_{\text{GH}}}{b}, \frac{\beta_{\text{GH}}}{b}) + \mathcal{D}_{e,\text{SH-h}} \right), \tag{2.46}$$

where $\mathcal{D}_{e,\mathrm{SH-h}}$ denotes the diversity gain with respect to ASEP of the SH-FSO/RF transmission and is calculated by

$$\mathcal{D}_{e,\mathrm{SH-h}} = \min\left(\min(\frac{\xi_{\mathrm{GS}}^2}{b}, \frac{\alpha_{\mathrm{GS}}}{b}, \frac{\beta_{\mathrm{GS}}}{b}) \ , \ \min(\frac{\xi_{\mathrm{GS}}^2}{b}, \frac{\alpha_{\mathrm{GS}}}{b}, \frac{\beta_{\mathrm{GS}}}{b}) + 1 \right). \tag{2.47}$$

After simplification, $\mathcal{D}_{e,\mathrm{SatCom}}$ is given by

$$\mathcal{D}_{e,\mathrm{SatCom}} \ = \ \min\left(\frac{\xi_{\mathrm{GH}}^2}{b} \ , \ \frac{\alpha_{\mathrm{GH}}}{b} \ , \ \frac{\beta_{\mathrm{GH}}}{b} \right). \tag{2.48}$$

2.6 Switching Threshold Optimization

In this section, we derive the optimum switching thresholds for both FSO links in terms of minimizing the overall system ASEP. First, we obtain the optimum switching threshold for SH-FSO transmission, $\gamma_{\mathrm{opt}}^{\mathrm{SH}}$, which is given by differentiating (2.30) for γ_{th} and equating it to zero, as

$$\frac{d}{\gamma_{\mathrm{th}}} \bar{P}_e^{\mathrm{SH}} + \frac{d}{\gamma_{\mathrm{th}}} \ P_{\mathrm{out}}^{\mathrm{SH}} \ \bar{P}_e^{\mathrm{RF}} = 0. \tag{2.49}$$

From (2.12) and (2.26), we can rewrite (2.49) as

$$-P(e|\gamma) \ f_{\gamma_{\mathrm{GS}}}(\gamma) + f_{\gamma_{\mathrm{GS}}}(\gamma) \ \bar{P}_e^{\mathrm{RF}} = 0. \tag{2.50}$$

With the application of (2.20), the optimum switching of the SH-FSO transmission is given by

$$\gamma_{\mathrm{opt}}^{\mathrm{SH}} = \left[\frac{1}{\sin\frac{\pi}{M}} \ \mathrm{erfc}^{-1}\left(\frac{2}{A} \ \bar{P}_e^{\mathrm{RF}} \right) \right]^2. \tag{2.51}$$

Now, we derive the optimum switching threshold for FSO transmission through the HAP $\gamma_{\mathrm{opt}}^{\mathrm{SAG}}$. By differentiating (2.24) for γ_{th} and equating it to zero, we can obtain

$$\frac{d}{\gamma_{\mathrm{th}}} \bar{P}_e^{\mathrm{SAG}} + \frac{d}{\gamma_{\mathrm{th}}} \ P_{\mathrm{out}}^{\mathrm{SAG}} \ \bar{P}_{e,\mathrm{opt}}^{\mathrm{SH-h}} = 0, \tag{2.52}$$

where $\bar{P}_{e,\text{opt}}^{\text{SH}-\text{h}}$ denotes the ASEP of the SH-FSO/RF transmission with optimum switching threshold, $\gamma_{\text{opt}}^{\text{SH}}$. Given that aerosols are typically concentrated within 2 km of the ground [23], the HAP-SAT hop experiences extremely weak turbulence with very large fading parameters in the order of 10^4. On the other hand, the ground–HAP hop is vulnerable to atmospheric-turbulence effects and weather conditions. Thus, it is more likely that $\gamma_{\text{HS}} > \gamma_{\text{GH}}$, and the effective instantaneous SNR of the FSO transmission through the HAP can be approximated as $\gamma_{\text{SAG}} \approx \gamma_{\text{GH}}$ [33]. Hence, (2.52) can be rewritten as

$$\frac{d}{\gamma_{\text{th}}} \bar{P}_e^{\text{GH}} + \frac{d}{\gamma_{\text{th}}} \, P_{\text{out}}^{\text{GH}} \, \bar{P}_{e,\text{opt}}^{\text{SH}-\text{h}} \approx 0. \tag{2.53}$$

Using (2.12), (2.20), and (2.26), the optimum switching for FSO transmission over the HAP is obtained as

$$\gamma_{\text{opt}}^{\text{SAG}} \approx \left[\frac{1}{\sin \frac{\pi}{M}} \, \text{erfc}^{-1} \left(\frac{2}{A} \, \bar{P}_{e,\text{opt}}^{\text{SH}-\text{h}} \right) \right]^2. \tag{2.54}$$

2.7 Numerical Results

We now illustrate the performance of the integrated transmission system using selected numerical examples. We also use Monte Carlo simulations to verify the obtained expressions. Unless otherwise stated, we assume an IM/DD scheme without losing generality, and the system parameters as listed in Table 2.1 [31]. Note also that using a 1550 nm wavelength is preferred for both uplink and downlink FSO transmissions to mitigate the atmospheric turbulence effects [24]. Furthermore, we assume that FSO and RF links have equal average SNR through power control. It should be noted that the zenith angles (θ_{HS} and θ_{GS}) vary with the satellite's position, whereas for θ_{GH} is independent of the satellite's location and remains fixed at a low value. The infinite summations are truncated to $v = 50$, $m = 30$, and $u = 30$

Table 2.1: Simulation parameters

Parameter	*Symbol*	*Value*
Ground station height	h_{G}	2 m
HAP relay altitude	h_{H}	20 km
SAT altitude	h_{S}	620 km
Ground-SAT and HAP-SAT zenith angle	θ_{HS}, θ_{GS}	$30^{\mathrm{o}} : 80^{\mathrm{o}}$
Ground-HAP zenith angle	θ_{GH}	5^{o}
Wind speed	ω	21 m/s
Ground level turbulence	$C_{\mathrm{n}}^2(0)$	$1.7 \times 10^{-14}\mathrm{m}^{\frac{-2}{3}}$
FSO subsystem [31]		
Optical bandwidth	BW_f	100 GHz
Optical wavelength	λ_f	1550 nm
Telescope Tx gain	G_f^{tx}	75 dB
Telescope Rx gain	G_f^{rx}	75 dB
Background noise power	σ_n^2	250μW [63]
Pointing error coefficients	ξ_{GS}, ξ_{GH}, and ξ_{HS}	5.2, 5.2, and 13.07
Optical-to-electrical efficiency	η	0.8
Beam divergence angle	ϕ	15μrad [63]
Telescope aperture diameter	D	0.2 m
Transmitting beam radius	W_0^{G}, W_0^{H}	0.02 m
Switching threshold	γ_{th}	10.5 dB
RF subsystem [64]		
RF carrier frequency	f_r	30 GHz
RF link bandwidth	BW_r	1 GHz
RF Transmit antenna gain	G_r^{tx}	52 dB
RF Receive antenna gain	G_r^{rx}	52 dB
RF Noise power spectral density	$P_{n_{\mathrm{o}}}$	-114 dBW/MHz
Noise figure	N_r	5 dB
Rician factor	K	6

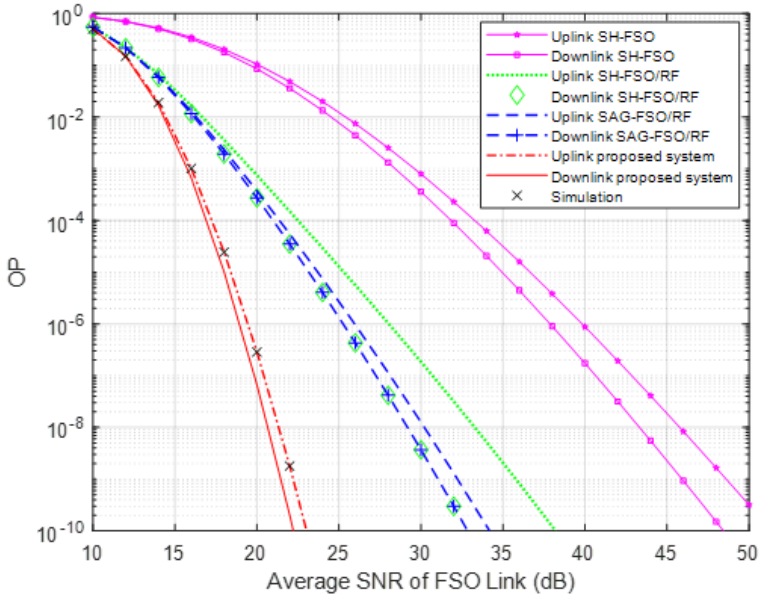

Figure 2.3: OP performance with varying average link SNRs.

since larger values have a minor impact on the obtained performance.

Figure 2.3 shows the OP of the integrated transmission system given by (2.18) as a function of average link SNR over uplink and downlink scenarios. The results of other transmission systems are also plotted for comparison purposes. We assume a 10.5 dB outage threshold and a 60° satellite zenith angle. From this figure, we can observe that the derived analytical expression for OP exactly matches the Monte-Carlo simulation. Because of the residual beam-wandering effects in the uplink scenario, all SatCom systems achieve better performance in the downlink scenario than in the uplink. Also, the SAG-FSO/RF design in [31] outperforms SH-FSO/RF transmission [27] over the uplink, while the downlink performance gain is negligible. With our integrated transmission system, we can achieve about 10 dB performance gain over the SAG-FSO/RF transmission [31] for both downlink and uplink scenarios, at an OP of 10^{-9}. The performance gain over downlink and uplink scenarios suggests that the proposed system is a promising solution for future SatCom systems.

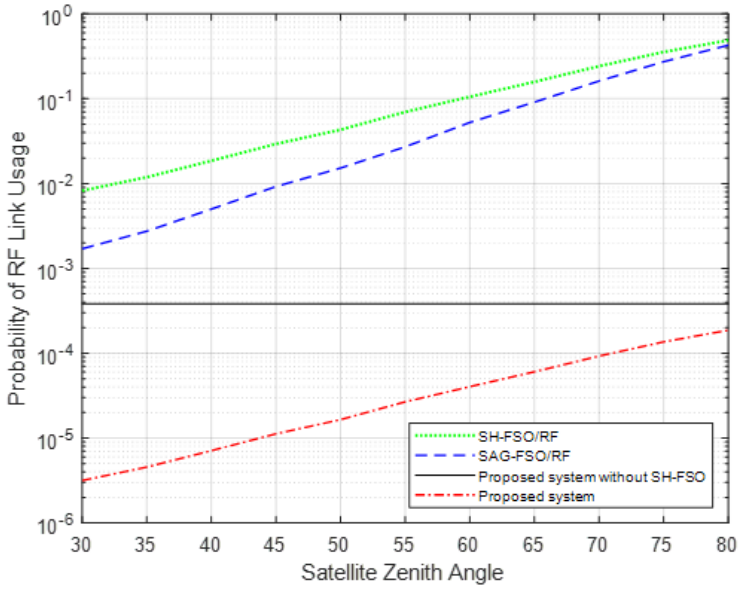

Figure 2.4: Probability of the RF-link usage for different satellite zenith angles over uplink scenario.

Because FSO transmissions typically have higher throughput than RF transmissions, a lower probability of RF-link usage denotes higher system throughput. Therefore, we show the probability of RF-link usage in Figure 2.4 to highlight the benefit of the suggested transmission system. To do so, we assume varying satellite zenith angles, an outage threshold of 10.5 dB, and a 20 dB average SNR. For the sake of comparison, we also plot the probability of RF-link usage for SH-FSO/RF [27], SAG-FSO/RF [31], and our proposed system without SH-FSO transmission. From this figure, we can see that the integrated transmission system results in substantially lower RF-link usage than SAG-FSO/RF [31], whereas SAG-FSO/RF [31] slightly outperforms SH-FSO/RF [27]. The probability of RF-link usage is decreased from 2×10^{-2} and 5×10^{-3} for SH-FSO/RF [27] and SAG-FSO/RF [31] systems to 7×10^{-6} for our proposed system, at 40^{o} satellite zenith angle. Importantly, the RF-link usage increases to 4×10^{-4} without the use of SH-FSO transmission as an additional backup. Despite its vulnerability to atmospheric turbulence, the SH-FSO contributes to improved system performance.

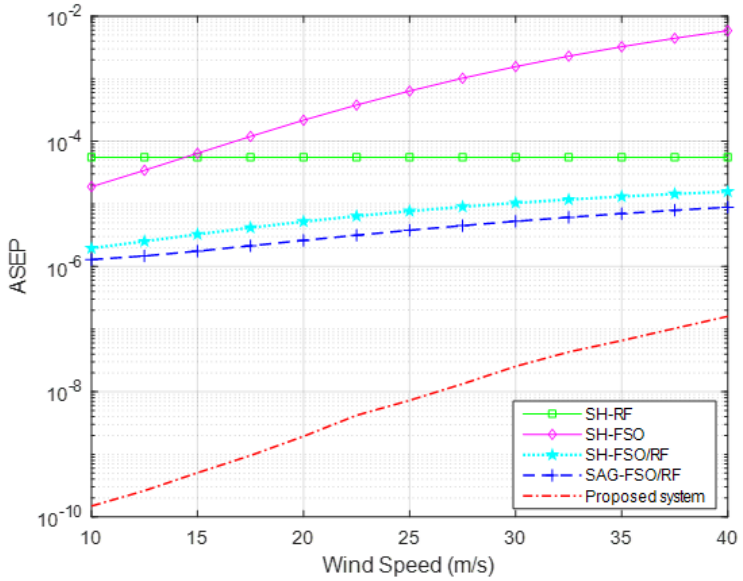

Figure 2.5: ASEP performance for different wind speeds.

Figure 2.5 presents the ASEP of the integrated transmission system given by (2.24) for different wind speeds, binary PSK modulation, a switching threshold of 10.5 dB, a 20 dB average link SNR, a 60° satellite zenith angle, and an uplink scenario. Note that high wind speeds cause vortex formation, which alters the refractive index structure of the air. Such a phenomenon leads to pointing errors and possible fluctuations in the amplitude of the received signal. Therefore, a degraded SatCom performance is expected. From this figure, the wind speed affects the SH-FSO link to a greater extent, and employing the RF link as a backup achieves a significant performance gain. The hybrid FSO/RF transmission benefits from the complementary property of available beamwidth. The SH-FSO beamwidth at the receiver can range from tens of meters to a few kilometers, while the RF beamwidth ranges from tens to hundreds of kilometers, depending on the satellite altitude and zenith angle. Furthermore, we can also see that the proposed SatCom system achieves the best ASEP among all transmission schemes thanks to the small zenith angle of HAP deployment. When the wind speed changes from 10 m/s to 40 m/s, β_{GH} and α_{GH} are changed from $(66.37, 46.31)$ to $(23.13, 19.79)$. Thus, the FSO transmission over

Table 2.2: Optimal switching thresholds for SAG-FSO link.

Average SNR of the Link	*Optimal Thresholds* (dB)	
	Analytical	Numerical
$\bar{\gamma}_{ij} = 20$ dB	9.088	9
$\bar{\gamma}_{ij} = 25$ dB	9.882	10
$\bar{\gamma}_{ij} = 30$ dB	10.515	10.5

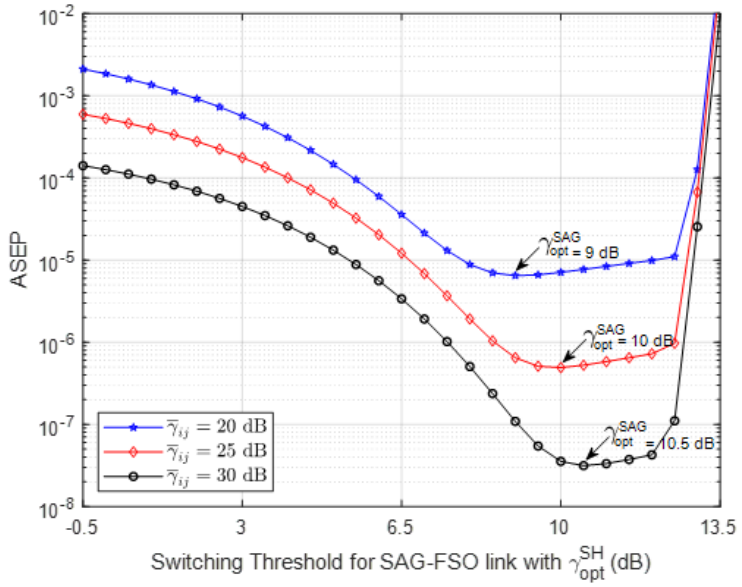

Figure 2.6: ASEP performance as a function of switching threshold values.

the HAP experiences a weak turbulence effect.

Figure 2.6 presents the ASEP of the proposed system with respect to the switching thresholds for different average SNRs. We assume a 65° satellite zenith angle, binary PSK modulation, a ground level turbulence $C_{\rm n}^2(0) = 4.69 \times 10^{-13} \mathrm{m}^{\frac{-2}{3}}$, and an uplink scenario. It is observed that there are optimum switching thresholds, $\gamma_{\rm opt}^{\rm SAG}$ and $\gamma_{\rm opt}^{\rm SH}$, at which the ASEP reaches its minimum value, and the optimal value choice increases with the average SNR. Table 2.2 shows the obtained numerical results of the optimum switching thresholds compared to the analytical values given by (2.51) and (2.54), verifying the accuracy of the analytical expressions.

Figure 2.7 shows the ergodic capacity performance given by (2.33), assuming a satellite zenith angle of 80° and an uplink scenario. We can observe that the

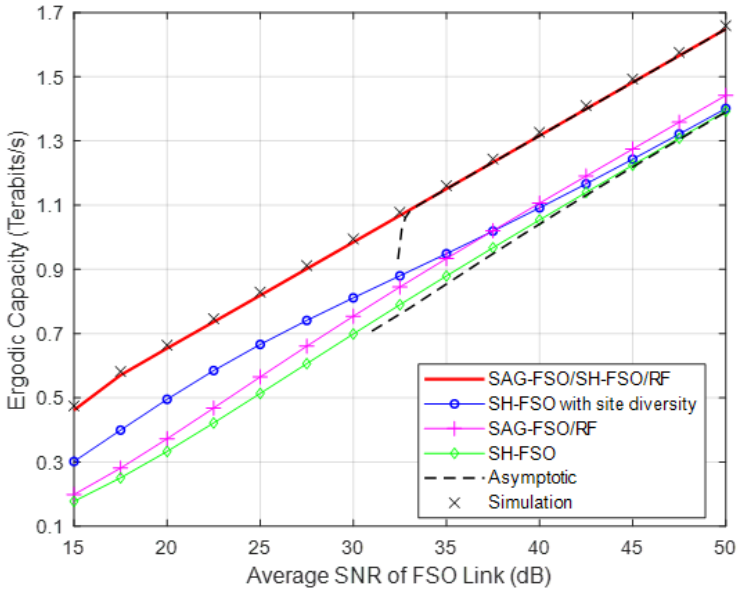

Figure 2.7: Ergodic capacity comparison of Satcom transmission systems.

asymptotic results closely match the exact expressions at high-SNR values. Also, the analytical results match the Monte-Carlo simulations perfectly. Further, the integrated SatCom system achieves the best performance over all SNR values. It can achieve capacity gains of about 190 Gbps, 245 Gbps, and 300 Gbps over SH-FSO with site diversity [65], hybrid SAG-FSO/RF in [31], and SH-FSO in [25], respectively, at an average SNR of 30 dB. This performance advantage originates from the minimization of the atmospheric turbulence effect with the low-zenith angle considered for the ground–HAP transmission. The frequency of switching to the RF link is also reduced to a large extent, which increases the overall system throughput.

In Figure 2.8, we compare the ergodic capacity of the integrated SatCom system with different detection techniques. From this figure, the integrated SatCom system with IM/DD scheme can achieve better capacity performance than that with HD scheme over all satellite zenith angles when the average received SNR increases. For example, we can obtain a capacity gain of about 25 Gbps over the HD technique at an average SNR of 17 dB. This somewhat surprising result can be explained as follows:

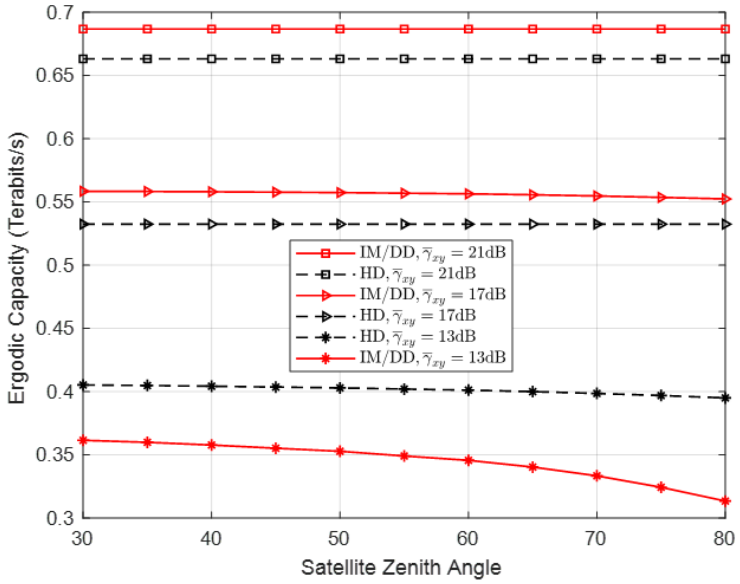

Figure 2.8: Ergodic capacity comparison of IM/DD and HD detection techniques.

HD generally outperforms IM/DD under severe atmospheric turbulence conditions and over low SNRs due to its coherent detection nature. With the proposed SAG-FSO transmission in a low-zenith-angle direction, the adverse effect of atmospheric turbulence will be successfully reduced. Therefore, over a high SNR region, the SAG-FSO with IM/DD can achieve a higher transmission rate than with the HD scheme. For example, the SAG-FSO with IM/DD can maintain a capacity gain of 15 Gbps, at an average SNR of 17 dB. Note that the threshold setting has an impact on this behavior. In particular, when the threshold is set too low, the system will use SAG-FSO over a low SNR scenario, where the system with HD outperforms that with IM/DD. The HD technique can also maintain a lower outage probability compared to the IM/DD technique. Therefore, the frequency of switching to the hybrid SH-FSO/RF is lower compared to the IM/DD case. The SAG-FSO with HD technique has an outage probability of 3.92×10^{-7} that increases to 2.21×10^{-2} in the case of IM/DD, at an average SNR of 17 dB. As such, the SatCom with IM/DD benefits more from the backup SH-FSO/RF links than with the HD detection technique.

Appendix: Asymptotic Analysis of Hybrid SAG-FSO/SH-FSO/RF Transmission System

Under the condition of a very small value of its argument, $Z \to 0^+$, the Meijer G-function can be represented in terms of the summation of basic elementary functions as [52, eq. (9.303)]

$$G_{p,q}^{\,s,t}\left(z \mid \begin{matrix} c_1,\ldots,c_t,\ldots,c_p \\ d_1,\ldots,d_s,\ldots,d_q \end{matrix}\right) = \sum_{g=1}^{s} z^{d_g} \frac{\prod_{j=1;j\neq g}^{s} \Gamma\left(d_j - d_g\right) \prod_{j=1}^{t} \Gamma\left(1 + d_g - c_j\right)}{\prod_{j=s+1}^{q} \Gamma\left(1 + d_g - d_j\right) \prod_{j=t+1}^{p} \Gamma\left(c_j - d_g\right)}, \quad (2.55)$$

where $p \leq q$ and no two d_j (for $j = 1, 2, ..., t$) differ by an integer.

Here, we apply the asymptotic expansion of the Meijer G-function in (2.55) to obtain the asymptotic SEP and outage probability, and ergodic capacity expressions. The asymptotic OP of the integrated transmission system is expressed by

$$P_{\text{out},a}^{\text{SatCom}} = P_{\text{out},a}^{\text{SAG}}\ P_{\text{out},a}^{\text{SH}}\ P_{\text{out},a}^{\text{RF}}\ , \quad (2.56)$$

where

$$P_{\text{out},a}^{\text{SAG}} = 1 - \left(1 - P_{\text{out},a}^{\text{GH}}\right)\left(1 - P_{\text{out},a}^{\text{HS}}\right). \quad (2.57)$$

Using (2.55) and (2.12), the asymptotic OP of the ground–HAP hop is given by

$$P_{\text{out},a}^{\text{GH}} = \sum_{g=1}^{3b} \frac{\mathcal{X}_{\text{GH}}}{\mathcal{B}_{\text{GH}}^{2,g}}\ \mathcal{H}_3\ \left(\frac{\mathcal{E}_{\text{GH}}\ \gamma_{\text{th}}}{\mu_{\text{GH},b}}\right)^{\mathcal{B}_{\text{GH}}^{2,g}}, \quad (2.58)$$

where $\mathcal{H}_3 = \frac{\prod_{z=1;z\neq g}^{3b} \Gamma\left(\mathcal{B}_{\text{GH}}^{2,z} - \mathcal{B}_{\text{GH}}^{2,g}\right)}{\prod_{z=1}^{b} \Gamma\left(\mathcal{B}_{\text{GH}}^{1,z} - \mathcal{B}_{\text{GH}}^{2,g}\right)}$. Similarly, $P_{\text{out},a}^{\text{HS}}$ and $P_{\text{out},a}^{\text{SH}}$ can be obtained, using the corresponding parameters $\mu_{ij,b}$, ξ_{ij}, β_{ij}, and α_{ij}. With the application of (2.55)

and (2.17), the asymptotic OP of the RF link, after some algebraic manipulations, is given by

$$P_{\text{out},a}^{\text{RF}} = \sum_{u=0}^{\infty} \frac{\exp(-K)\ K^{u}\ (K+1)^{u+1}\ (\gamma_{\text{th}})^{u+1}}{(1+u)\ (u!)^{2}}\ (\bar{\gamma}_{r})^{-(u+1)}. \tag{2.59}$$

The asymptotic ASEP of the integrated transmission system is as follows

$$\bar{P}_{e,a}^{\text{SatCom}} = \bar{P}_{e,a}^{\text{SAG}} \ + \ P_{\text{out},a}^{\text{SAG}} \left[\bar{P}_{e,a}^{\text{SH}} \ + \ P_{\text{out},a}^{\text{SH}}\ \bar{P}_{e,a}^{\text{RF}}\right], \tag{2.60}$$

where

$$\bar{P}_{e,a}^{\text{SAG}} = \bar{P}_{e,a}^{\text{GH}} \ + \ \bar{P}_{e,a}^{\text{HS}} \ - \ \bar{P}_{e,a}^{\text{GH}}\ \bar{P}_{e,a}^{\text{HS}}. \tag{2.61}$$

The asymptotic ASEP of the FSO transmission over the ground–HAP hop is given by $\bar{P}_{e,a}^{\text{GH}} = I_{e_1}^{a} - I_{e_2}^{a}$, where

$$I_{e_1}^{a} = \frac{A\ \mathcal{X}_{\text{GH}}}{2\sqrt{\pi}} \sum_{g=1}^{3b} \mathcal{H}_{3}\ \frac{\Gamma\left(\frac{1}{2} + \mathcal{B}_{\text{GH}}^{2,g}\right)}{\mathcal{B}_{\text{GH}}^{2,g}} \left(\frac{\mathcal{E}_{\text{GH}}}{\left(\sin\frac{\pi}{M}\right)^{2} \mu_{\text{GH},b}}\right)^{\mathcal{B}_{\text{GH}}^{2,g}}, \tag{2.62}$$

and

$$I_{e_2}^{a} = A\ \mathcal{X}_{\text{GH}}\ \sum_{g=1}^{3b} \mathcal{H}_{3}\ \left(\frac{\mathcal{E}_{\text{GH}}\ \gamma_{\text{th}}}{\mu_{\text{GH},b}}\right)^{\mathcal{B}_{\text{GH}}^{2,g}}\ \left[\frac{1}{2\ \mathcal{B}_{\text{GH}}^{2,g}} \ - \ \frac{\mathcal{H}_{2}\ \gamma_{\text{th}}^{v+\frac{1}{2}}}{\sqrt{\pi}\ (v\ +\ \frac{1}{2}\ +\ \mathcal{B}_{\text{GH}}^{2,g})}\right], \tag{2.63}$$

respectively. Similarly, $\bar{P}_{e,a}^{\text{HS}}$ and $\bar{P}_{e,a}^{\text{SH}}$ can be obtained, using the corresponding parameters $\mu_{ij,b}$, ξ_{ij}, β_{ij}, and α_{ij}. For the RF link, the asymptotic ASEP is represented by

$$\bar{P}_{e,a}^{\text{RF}} = \sum_{u=0}^{\infty} \frac{A \exp(-K) K^{u} (K+1)^{u+1} \Gamma(\frac{3}{2}+u)}{2\sqrt{\pi}\ \left(\sin\frac{\pi}{M}\right)^{2u+2}\ (1+u)\ (u!)^{2}}\ (\bar{\gamma}_{r})^{-(u+1)}. \tag{2.64}$$

The asymptotic ergodic capacity can be expressed by

$$\bar{C}_a^{\text{SatCom}} = \min\left\{\bar{C}_a^{\text{GH}}, \bar{C}_a^{\text{HS}}\right\} + \left[1 - \left(1 - P_{a\text{out}}^{\text{GH}}\right)\left(1 - P_{\text{out},a}^{\text{HS}}\right)\right]\left[\bar{C}_a^{\text{SH}} + P_{\text{out},a}^{\text{SH}}\bar{C}_a^{\text{RF}}\right]. \quad (2.65)$$

The asymptotic ergodic capacity of the ground–HAP link can be written as $\bar{C}_a^{\text{GH}} = I_{c_1}^a - I_{c21}^a - I_{c22}^a$, where

$$I_{c_1}^a = \frac{\text{BW}_f\, \mathcal{X}_{\text{GH}}}{\ln(2)} \sum_{g=1}^{3b+2} \mathcal{H}_4\, \frac{\Gamma\left(1 + \mathcal{B}_{\text{GH}}^{3,g}\right)}{\Gamma\left(1 - \mathcal{B}_{\text{GH}}^{3,g}\right)} \left(\frac{\mathcal{E}_{\text{GH}}}{\epsilon\, \mu_{\text{GH},b}}\right)^{\mathcal{B}_{\text{GH}}^{3,g}}, \quad (2.66)$$

$$I_{c21}^a = \text{BW}_f\, \log_2(1 + \epsilon\, a)\, P_{\text{out},a}^{\text{GH}}, \quad (2.67)$$

and

$$I_{c22}^a = \frac{\text{BW}_f\, \mathcal{X}_{\text{GH}}}{\ln(2)} \sum_{g=1}^{3b} \mathcal{H}_3 \left(\frac{\mathcal{E}_{\text{GH}}\, \gamma_{\text{th}}}{\mu_{\text{GH},b}}\right)^{\mathcal{B}_{\text{GH}}^{2,g}} \sum_{m=1}^{\infty} \frac{(-1)^{m+1}\, \epsilon^m}{m(1 + \epsilon\, a)^m} \sum_{n=0}^{m} \binom{m}{n} (-a)^{m-n}\, \frac{\gamma_{\text{th}}^n}{n + \mathcal{B}_{\text{GH}}^{2,g}}. \quad (2.68)$$

Here, we define $\mathcal{H}_4 = \frac{\prod_{z=1;z\neq g}^{3b+2} \Gamma\left(\mathcal{B}_{\text{GH}}^{3,z} - \mathcal{B}_{\text{GH}}^{3,g}\right)}{\prod_{z=1}^{b} \Gamma\left(\mathcal{B}_{\text{GH}}^{1,z} - \mathcal{B}_{\text{GH}}^{3,g}\right)}$ and $\mathcal{B}_{\text{GH}}^{3,g} = \{\mathcal{B}_{\text{GH}}^{2,g}, 0, 0\}$. Similarly, $\bar{C}_a^{\text{HS}}$ and $\bar{C}_a^{\text{GS}}$ can be obtained, using the corresponding parameters α_{ij}, β_{ij}, ξ_{ij}, and $\mu_{ij,b}$. The asymptotic ergodic capacity of the RF link can be written as

$$\bar{C}_a^{\text{RF}} = \frac{BW_{\text{RF}}}{\ln(2)}\, \exp(-K) \sum_{u=0}^{\infty} \frac{(K)^u}{(u!)^2} \sum_{g=1}^{3} \mathcal{H}_5\, \frac{\Gamma\left(1 + \mathcal{B}_{\text{RF}}^{4,g}\right)}{\Gamma\left(1 - \mathcal{B}_{\text{RF}}^{4,g}\right)} \left(\frac{K+1}{\bar{\gamma}_r}\right)^{\mathcal{B}_{\text{RF}}^{4,g}}, \quad (2.69)$$

where $\mathcal{H}_5 = \prod_{z=1;z\neq g}^{3} \Gamma\left(\mathcal{B}_{\text{RF}}^{4,z} - \mathcal{B}_{\text{RF}}^{4,g}\right)$ and $\mathcal{B}_{\text{RF}}^{4,g} = \{1 + u, 0, 0\}$.

Chapter 3

Reliable Terabits Feeder Link for Satellite Communications with SAG-FSO transmission through Multiple HAP Relays

Clouds represent a considerable barrier to optical communications. In addition, FSO transmissions are susceptible to the adverse impacts of atmospheric turbulence. In the following, we present two candidate solutions for Terabits satellite feeder links based on SAG-FSO networks [66]. In particular, we propose to combine SAG-FSO transmission with site diversity to mitigate weather effects and increase the reliability of SAG-FSO networks. A HAP-based FSO relay hovering directly above a ground station can successfully mitigate atmospheric turbulence impacts, while site diversity is an effective solution for addressing weather effects. To achieve a similar diversity benefit with reduced cost and lower complexity, we also propose switching-based HAP relays with a hybrid SAG-FSO/RF transmission. The proposed solution switches between HAPs depending on the ground–HAP channel quality.

3.1 Related Work

Cloudy weather conditions represent a primary obstacle to reliable FSO transmissions. Site diversity demonstrates as one of the most effective solutions to mitigate cloud effects. It can sustain feeder link availability with the use of geographically dispersed ground sites such that at least one site is visible to the satellite at any given time. Remotely distributed ground stations have a higher probability of experiencing uncorrelated weather conditions. In [67], the SH-FSO transmission was combined with site diversity to provide reliable connectivity. In particular, the downlink SH-FSO transmission with the highest received SNR was selected among multiple ground stations. The numerical results in [67] showed that SH-FSO transmission with site diversity achieved a considerable performance gain when the zenith angle of satellites was relatively small. Nonetheless, it had a limited performance gain when the satellite zenith angle became larger as FSO transmissions were exposed to higher atmospheric-turbulence fading effects. Site diversity cannot efficiently mitigate beam wandering and atmospheric turbulence as their effects become more severe as the propagation distance of the FSO link increases in high-turbulence environments.

3.2 SAG-FSO Transmission with Site Diversity

Taking advantage of the SAG-FSO design's excellent performance in [41], we can combine site diversity with SAG-FSO transmission to increase the FSO feeder link's reliability, as illustrated in Figure 3.1. In the suggested setup, we adopt a hard-switching scheme due to its low complexity and practical relevance. The sites are connected through fiber-optic lines and can share information with each other. By dynamically switching between the two SAG-FSO transmissions at the main and backup sites, the integrated SAG-FSO networks can successfully alleviate both at-

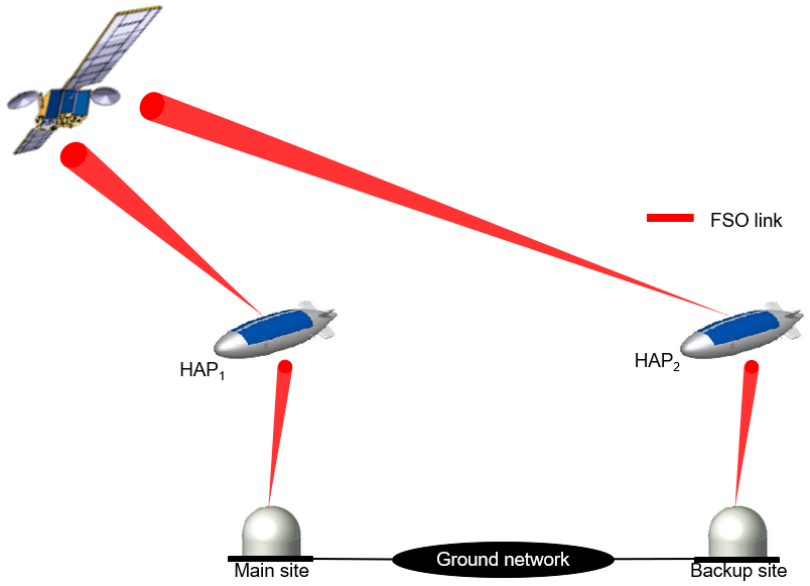

Figure 3.1: SAG-FSO transmission with site diversity for reliable SatCom feeder link.

mospheric turbulence and weather effects. From a practical perspective, the proposed SatCom system enjoys several additional advantages, as its performance is insensitive to variations in the zenith angle of satellites. It can work well for GEO satellites with fixed zenith angles as well as LEO satellites with varying zenith angles. Besides, it enjoys more independent weather effects when compared to SH-FSO transmission with site diversity proposed in [67], especially at high satellite zenith angles. With the design in [67], the probability of uncorrelated weather conditions between remotely separated ground sites decreases as the zenith angle of satellites increases.

In Figure 3.2, we plot the ergodic capacity of the SAG-FSO transmission with site diversity as a function of the target BER for binary PSK modulation with a satellite zenith angle of 60^{o} and a 15 dB average link SNR [66]. We can see from this figure that the proposed satellite feeder link solution outperforms other transmission schemes over all target BER values. Specifically, at a BER of 10^{-9}, we can obtain a capacity of 0.335 Terabits/s, leading to a spectral efficiency of 3.35 bps/Hz. On

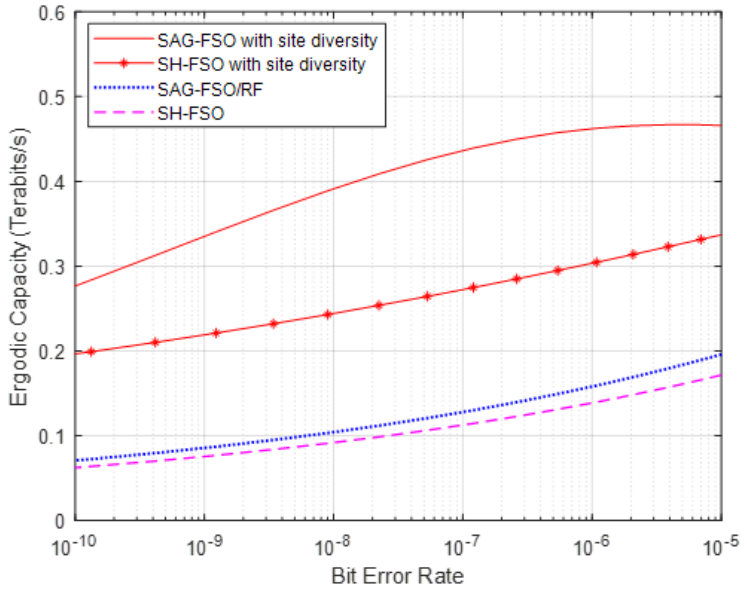

Figure 3.2: Ergodic capacity performance with varying targeted BER values.

the other hand, the SH-FSO with site diversity [67] and hybrid SAG-FSO/RF [31] transmission schemes only achieve a capacity of 218 Gbps and 85 Gbps, respectively. The obtained performance gain of the proposed feeder link solution is mainly due to deploying HAP relays for FSO transmissions, which significantly mitigates the adverse effects of atmospheric turbulence and attenuation. Furthermore, the two-step optical amplification helps reduce the required transmit power for SAG-FSO transmission compared to that for SH-FSO transmission [37].

Meanwhile, site diversity typically entails high costs due to the required terrestrial infrastructure. The primary criterion for choosing suitable sites is the prerequisite of a clear sky as much as possible during the year. To get such clear-sky conditions, a ground station may need to be placed on a mountaintop. For example, NASA's laser communications relay demonstration (LCRD) mission deploys ground stations on Table Mountain in Southern California and on Haleakalā Volcano in Hawaii [65]. Such ground stations, on the other hand, require additional terrestrial infrastructure investment because they are located far from the commer-

cial markets they are supposed to serve. The cost and complexity of the required terrestrial infrastructure will increase exponentially as the number of backup sites increases [68].

3.3 Hybrid SAG-FSO/RF Transmission with Multiple HAP Relays

In order to achieve a similar benefit of site diversity at a reduced cost, a SatCom system with multiple HAP relays could be a promising solution. The use of multiple HAPs was recently proposed to improve SatCom performance in the downlink [69]. With this design in [69], the satellite selects the HAP node that provides the best channel quality depending on the feedback channel state information from each HAP node. In the second hop, the selected HAP decodes and forwards the received optical signal to the ground station using hybrid FSO/RF transmission. The authors adopted the same data transmission scheme over both RF and FSO links. At the ground station, the highest received SNR is selected. According to [69], selecting a HAP depending on the SAT–HAP channel quality was shown to improve the SatCom system performance. However, transmitting the same data simultaneously over both RF and FSO links limits the overall SatCom system's throughput and wastes the transmit power over the RF link when the FSO link experiences weak turbulence effects.

In contrast to the current literature, we propose a reliable SatCom strategy for FSO feeder links using a single ground station and multiple HAP relays. More precisely, our proposed design switches between HAP relays depending on the ground–HAP channel quality, as there are more atmospheric turbulence and weather effects. We also propose a hybrid SAG-FSO/RF transmission system to further increase the SatCom system reliability and make use of the conventional RF transmission to the

satellite. For the system mode of operation, we adopt a hard-switching scheme to benefit from the FSO link's higher transmission rate while simplifying the design of the receiver. Moreover, we recommend HAPs with purely FSO communication payloads to minimize their power consumption and hardware complexity as they are resource-limited systems.

Meanwhile, the ground-HAP links corresponding to different HAP relays may experience correlated atmospheric turbulence. It is of great practical interest to analyze the performance of the proposed transmission system over correlated FSO links. The effect of correlation between FSO branches was analyzed over G-G fading for several scenarios. In [50, 70, 71], the outage probability and error rate performance were analyzed for single-input-multiple-output (SIMO) FSO systems, assuming selection combining and maximal ratio combining receivers. In [49, 72], the error rate performance was investigated for a multiple-input-single-output (MISO) FSO system with simultaneous FSO transmissions and a single aperture-based receiver. To the best of my knowledge, no previous work has yet analyzed the effect of correlated turbulence on the performance of switching-based FSO transmissions. This motivates my work to analyze the performance of the hybrid SAG-FSO/RF transmission system over correlated atmospheric turbulence channels.

3.4 System and Channel Models

We consider a SatCom system, as shown in Figure 3.3, where a ground station communicates with a satellite with the help of two HAPs acting as FSO relays. In particular, the ground station can establish the communication link with the satellite over dual-hop FSO links through HAP relays or directly over an RF link. To simplify the receiver design at the satellite, only one link will be active at a time. The ground station switches to the most favorable channel based on a feedback signal from the satellite. A feedback signal of 2 bits is required to transmit using

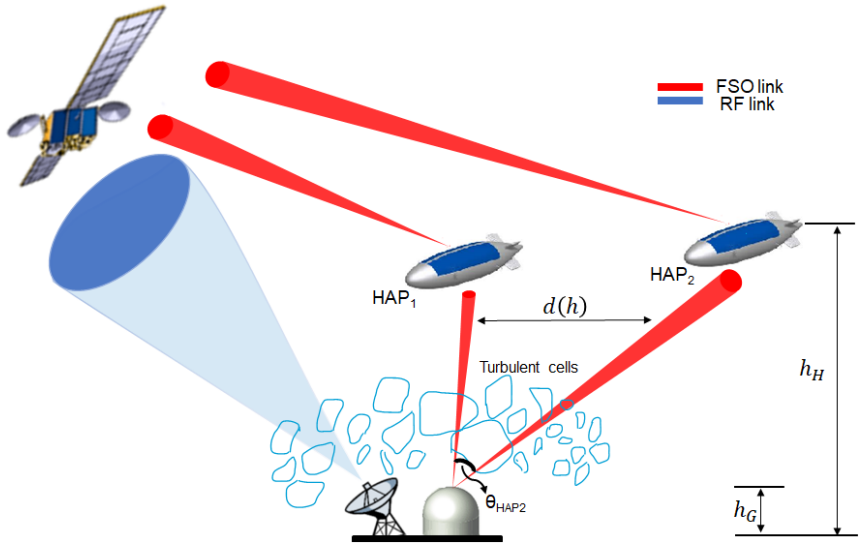

Figure 3.3: Proposed switching-based HAP relays with a hybrid SAG-FSO/RF transmission.

the best link. The proposed system with HAP-based FSO relays can mitigate the blocking effects of flying drones, birds, and clouds. The system can also alleviate weather and turbulence effects by adaptively switching between two FSO links, achieving similar diversity benefits of geographically dispersed ground stations with much lower complexity and cost [68].

We adopt a single-threshold hard-switching scheme due to its low complexity. Without losing generality, we assume HAP_1 has a smaller zenith angle than HAP_2, i.e., HAP_1 hovers directly above the ground station. We prefer the FSO transmission through HAP_1 [73], and use it whenever the link quality is acceptable. To eliminate the noise in the forward signal, we used a decode-and-forward relaying scheme at HAPs. The effective instantaneous SNR of the FSO transmission through HAP_1 is $\gamma_{\text{SAG}_1} = \min(\gamma_{\text{GH}_1}, \gamma_{\text{H}_1\text{S}})$, where γ_{GH_1} and $\gamma_{\text{H}_1\text{S}}$ denote the instantaneous receive SNR of the ground-HAP_1 (GH_1) and HAP_1-SAT (H_1S) hop, respectively [74, eq. (26)]. When the FSO transmission over HAP_1 experiences unfavorable channel conditions, i.e., γ_{SAG_1} is smaller than a threshold γ_{th}, the system switches to FSO transmission

through HAP_2. Note that γ_{th} is selected to satisfy a predefined QoS, typically in terms of SEP [31,36,39]. Since HAP_2 is at a longer distance from the ground station, the FSO transmission over HAP_2 will require more transmit power than HAP_1 to maintain the target SEP. Aerosol particles in the atmosphere scatter and/or absorb optical signals [23]. Note also that the FSO link through HAP_2 can sustain higher data rates than the RF link despite experiencing more atmospheric turbulence [41]. The transmission system will restore the single-hop RF link only if both SAG-FSO links are unacceptable. According to the above operation mode, the overall effective SNR of the system is given by

$$\gamma_{\text{o}} = \begin{cases} \gamma_{\text{SAG}_1}, & \gamma_{\text{SAG}_1} \geq \gamma_{\text{th}}; \\ \gamma_{\text{SAG}_2}, & \gamma_{\text{SAG}_1} < \gamma_{\text{th}}, \gamma_{\text{SAG}_2} \geq \gamma_{\text{th}}; \\ \gamma_r, & \gamma_{\text{SAG}_1} < \gamma_{\text{th}}, \gamma_{\text{SAG}_2} < \gamma_{\text{th}}, \end{cases} \tag{3.1}$$

where γ_r is the instantaneous receive SNR of the RF link. We adopt uncoded signal with MPSK modulation for data transmission over FSO and RF links. SEP may still be a relevant performance metric that ensures the demodulated data bits can be retrieved at the receiver satisfactorily. It measures the reliability of the transmission link. It also applies to both coded and uncoded systems. The conditional SEP of MPSK given the instantaneous SNR of the link, γ, can be written as [57, eq. (8.25)]

$$P(e|\gamma) = \frac{A}{2} \operatorname{erfc}\left(\sqrt{\gamma}\ \sin\frac{\pi}{M}\right), \tag{3.2}$$

where $A = 1$ for binary PSK modulation (i.e., $M = 2$), $A = 2$ for higher order modulations (i.e., $M > 2$), and erfc $(\cdot)$ denotes the complementary error function.

3.4.1 FSO Channel Model

In this work, we assume the FSO transmissions experience G-G fading [44]. The pdf of the instantaneous receive SNR can be generally represented by [75, eq. (2)]

$$f_{\gamma_l}(\gamma) = \frac{\gamma^{-1}}{b\Gamma(\alpha_l)\Gamma(\beta_l)} G_{0,2}^{2,0}\left(\alpha_l\beta_l\left(\frac{\gamma}{\mu_l}\right)^{\frac{1}{b}}\middle|\begin{matrix} - \\ \alpha_l, \beta_l \end{matrix}\right), \tag{3.3}$$

where $l \in \{\mathrm{GH_1}, \mathrm{H_1S}, \mathrm{GH_2}, \mathrm{H_2S}\}$, b defines the detection type at the optical receiver (i.e., $b = 1$ for HD and $b = 2$ for IM/DD), μ_l is the average electrical SNR [76], $\Gamma(\cdot)$ is the Gamma function [52, eq. (8.310)], and α_l and β_l are large-scale and small-scale fading parameters related to the atmospheric conditions. For the ground-$\mathrm{HAP_1}$ hop, $\alpha_{\mathrm{GH_1}}$ and $\beta_{\mathrm{GH_1}}$ can be calculated as [31, eq. (49, 50)]

$$\alpha_{\mathrm{GH_1}} = \Bigg[5.95(h_{\mathrm{H_1}} - h_{\mathrm{G}})^2 \sec^2(\theta_{\mathrm{GH_1}}) \left(\frac{2W_{\mathrm{o}}}{r_{\mathrm{GH_1}}}\right)^{\frac{5}{3}} \left(\frac{\Delta_{\mathrm{GH_1}}}{W_{\mathrm{GH_1}}}\right)^2 + \exp\left(\frac{0.49\ \sigma_{\mathrm{GH_1}}^2}{\left(1 + 0.56\ \sigma_{\mathrm{GH_1}}^{\frac{12}{5}}\right)^{\frac{7}{6}}}\right) - 1\Bigg]^{-1}, \tag{3.4}$$

$$\beta_{\mathrm{GH_1}} = \left[\exp\left(\frac{0.51\ \sigma_{\mathrm{GH_1}}^2}{\left(1 + 0.69\ \sigma_{\mathrm{GH_1}}^{\frac{12}{5}}\right)^{\frac{5}{6}}}\right) - 1\right]^{-1}, \tag{3.5}$$

where $h_{\mathrm{H_1}}$, h_{G}, $\theta_{\mathrm{GH_1}}$, $\Delta_{\mathrm{GH_1}}$, $r_{\mathrm{GH_1}}$, W_{o}, $W_{\mathrm{GH_1}}$, and $\sigma_{\mathrm{GH_1}}^2$ denote the $\mathrm{HAP_1}$ altitude, the aperture height of the ground station, the zenith angle of the $\mathrm{HAP_1}$, the beam-wandering-induced pointing error, the Fried parameter, the optical beam radius at the ground station, the optical beam radius at the $\mathrm{HAP_1}$, and Rytov variance, respectively [16]. The strength of atmospheric turbulence is often measured by $\sigma_{\mathrm{GH_1}}^2$,

which is calculated for the slant path of the ground-HAP$_1$ hop as [16, eq. (6)]

$$\sigma^2_{\mathrm{GH_1}} = 2.25\, k^{\frac{7}{6}} (h_{\mathrm{H_1}} - h_{\mathrm{G}})^{\frac{5}{6}} \sec^{\frac{11}{6}}(\theta_{\mathrm{GH_1}}) \int_{h_{\mathrm{G}}}^{h_{\mathrm{H_1}}} C_n^2(h) \left(1 - \frac{h - h_{\mathrm{G}}}{h_{\mathrm{H_1}} - h_{\mathrm{G}}}\right)^{\frac{5}{6}} \left(\frac{h - h_{\mathrm{G}}}{h_{\mathrm{H_1}} - h_{\mathrm{G}}}\right)^{\frac{5}{6}} dh, \quad (3.6)$$

where $k = 2\pi/\lambda$ and $C_n^2(h)$ denotes the refractive index structure [33]. Similarly, α_l and β_l for other hops can be evaluated.

Atmospheric turbulence is induced by aerosols experiencing solar heating and wind. Turbulent inhomogeneity along the propagation distance leads to the formation of turbulent eddies of different sizes. They range from tens of centimeters to meters in size [77]. Note also that aerosol particles such as haze, smoke, dust, and smog are mainly concentrated near the earth's surface [38]. Hence, the ground-HAP links experience more atmospheric turbulence and are likely to experience a spatial correlation of atmospheric turbulence. We adopt a scenario where correlation exists only between large-scale turbulent eddies [50]. In practice, this is the real scenario that is verified in [78] and validated by an acceptable simulation model in [79]. We assume a correlated Gamma-Gamma fading environment for ground station to HAP hops with identical fading parameters, i.e., $\alpha_{\mathrm{GH_1}} = \alpha_{\mathrm{GH_2}} = \alpha_{\mathrm{GH}}$ and $\beta_{\mathrm{GH_1}} = \beta_{\mathrm{GH_2}} = \beta_{\mathrm{GH}}$. The joint pdf of the received SNR at HAP$_1$ and HAP$_2$ is given by [50, eq. (7)]

$$f_{\gamma_{\mathrm{GH_1}},\gamma_{\mathrm{GH_2}}}(\gamma_{\mathrm{GH_1}}, \gamma_{\mathrm{GH_2}}) = \frac{\left(1-\sqrt{\rho}\right)^{\alpha_{\mathrm{GH}}}}{\Gamma\left(\alpha_{\mathrm{GH}}\right)\Gamma(\beta_{\mathrm{GH}})^2} \sum_{k_{\mathrm{GH_1}}=0}^{\infty} \sum_{k_{\mathrm{GH_2}}=0}^{\infty} \frac{\Gamma\left(\alpha_{\mathrm{GH}} + k_{\mathrm{GH_1}} + k_{\mathrm{GH_2}}\right) \rho^{\frac{k_{\mathrm{GH_1}}+k_{\mathrm{GH_2}}}{2}}}{\left(1+\sqrt{\rho}\right)^{\alpha_{\mathrm{GH}}+k_{\mathrm{GH_1}}+k_{\mathrm{GH_2}}}}$$
$$\Xi^{\frac{2\alpha_{\mathrm{GH}}+k_{\mathrm{GH_1}}+k_{\mathrm{GH_2}}+2\beta_{\mathrm{GH}}}{2}} \prod_{i\in\{\mathrm{GH_1},\mathrm{GH_2}\}} \frac{1}{b\,\Gamma\left(\alpha_{\mathrm{GH}}+k_i\right) k_i!} \left(\gamma_i\right)^{\frac{\alpha_{\mathrm{GH}}+k_i+\beta_{\mathrm{GH}}}{2b}-1} \left(\frac{1}{\mu_i}\right)^{\frac{\alpha_{\mathrm{GH}}+k_i+\beta_{\mathrm{GH}}}{2b}}$$
$$G_{0,2}^{2,0}\left(\Xi\left(\frac{\gamma_i}{\mu_i}\right)^{\frac{1}{b}} \middle| \begin{matrix} - \\ \left(\frac{\alpha_{\mathrm{GH}}+k_i-\beta_{\mathrm{GH}}}{2}\right), -\left(\frac{\alpha_{\mathrm{GH}}+k_i-\beta_{\mathrm{GH}}}{2}\right) \end{matrix}\right), \quad (3.7)$$

where $\Xi = \alpha_{\text{GH}}\beta_{\text{GH}}/(1-\sqrt{\rho})$. $\rho \in [0,1)$ represents the correlation coefficient. On the other hand, the HAP-SAT links encounter extremely weak turbulence. The fading parameters $\alpha_{\text{H}_1\text{S}}$, $\alpha_{\text{H}_2\text{S}}$, $\beta_{\text{H}_1\text{S}}$, and $\beta_{\text{H}_2\text{S}}$ are very large [33]. We assume that with sufficient transmit power level, the HAP-SAT hops for both HAPs enjoy high reliability, with SNR always greater than γ_{th}, i.e., $\gamma_{\text{H}_1\text{S}}$ and $\gamma_{\text{H}_2\text{S}} \geq \gamma_{\text{th}}$.

3.4.2 RF Channel Model

RF transmissions between ground station and satellite experience a strong line-of-sight communication link and weak scattered paths. Therefore, the Rician fading model is adopted to model the RF link over the SatCom environment. The pdf of the instantaneous receive SNR can be expressed by [57, eq. (2.16)]

$$f_{\gamma_{\text{RF}}}(\gamma) = \frac{K+1}{\bar{\gamma}_r} \exp\left(-(K+1)\frac{\gamma}{\bar{\gamma}_r} - K\right) I_0\left(2\sqrt{K(K+1)\frac{\gamma}{\bar{\gamma}_r}}\right), \tag{3.8}$$

where $I_0(\cdot)$ denotes the 0_{th} modified Bessel function of the first kind, K represents the ratio of the power contribution from line-of-sight path to the remaining multi-paths, and $\bar{\gamma}_r$ is the average SNR as given by [80, eq. (18)].

3.5 ASEP Performance Analysis

The average SEP of the hybrid SAG-FSO/RF transmission system can be written as [36, eq. (25)]

$$\bar{P}_e = \bar{P}_e^{\text{SAG}_1} + P_{\text{out}}^{\text{SAG}_1} \bar{P}_e^{\text{SAG}_2} + P_{\text{out}}^{\text{SAG}_{1,2}} \bar{P}_e^{\text{RF}}, \tag{3.9}$$

where $\bar{P}_e^{\text{SAG}_1}$ represents the average SEP of the FSO link through HAP_1 when $\gamma_{\text{SAG}_1} \geq \gamma_{\text{th}}$, and $P_{\text{out}}^{\text{SAG}_1}$ denotes its outage probability. The average SEP of the FSO link through HAP_2 when $\gamma_{\text{SAG}_1} < \gamma_{\text{th}}$ and $\gamma_{\text{SAG}_2} \geq \gamma_{\text{th}}$ is given by $\bar{P}_e^{\text{SAG}_2}$, $P_{\text{out}}^{\text{SAG}_{1,2}}$

defines the probability that both FSO links are in an outage, and $\bar{P}_e^{\mathrm{RF}}$ is the average SEP of the RF link.

With the decode-and-forward relaying scheme at HAP_1, the average SEP of the FSO link is given by [60, eq. (22)]

$$\bar{P}_e^{\mathrm{SAG}_1} = \bar{P}_e^{\mathrm{GH}_1} + \bar{P}_e^{\mathrm{H}_1\mathrm{S}} - \bar{P}_e^{\mathrm{GH}_1}\ \bar{P}_e^{\mathrm{H}_1\mathrm{S}}, \tag{3.10}$$

where $\bar{P}_e^{\mathrm{GH}_1}$ and $\bar{P}_e^{\mathrm{H}_1\mathrm{S}}$ denote the average SEP of the ground–HAP_1 and HAP_1–SAT hops, respectively. The analytical expression of $\bar{P}_e^{\mathrm{GH}_1}$ when γ_{GH_1} is greater than γ_{th} can be obtained as [37, eq. (9)]

$$\begin{aligned}\bar{P}_e^{\mathrm{GH}_1} &= \int_{\gamma_{\mathrm{th}}}^{\infty} P(e|\gamma)\ f_{\gamma_{\mathrm{GH}_1}}(\gamma)\ d\gamma \\ &= \underbrace{\int_0^{\infty} P(e|\gamma)\ f_{\gamma_{\mathrm{GH}_1}}(\gamma)\ d\gamma}_{I_{e_1}} - \underbrace{\int_0^{\gamma_{\mathrm{th}}} P(e|\gamma)\ f_{\gamma_{\mathrm{GH}_1}}(\gamma)\ d\gamma}_{I_{e_2}}\ .\end{aligned} \tag{3.11}$$

The expression of I_{e_1} can be analytically expressed using (2.22), (3.3), and [55, eq. (07.34.21.0013.01)] as

$$I_{e_1} = \frac{A\ b^{\alpha_{\mathrm{GH}}+\beta_{\mathrm{GH}}-1}}{(2\pi)^{b-1}\ 2\sqrt{\pi}\ \Gamma(\alpha_{\mathrm{GH}})\ \Gamma(\beta_{\mathrm{GH}})}\ G_{2,2b+1}^{2b,2}\left(\frac{(\alpha_{\mathrm{GH}}\beta_{\mathrm{GH}})^b}{b^{2b}\left(\sin\frac{\pi}{M}\right)^2\mu_{\mathrm{GH}_1}}\middle|\begin{matrix}1,\frac{1}{2}\\ \mathcal{B}^1_{\mathrm{GH}},0\end{matrix}\right). \tag{3.12}$$

With the application of (2.23), (3.3), and [55, eq. (07.34.21.0084.01)], I_{e_2} is given by

$$\begin{aligned}I_{e_2} = {}& \frac{A}{2\Gamma(\alpha_{\mathrm{GH}})\Gamma(\beta_{\mathrm{GH}})}G_{1,3}^{2,1}\left(\alpha_{\mathrm{GH}}\beta_{\mathrm{GH}}\left(\frac{\gamma_{\mathrm{th}}}{\mu_{\mathrm{GH}_1}}\right)^{\frac{1}{b}}\middle|\begin{matrix}1\\ \alpha_{\mathrm{GH}},\beta_{\mathrm{GH}},0\end{matrix}\right) - \frac{A\ b^{\alpha_{\mathrm{GH}}+\beta_{\mathrm{GH}}-1}}{(2\pi)^{b-1}\sqrt{\pi}} \\ & \sum_{j=0}^{\infty}\frac{(-1)^j\gamma_{\mathrm{th}}^{j+\frac{1}{2}}\left(\sin\frac{\pi}{M}\right)^{2j+1}}{j!\ (2j+1)\ \Gamma(\alpha_{\mathrm{GH}})\Gamma(\beta_{\mathrm{GH}})}G_{1,2b+1}^{2b,1}\left(\left(\frac{\alpha_{\mathrm{GH}}\beta_{\mathrm{GH}}}{b^2}\right)^b\ \frac{\gamma_{\mathrm{th}}}{\mu_{\mathrm{GH}_1}}\middle|\begin{matrix}1-j-\frac{1}{2}\\ \mathcal{B}^1_{\mathrm{GH}},-j-\frac{1}{2}\end{matrix}\right),\end{aligned} \tag{3.13}$$

where $\mathcal{B}^1_{\text{GH}} = \{\frac{\alpha_{\text{GH}}}{b}, \ldots, \frac{\alpha_{\text{GH}}+b-1}{b}, \frac{\beta_{\text{GH}}}{b}, \ldots, \frac{\beta_{\text{GH}}+b-1}{b}\}$ consists of $2b$ terms. The ASEP of the FSO transmission over HAP$_1$-SAT hop with $\gamma_{\text{H}_1\text{S}}$ always greater than γ_{th}, $\bar{P}_e^{\text{H}_1\text{S}}$, can be analytically expressed by

$$\bar{P}_e^{\text{H}_1\text{S}} = \int_0^\infty P(e|\gamma)\ f_{\gamma_{\text{H}_1\text{S}}}(\gamma)\ d\gamma. \tag{3.14}$$

Hence, $\bar{P}_e^{\text{H}_1\text{S}}$ can be expressed similar to (3.12) using the corresponding parameters $\mu_{\text{H}_1\text{S}}$, $\alpha_{\text{H}_1\text{S}}$, and $\beta_{\text{H}_1\text{S}}$.

Since we assume $\gamma_{\text{H}_1\text{S}} \geq \gamma_{\text{th}}$, if γ_{GH_1} falls below γ_{th}, the SAG$_1$-FSO link cannot satisfy the target SEP and the system switches to the backup SAG$_2$-FSO or RF links. $P_{\text{out}}^{\text{SAG}_1}$ can be evaluated by [75, eq. (2)]

$$P_{\text{out}}^{\text{SAG}_1} = \frac{1}{b\ \Gamma(\alpha_{\text{GH}})\ \Gamma(\beta_{\text{GH}})}\ G_{1,3}^{2,1}\left(\alpha_{\text{GH}}\beta_{\text{GH}}\left(\frac{\gamma_{\text{th}}}{\mu_{\text{GH}_1}}\right)^{\frac{1}{b}}\middle|\begin{matrix}1\\ \alpha_{\text{GH}}, \beta_{\text{GH}}, 0\end{matrix}\right). \tag{3.15}$$

The average SEP of the FSO link through HAP$_2$, $\bar{P}_e^{\text{SAG}_2}$, can be similarly calculated as (3.10), whereas $\bar{P}_e^{\text{H}_2\text{S}}$ is given by

$$\bar{P}_e^{\text{H}_2\text{S}} = \int_{\gamma_{\text{th}}}^\infty P(e|\gamma)\ f_{\gamma_{\text{H}_2\text{S}}}(\gamma \mid \gamma_{\text{SAG}_1} < \gamma_{\text{th}})\ d\gamma. \tag{3.16}$$

Because correlated turbulence only affects ground–HAP FSO transmissions, the HAP–SAT FSO transmissions can be considered to experience independent turbulence effects [69]. As a result, (3.16) can be simplified to

$$\bar{P}_e^{\text{H}_2\text{S}} = \int_{\gamma_{\text{th}}}^\infty P(e|\gamma)\ f_{\gamma_{\text{H}_2\text{S}}}(\gamma)\ d\gamma, \tag{3.17}$$

which is analytically expressed using (3.12) with the corresponding parameters $\alpha_{\text{H}_2\text{S}}$,

$\beta_{\mathrm{H_2S}}$, and $\mu_{\mathrm{H_2S}}$. The average SEP of the ground–HAP$_2$ hop is given by

$$\bar{P}_e^{\mathrm{GH_2}} = \int_{\gamma_{\mathrm{th}}}^{\infty} P(e|\gamma)\; f_{\gamma_{\mathrm{GH_2}}}(\gamma \mid \gamma_{\mathrm{SAG_1}} < \gamma_{\mathrm{th}})\; d\gamma. \tag{3.18}$$

Since $\gamma_{\mathrm{H_1S}} \geq \gamma_{\mathrm{th}}$, (3.18) can be equivalently calculated as

$$\bar{P}_e^{\mathrm{GH_2}} = \int_{\gamma_{\mathrm{th}}}^{\infty} P(e|\gamma)\; f_{\gamma_{\mathrm{GH_2}}}(\gamma \mid \gamma_{\mathrm{GH_1}} < \gamma_{\mathrm{th}})\; d\gamma, \tag{3.19}$$

where

$$f_{\gamma_{\mathrm{GH_2}}}(\gamma \mid \gamma_{\mathrm{GH_1}} < \gamma_{\mathrm{th}}) = \int_0^{\gamma_{\mathrm{th}}} f_{\gamma_{\mathrm{GH_1}},\gamma_{\mathrm{GH_2}}}(\gamma_{\mathrm{GH_1}}, \gamma_{\mathrm{GH_2}})\; d\gamma_{\mathrm{GH_1}}. \tag{3.20}$$

With the application of (3.7), [58, eq. (26)], and [52, eq. (9.31.5)], the expression of $f_{\gamma_{\mathrm{GH_2}}}(\gamma|\gamma_{\mathrm{GH_1}} < \gamma_{\mathrm{th}})$ is given by

$$f_{\gamma_{\mathrm{GH_2}}}(\gamma \mid \gamma_{\mathrm{GH_1}} < \gamma_{\mathrm{th}}) = \frac{\mathcal{Y}\; \Xi^{\frac{\alpha_{\mathrm{GH}}+k_2+\beta_{\mathrm{GH}}}{2}}}{b\; \Gamma\left(\alpha_{\mathrm{GH}}+k_2\right) k_2!} \left(\frac{1}{\mu_{\mathrm{GH_2}}}\right)^{\frac{\alpha_{\mathrm{GH}}+k_2+\beta_{\mathrm{GH}}}{2b}} \left(\gamma\right)^{\frac{\alpha_{\mathrm{GH}}+k_2+\beta_{\mathrm{GH}}}{2b}-1} G_{0,2}^{2,0}\left(\Xi\left(\frac{\gamma}{\mu_{\mathrm{GH_2}}}\right)^{\frac{1}{b}}\middle| \begin{matrix} - \\ \left(\frac{\alpha_{\mathrm{GH}}+k_2-\beta_{\mathrm{GH}}}{2}\right), -\left(\frac{\alpha_{\mathrm{GH}}+k_2-\beta_{\mathrm{GH}}}{2}\right) \end{matrix}\right), \tag{3.21}$$

where

$$\mathcal{Y} = \frac{\left(1-\sqrt{\rho}\right)^{\alpha_{\mathrm{GH}}}}{\Gamma\left(\alpha_{\mathrm{GH}}\right)\Gamma(\beta_{\mathrm{GH}})^2} \sum_{k_1=0}^{\infty}\sum_{k_2=0}^{\infty} \frac{\Gamma\left(\alpha_{\mathrm{GH}}+k_1+k_2\right)\rho^{\frac{k_1+k_2}{2}}}{\left(1+\sqrt{\rho}\right)^{\alpha_{\mathrm{GH}}+k_1+k_2}} \times \frac{1}{\Gamma\left(\alpha_{\mathrm{GH}}+k_1\right)k_1!}\; G_{1,3}^{2,1}\left(\Xi\left(\frac{\gamma_{\mathrm{th}}}{\mu_{\mathrm{GH_1}}}\right)^{\frac{1}{b}}\middle| \begin{matrix} 1 \\ \alpha_{\mathrm{GH}}+k_1, \beta_{\mathrm{GH}}, 0 \end{matrix}\right). \tag{3.22}$$

To obtain the average SEP of the ground–HAP$_2$ hop over correlated atmospheric turbulence, we rewrite (3.19) as

$$\bar{P}_e^{\mathrm{GH}_2} = \underbrace{\int_0^{\infty} P(e|\gamma)\; f_{\gamma_{\mathrm{GH}_2}}(\gamma \mid \gamma_{\mathrm{GH}_1} < \gamma_{\mathrm{th}})\; d\gamma}_{I_{e_3}} - \underbrace{\int_0^{\gamma_{\mathrm{th}}} P(e|\gamma)\; f_{\gamma_{\mathrm{GH}_2}}(\gamma \mid \gamma_{\mathrm{GH}_1} < \gamma_{\mathrm{th}})\; d\gamma}_{I_{e_4}} . \tag{3.23}$$

The analytical expression of I_{e_3} can be obtained after some algebraic manipulations, using (2.22), (3.21), [55, eq. (07.34.21.0013.01)], and [52, eq. (9.31.5)], as

$$I_{e_3} = \frac{\mathcal{Y}\; A\; b^{\alpha_{\mathrm{GH}}+k_2+\beta_{\mathrm{GH}}-1}}{(2\pi)^{b-1}\; 2\sqrt{\pi}\; \Gamma(\alpha_{\mathrm{GH}}+k_2)\; k_2!} G_{2,2b+1}^{2b,2}\left(\frac{\Xi^b}{b^{2b}\left(\sin\frac{\pi}{M}\right)^2 \mu_{\mathrm{GH}_2}} \middle| \begin{matrix} 1, \frac{1}{2} \\ \mathcal{B}_{\mathrm{GH}}^2, 0 \end{matrix} \right), \tag{3.24}$$

where $\mathcal{B}_{\mathrm{GH}}^2 = \{\frac{\alpha_{\mathrm{GH}}+k_2}{b}, \ldots, \frac{\alpha_{\mathrm{GH}}+k_2+b-1}{b}, \frac{\beta_{\mathrm{GH}}}{b}, \ldots, \frac{\beta_{\mathrm{GH}}+b-1}{b}\}$ consists of $2b$ terms. With the application of (2.23), (3.21), [55, eq. (07.34.21.0084.01)], and [52, eq. (9.31.5)], I_{e_4} can be analytically expressed as

$$I_{e_4} = \frac{\mathcal{Y}\; A}{2\Gamma(\alpha_{\mathrm{GH}}+k_2)\; k_2!}\; G_{1,3}^{2,1}\left(\Xi\left(\frac{\gamma_{\mathrm{th}}}{\mu_{\mathrm{GH}_2}}\right)^{\frac{1}{b}} \middle| \begin{matrix} 1 \\ \alpha_{\mathrm{GH}}+k_2, \beta_{\mathrm{GH}}, 0 \end{matrix} \right) - \frac{\mathcal{Y}\; A}{(2\pi)^{b-1}} \frac{b^{\alpha_{\mathrm{GH}}+k_2+\beta_{\mathrm{GH}}-1}}{\sqrt{\pi}\Gamma(\alpha_{\mathrm{GH}}+k_2)k_2!} \sum_{j=0}^{\infty} \frac{(-1)^j \gamma_{\mathrm{th}}^{j+\frac{1}{2}} \left(\sin\frac{\pi}{M}\right)^{2j+1}}{j!\;(2j+1)} G_{1,2b+1}^{2b,1}\left(\left(\frac{\Xi}{b^2}\right)^b \frac{\gamma_{\mathrm{th}}}{\mu_{\mathrm{GH}_2}} \middle| \begin{matrix} 1-j-\frac{1}{2} \\ \mathcal{B}_2, -j-\frac{1}{2} \end{matrix} \right). \tag{3.25}$$

The SAG-FSO links will be in outage if both γ_{GH_1} and γ_{GH_2} are below γ_{th}. As the ground–HAP FSO transmissions experience correlated turbulence, $P_{\mathrm{out}}^{\mathrm{SAG}_{1,2}}$ can

be written as

$$P_{\text{out}}^{\text{SAG}_{1,2}} = \int_0^{\gamma_{\text{th}}} \int_0^{\gamma_{\text{th}}} f_{\gamma_{\text{GH}_1},\gamma_{\text{GH}_2}}\left(\gamma_{\text{GH}_1},\gamma_{\text{GH}_2}\right)\, d\gamma_{\text{GH}_1}\, d\gamma_{\text{GH}_2}. \tag{3.26}$$

Substituting (3.7) in (3.26), the double integrations are carried out with the help of [58, eq. (26)] and [52, eq. (9.31.5)]. The final expression of the outage probability over correlated G-G is given by

$$P_{\text{out}}^{\text{SAG}_{1,2}} = \frac{\left(1-\sqrt{\rho}\right)^{\alpha_{\text{GH}}}}{\Gamma\left(\alpha_{\text{GH}}\right)\Gamma(\beta_{\text{GH}})^2} \sum_{k_{\text{GH}_1}=0}^{\infty}\sum_{k_{\text{GH}_2}=0}^{\infty} \frac{\Gamma\left(\alpha_{\text{GH}}+k_{\text{GH}_1}+k_{\text{GH}_2}\right)}{\left(1+\sqrt{\rho}\right)^{\alpha_{\text{GH}}+k_{\text{GH}_1}+k_{\text{GH}_2}}} \prod_{i\in\{\text{GH}_1,\text{GH}_2\}} \frac{\rho^{\frac{k_{\text{GH}_1}+k_{\text{GH}_2}}{2}}}{\Gamma\left(\alpha_{\text{GH}}+k_i\right)k_i!} G_{1,3}^{2,1}\left(\Xi\left(\frac{\gamma_{\text{th}}}{\mu_i}\right)^{\frac{1}{b}} \,\middle|\, \begin{matrix} 1 \\ \alpha_{\text{GH}}+k_i, \beta_{\text{GH}}, 0 \end{matrix}\right). \tag{3.27}$$

Since the RF and FSO links experience independent fading effects, the average SEP of the RF link is expressed as

$$\bar{P}_e^{\text{RF}} = \int_0^{\infty} P(e|\gamma)\; f_{\gamma_r}(\gamma)\; d\gamma. \tag{3.28}$$

With the application of (3.8), series expansion to the modified Bessel function using [52, eq. (8.447.1)], and rewriting the exponential function in terms of the Meijer G-function using [58, eq. (11)], the analytical expression of $\bar{P}_e^{\text{RF}}$ is obtained after some algebraic manipulations using [55, eq. (07.34.21.0013.01)] as

$$\bar{P}_e^{\text{RF}} = \mathcal{F}\; \exp(-K) \sum_{u=0}^{\infty} \frac{A\;(K\mathcal{F})^u}{2\sqrt{\pi}\left(\sin\frac{\pi}{M}\right)^{2u+2}\;(u!)^2} \times\; G_{2,2}^{1,2}\left(\frac{\mathcal{F}}{\left(\sin\frac{\pi}{M}\right)^2} \,\middle|\, \begin{matrix} -u\;, & -u-\frac{1}{2} \\ 0\;, & -u-1 \end{matrix}\right), \tag{3.29}$$

where $\mathcal{F} = \frac{K+1}{\bar{\gamma}_r}$. Note that the terms of the infinite summation in (3.13), (3.24), (3.25), (3.27), and (3.29) converge since the terms decrease at the rate of $\frac{1}{j!}$, $\frac{1}{k_i!}$,

Table 3.1: Computation time for asymptotic and exact SEP expressions

Parameters		*Execution time (sec)*	
Correlation coefficient	Truncation value	Exact	Asymptotic
0.2	$j = 50, u = 20, k_i = 21$	276	0.83
0.5	$j = 50, u = 20, k_i = 41$	382	3.02
0.8	$j = 50, u = 20, k_i = 71$	534	8.52

and $\frac{1}{(u!)^2}$, respectively. In addition, the obtained expressions are applicable for both downlink and uplink scenarios, using the suitable expressions for large-scale and small-scale fading parameters [31].

3.6 Overall System Diversity Gain

To calculate the overall system diversity gain, we perform asymptotic analysis at high SNRs. With the application of [52, eq. (9.303)] on (3.9), we can represent the Meijer G-function by its basic elementary form and obtain the asymptotic SEP and outage probability expressions as given in the Appendix of this chapter. Such expressions are analytically more tractable because they involve the summation of much simpler functions and are computationally less intensive, as shown in Table 3.1. At high SNR, the ASEP expression of a particular system should have the form $\mathcal{C}(\text{SNR})^{-\mathcal{D}}$, where $\mathcal{D}$ denote the diversity gain of the system [62, eq. (1)].

From (3.32), (3.33), and (3.34), we can observe that $\bar{P}_{ae}^{\text{SAG}_1} \propto (\mu_l)^{-\mathcal{D}_{e,\text{SAG}_1}}$, where $\mathcal{D}_{e,\text{SAG}_1} = \min(\frac{\alpha_{\text{GH}}}{b}, \frac{\beta_{\text{GH}}}{b}, \frac{\alpha_{\text{H}_1\text{S}}}{b}, \frac{\beta_{\text{H}_1\text{S}}}{b})$ is the diversity gain of the SAG_1-FSO link with respect to SEP. Since $\alpha_{\text{GH}} \ll \alpha_{\text{H}_1\text{S}}$ and $\beta_{\text{GH}} \ll \beta_{\text{H}_1\text{S}}$, $\mathcal{D}_{e,\text{SAG}_1} = \min(\frac{\alpha_{\text{GH}}}{b}, \frac{\beta_{\text{GH}}}{b})$. From (3.35), it is observed that $P_{a\text{out}}^{\text{SAG}_1} \propto (\mu_l)^{-\mathcal{D}_{\text{O},\text{SAG}_1}}$, where $\mathcal{D}_{\text{O},\text{SAG}_1} = \min(\frac{\alpha_{\text{GH}}}{b}, \frac{\beta_{\text{GH}}}{b})$ is the diversity gain of the SAG_1-FSO link with respect to outage. Using only the dominant terms, we can conclude from (3.32), (3.36), (3.37), and (3.38) that $\bar{P}_{ae}^{\text{SAG}_2} \propto (\mu_l)^{-\mathcal{D}_{e,\text{SAG}_2}}$, where $\mathcal{D}_{e,\text{SAG}_2} = 2\min(\frac{\alpha_{\text{GH}}}{b}, \frac{\beta_{\text{GH}}}{b})$ is the diversity gain of the SAG_2-FSO transmission with respect to SEP. From (3.39), we can find that $P_{a\text{out}}^{\text{SAG}_{1,2}} \propto$

$(\mu_l)^{-\mathcal{D}_{\mathrm{O,SAG}_{1,2}}}$, where $\mathcal{D}_{\mathrm{O,SAG}_{1,2}} = 2\min(\frac{\alpha_{\mathrm{GH}}}{b}, \frac{\beta_{\mathrm{GH}}}{b})$ is the diversity gain of both FSO links with respect to outage over correlated turbulence. Because the higher-order terms are insignificant, just the first term in (3.40) is considered, $\bar{P}_{ae}^{\mathrm{RF}} \propto (\bar{\gamma}_r)^{-1}$. Thus, the diversity gain of the RF link is unity. As a result, the diversity gain of the transmission system can be expressed as

$$\mathcal{D} = \min\left(\mathcal{D}_{e,\mathrm{SAG}_1}\ ,\ \mathcal{D}_{\mathrm{O,SAG}_1} + \mathcal{D}_{e,\mathrm{SAG}_2}\ ,\ \mathcal{D}_{\mathrm{O,SAG}_{1,2}} + 1\right). \tag{3.30}$$

After simplification, $\mathcal{D}$ can be written as

$$\mathcal{D} \ = \ \min\left(\frac{\alpha_{\mathrm{GH}}}{b}\ ,\ \frac{\beta_{\mathrm{GH}}}{b}\right). \tag{3.31}$$

This indicates that the overall diversity gain of the transmission system is mainly dependent on atmospheric turbulence between the ground station and HAP and is unaffected by the correlation effect. Correlated turbulence only affects the code gain of the system.

3.7 Numerical Results

We present the effect of correlated turbulence on the switching-based HAP relays with hybrid SAG-FSO/RF transmission in terms of ASEP. The numerical results are obtained based on the derived analytical expressions and confirmed by Monte-Carlo simulations. The correlated fading envelope samples are generated in MATLAB using [81]. We assume the transmission system parameters as listed in Table 3.2. We also adopt an uplink SatCom scenario. The infinite summations in (3.13), (3.25), and (3.29) are truncated to $u = 20$ and $j = 50$ as larger values have a negligible impact. The number of required terms for the infinite summation in (3.27) is highly dependent on the correlation coefficient (see Table I in [50] for k_i truncated values).

Table 3.2: Simulation parameters

Parameter	*Value*
Satellite altitude	620 km
HAP altitude	20 km
Ground station aperture height	2 m
HAP_1 zenith angle	0^o
HAP_2 zenith angle	$\geq 0^o$
FSO wavelength	1550 nm
Telescope aperture diameter	20 cm
Beam radius at optical transmitter	2 cm
Optical-to-electrical conversion efficiency	0.8
Wind speed	21 m/s
RF carrier frequency	30 GHz
Rician factor	6
Switching threshold	10.5 dB

In Figure 3.4, we examine the ASEP performance of the proposed transmission system as a function of correlation coefficient values. We assume BPSK, an IM/DD scheme, refractive index structure of 1×10^{-13} $\mathrm{m}^{\frac{-2}{3}}$, a switching threshold of 10.5 dB, $\mu_l = 25$ dB, and $\bar{\gamma}_r = 25$ dB. The results of RF-only [57], FSO-only [25], hybrid FSO/RF [27], and SAG-FSO/RF [31] SatCom systems are also plotted for comparison purposes. We can see that the performance of the proposed system degrades as the correlation coefficient value increases, as expected. The ASEP changes from 5×10^{-11} to 3.7×10^{-9} when ρ increases from 0.1 to 0.9. Despite the ASEP performance variation, the transmission system with switching-based HAP relays performs better than existing solutions across the entire range of ρ values. The improved performance of the proposed system is attributed to the use of the SAG_2-FSO link as an additional backup. Although FSO transmission over HAP_2 is

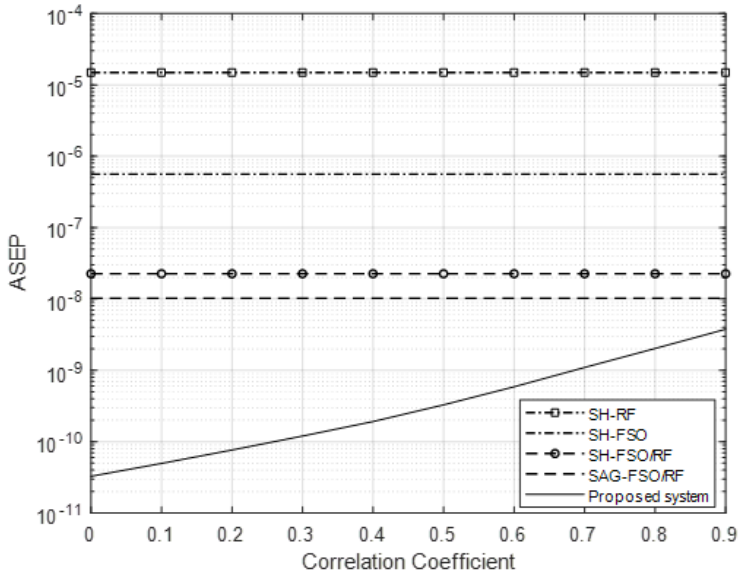

Figure 3.4: Effect of correlation coefficient values on the ASEP performance.

more vulnerable to atmospheric turbulence, the two-step optical amplification helps mitigate its effects, thereby increasing the FSO's usability even further.

In Figure 3.5, we plot the ASEP of the proposed transmission system with HD and IM/DD receivers. The ASEP versus SNR plots are obtained for correlated turbulence levels $\rho = 0.8, 0.5, 0.2$, and 0. We also assume BPSK modulation, a refractive index structure of 4.69×10^{-13} $\mathrm{m}^{\frac{-2}{3}}$, a switching threshold of 10.5 dB, and both RF and FSO links have equal average SNR. As we can see, the analytical results perfectly match Monte-Carlo simulations. The asymptotic expressions are also presented to verify their accuracy. Furthermore, the impairment of the ASEP performance is noticed with the increase in correlation coefficient value. If there is no correlated turbulence between the FSO links, the system attains its best ASEP performance. The transmission system with HD receiver encounters a performance loss of 2.5 dB when ρ increases from 0 to 0.8, at ASEP of 1×10^{-10}. Even under such a correlation effect (i.e., $\rho = 0.8$), the transmission system with an HD receiver can maintain a performance gain over that with an IM/DD receiver over independent turbulence.

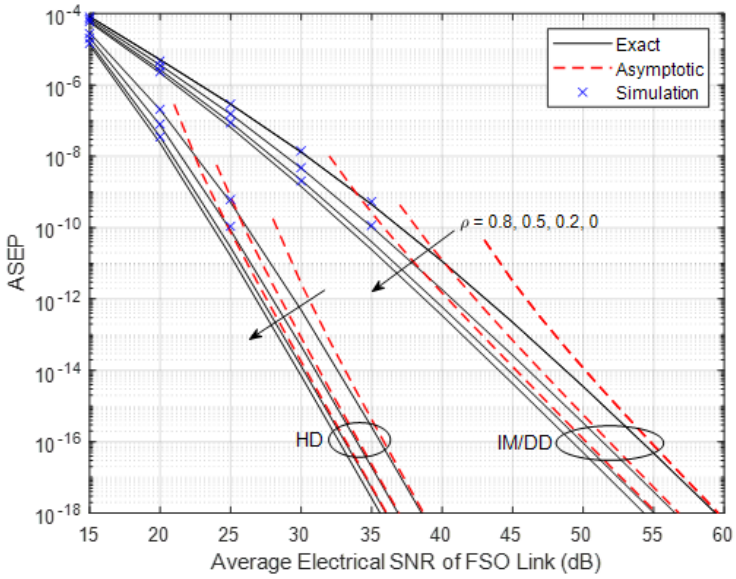

Figure 3.5: ASEP versus average SNR for different correlation coefficient values.

As a final numerical example, in Figure 3.6, we investigate the ASEP performance dependence on the refractive index structure parameter, assuming different correlation coefficient values. We also assume BPSK modulation, a switching threshold of 10.5 dB, $\mu_l = 25$ dB, and $\bar{\gamma}_r = 25$ dB. As seen in this figure, lower values of the refractive index parameter lead to better ASEP performance as the FSO transmissions are impaired by weak turbulence effects. The increase in the index value results in a noticeable deterioration of the ASEP performance. We can also see that the change in the correlation coefficient has a substantial effect in the case of weak atmospheric turbulence compared to strong ones. Even though the transmission system with the HD scheme outperforms the IM/DD scheme across the entire range of refractive index structure values, it suffers a greater ASEP performance penalty with the change in the correlation coefficient.

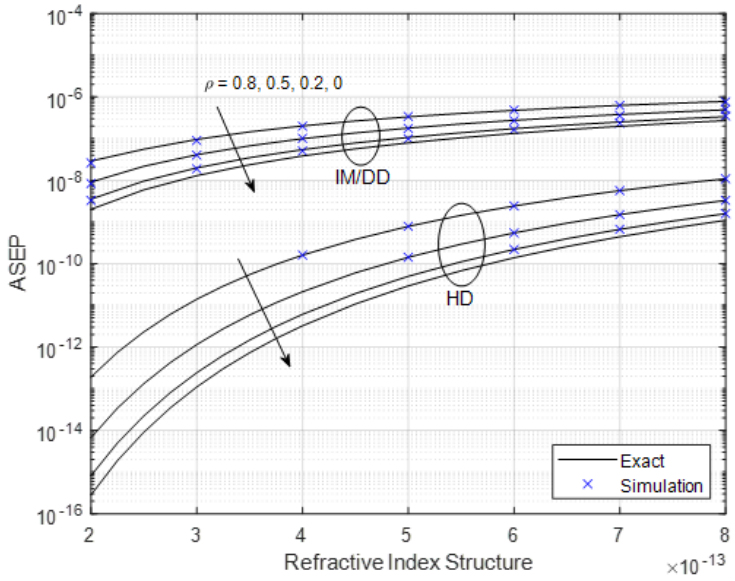

Figure 3.6: ASEP versus refractive index for different correlation coefficient values.

Appendix: Asymptotic Analysis of SAG-FSO/RF Transmission with Multiple HAP Relays

The asymptotic ASEP of the SAG_1-FSO link can be expressed as

$$\bar{P}_{ae}^{\mathrm{SAG}_1} = \bar{P}_{ae}^{\mathrm{GH}_1} + \bar{P}_{ae}^{\mathrm{HS}_1} - \bar{P}_{ae}^{\mathrm{GH}_1}\,\bar{P}_{ae}^{\mathrm{HS}_1}, \tag{3.32}$$

where

$$\begin{aligned}\bar{P}_{ae}^{\mathrm{GH}_1} = {} & \frac{A\, b^{\alpha_{\mathrm{GH}}+\beta_{\mathrm{GH}}-1}}{(2\pi)^{b-1}\, 2\sqrt{\pi}\,\Gamma(\alpha_{\mathrm{GH}})\Gamma(\beta_{\mathrm{GH}})} \sum_{z=1}^{2b} \Lambda_1\, \Gamma\left(\frac{1}{2}+\mathcal{B}_{\mathrm{GH}}^{1,z}\right) \left(\frac{(\alpha_{\mathrm{GH}}\beta_{\mathrm{GH}})^b}{b^{2b}\left(\sin\frac{\pi}{M}\right)^2 \mu_{\mathrm{GH}_1}}\right)^{\mathcal{B}_{\mathrm{GH}}^{1,z}} \\ & - \frac{A}{2\Gamma(\alpha_{\mathrm{GH}})\Gamma(\beta_{\mathrm{GH}})} \sum_{z=1}^{2} \Lambda_3 \left(\alpha_{\mathrm{GH}}\beta_{\mathrm{GH}} \left(\frac{\gamma_{\mathrm{th}}}{\mu_{\mathrm{GH}_1}}\right)^{\frac{1}{b}}\right)^{\mathcal{B}_{\mathrm{GH}}^{3,z}} + \frac{A\, b^{\alpha_{\mathrm{GH}}+\beta_{\mathrm{GH}}-1}}{(2\pi)^{b-1}\sqrt{\pi}\,\Gamma(\alpha_{\mathrm{GH}})\Gamma(\beta_{\mathrm{GH}})} \\ & \sum_{j=0}^{\infty} \frac{(-1)^j \gamma_{\mathrm{th}}^{j+\frac{1}{2}} \left(\sin\frac{\pi}{M}\right)^{2j+1}}{j!\,(2j+1)} \sum_{z=1}^{2b} \frac{\Lambda_1\, \mathcal{B}_{\mathrm{GH}}^{1,z}}{j+\frac{1}{2}+\mathcal{B}_{\mathrm{GH}}^{1,z}} \left(\left(\frac{\alpha_{\mathrm{GH}}\beta_{\mathrm{GH}}}{b^2}\right)^b \frac{\gamma_{\mathrm{th}}}{\mu_{\mathrm{GH}_1}}\right)^{\mathcal{B}_{\mathrm{GH}}^{1,z}}, \end{aligned} \tag{3.33}$$

is the asymptotic ASEP of the ground-HAP$_1$ hop, $\Lambda_1 = \frac{\prod_{g=1;g\neq z}^{2b}\Gamma\left(\mathcal{B}_{\text{GH}}^{1,g}-\mathcal{B}_{\text{GH}}^{1,z}\right)}{\mathcal{B}_{\text{GH}}^{1,z}}$, $\Lambda_3 = \frac{\prod_{g=1;g\neq z}^{2}\Gamma\left(\mathcal{B}_{\text{GH}}^{3,g}-\mathcal{B}_{\text{GH}}^{3,z}\right)}{\mathcal{B}_{\text{GH}}^{3,z}}$, and $\mathcal{B}_{\text{GH}}^{n,z}$ is the z^{th} term in $\mathcal{B}_{\text{GH}}^{n}$, i.e., $\mathcal{B}_{\text{GH}}^{3} = \{\alpha_{\text{GH}}, \beta_{\text{GH}}\} = \{\mathcal{B}_{\text{GH}}^{3,1}, \mathcal{B}_{\text{GH}}^{3,2}\}$. The asymptotic ASEP of the HAP$_1$-SAT hop is given by

$$\bar{P}_{ae}^{\text{H}_1\text{S}} = \frac{A\ b^{\alpha_{\text{H}_1\text{S}}+\beta_{\text{H}_1\text{S}}-1}\sum_{z=1}^{2b}\prod_{g=1;g\neq z}^{2b}\Gamma\left(\mathcal{B}_{\text{H}_1\text{S}}^{1,g}-\mathcal{B}_{\text{H}_1\text{S}}^{1,z}\right)}{(2\pi)^{b-1}\ 2\sqrt{\pi}\ \Gamma(\alpha_{\text{H}_1\text{S}})\ \Gamma(\beta_{\text{H}_1\text{S}})\ \mathcal{B}_{\text{H}_1\text{S}}^{1,z}} \Gamma\left(\frac{1}{2}+\mathcal{B}_{\text{H}_1\text{S}}^{1,z}\right)\left(\frac{\left(\alpha_{\text{H}_1\text{S}}\beta_{\text{H}_1\text{S}}\right)^{b}}{b^{2b}\left(\sin\frac{\pi}{M}\right)^{2}\mu_{\text{H}_1\text{S}}}\right)^{\mathcal{B}_{\text{H}_1\text{S}}^{1,z}}. \quad (3.34)$$

The asymptotic outage probability of the FSO transmission through HAP$_1$ is given by

$$P_{a\text{out}}^{\text{SAG}_1} = \sum_{z=1}^{2}\frac{\Lambda_3}{\Gamma(\alpha_{\text{GH}})\Gamma(\beta_{\text{GH}})}\left(\alpha_{\text{GH}}\beta_{\text{GH}}\left(\frac{\gamma_{\text{th}}}{\mu_{\text{GH}_1}}\right)^{\frac{1}{b}}\right)^{\mathcal{B}_{\text{GH}}^{3,z}}. \quad (3.35)$$

The asymptotic ASEP of the FSO transmission through HAP$_2$, $\bar{P}_{ae}^{\text{SAG}_2}$, is obtained similar to (3.32) with $\bar{P}_{ae}^{\text{H}_2\text{S}}$ analytically expressed using (3.34) with the corresponding fading parameters $\beta_{\text{H}_2\text{S}}$, $\alpha_{\text{H}_2\text{S}}$, and $\mu_{\text{H}_2\text{S}}$. The asymptotic SEP of the ground-HAP$_2$ hop is given by $\bar{P}_{ae}^{\text{GH}_2} = I_{ae_3} - I_{ae_4}$, where

$$I_{ae_3} = \frac{\mathcal{Y}_a\ A\ b^{\alpha_{\text{GH}}+k_2+\beta_{\text{GH}}-1}}{(2\pi)^{b-1}\ 2\sqrt{\pi}\ \Gamma(\alpha_{\text{GH}}+k_2)k_2!} \sum_{z=1}^{2b}\Lambda_2\ \Gamma\left(\frac{1}{2}+\mathcal{B}_{\text{GH}}^{2,z}\right)\left(\frac{\Xi^{b}}{b^{2b}\left(\sin\frac{\pi}{M}\right)^{2}\mu_{\text{GH}_2}}\right)^{\mathcal{B}_{\text{GH}}^{2,z}}, \quad (3.36)$$

and

$$I_{ae_4} = \frac{\mathcal{Y}_a\ A}{2\Gamma(\alpha_{\rm GH}+k_2)k_2!}\sum_{z=1}^{2}\ \Lambda_5\left(\Xi\left(\frac{\gamma_{\rm th}}{\mu_{\rm GH_2}}\right)^{\frac{1}{b}}\right)^{\mathcal{B}_{\rm GH}^{5,z}} - \frac{\mathcal{Y}_a\ A\ b^{\alpha_{\rm GH}+k_2+\beta_{\rm GH}-1}}{(2\pi)^{b-1}\sqrt{\pi}\ \Gamma(\alpha_{\rm GH}+k_2)k_2!}$$
$$\sum_{j=0}^{\infty}\frac{(-1)^j\gamma_{\rm th}^{j+\frac{1}{2}}\left(\sin\frac{\pi}{M}\right)^{2j+1}}{j!\ (2j+1)}\ \ \sum_{z=1}^{2b}\frac{\Lambda_2\ \mathcal{B}_{\rm GH}^{2,z}}{j+\frac{1}{2}+\mathcal{B}_{\rm GH}^{2,z}}\left(\left(\frac{\Xi}{b^2}\right)^b\ \frac{\gamma_{\rm th}}{\mu_{\rm GH_2}}\right)^{\mathcal{B}_{\rm GH}^{2,z}}. \quad (3.37)$$

Here $\Lambda_2 = \frac{\Pi_{g=1;g\neq z}^{2b}\Gamma\left(\mathcal{B}_{\rm GH}^{2,g}-\mathcal{B}_{\rm GH}^{2,z}\right)}{\mathcal{B}_{2,z}}$, $\Lambda_4 = \frac{\Pi_{g=1;g\neq z}^{2}\Gamma\left(\mathcal{B}_{\rm GH}^{4,g}-\mathcal{B}_{\rm GH}^{4,z}\right)}{\mathcal{B}_{\rm GH}^{4,z}}$, $\mathcal{B}_{\rm GH}^{4} = \{\alpha_{\rm GH}+k_1,\beta_{\rm GH}\}$, $\Lambda_5 = \frac{\Pi_{g=1;g\neq z}^{2}\Gamma\left(\mathcal{B}_{\rm GH}^{5,g}-\mathcal{B}_{\rm GH}^{5,z}\right)}{\mathcal{B}_{\rm GH}^{5,z}}$, $\mathcal{B}_{\rm GH}^{5} = \{\alpha_{\rm GH}+k_2,\beta_{\rm GH}\}$, and

$$\mathcal{Y}_a = \frac{\left(1-\sqrt{\rho}\right)^{\alpha_{\rm GH}}}{\Gamma\left(\alpha_{\rm GH}\right)\Gamma(\beta_{\rm GH})^2}\sum_{k_1=0}^{\infty}\sum_{k_2=0}^{\infty}\frac{\Gamma\left(\alpha_{\rm GH}+k_1+k_2\right)\rho^{\frac{k_1+k_2}{2}}}{\left(1+\sqrt{\rho}\right)^{\alpha_{\rm GH}+k_1+k_2}}$$
$$\sum_{z=1}^{2}\frac{\Lambda_4}{\Gamma\left(\alpha_{\rm GH}+k_1\right)k_1!}\left(\Xi\left(\frac{\gamma_{\rm th}}{\mu_{\rm GH_1}}\right)^{\frac{1}{b}}\right)^{\mathcal{B}_{\rm GH}^{4,z}}. \quad (3.38)$$

The asymptotic outage probability of both SAG-FSO links can be expressed as

$$P_{a\rm out}^{\rm SAG_{1,2}} = \frac{\left(1-\sqrt{\rho}\right)^{\alpha_{\rm GH}}}{\Gamma\left(\alpha_{\rm GH}\right)\Gamma(\beta)^2}\sum_{k_1=0}^{\infty}\sum_{k_2=0}^{\infty}\frac{\Gamma\left(\alpha_{\rm GH}+k_1+k_2\right)\rho^{\frac{k_1+k_2}{2}}}{\left(1+\sqrt{\rho}\right)^{\alpha_{\rm GH}+k_1+k_2}}$$
$$\prod_{i=1}^{2}\sum_{z=1}^{2}\frac{\Lambda_6}{\Gamma\left(\alpha_{\rm GH}+k_i\right)k_i!}\left(\Xi\left(\frac{\gamma_{\rm th}}{\mu_i}\right)^{\frac{1}{b}}\right)^{\mathcal{B}_{\rm GH}^{6,z}}, \quad (3.39)$$

where $\Lambda_6 = \frac{\Pi_{g=1;g\neq z}^{2}\Gamma\left(\mathcal{B}_{\rm GH}^{6,g}-\mathcal{B}_{\rm GH}^{6,z}\right)}{\mathcal{B}_{\rm GH}^{6,z}}$ and $\mathcal{B}_{\rm GH}^{6} = \{\alpha_{\rm GH}+k_i,\beta_{\rm GH}\}$.

The asymptotic ASEP of the RF link can be written as

$$\bar{P}_{ae}^{\rm RF} = \sum_{u=0}^{\infty}\frac{A\exp(-K)K^u(K+1)^{u+1}\Gamma(\frac{3}{2}+u)}{2\sqrt{\pi}\ \left(\sin\frac{\pi}{M}\right)^{2u+2}\ (1+u)\ (u!)^2}\ (\bar{\gamma}_r)^{-(u+1)}. \quad (3.40)$$

Chapter 4

Parallel FSO-RF Transmissions for High-Throughput Remote Access

Mixed usage of RF and FSO transmissions can improve the reliability and throughput of future SatCom systems. To overcome the rate limitation of conventional hybrid implementations, we propose parallel FSO and RF transmissions for end users to explore their complementary properties in beamwidth and bandwidth. In particular, RF transmission serves the users over a large geographical area, while the FSO link is employed to increase the throughput to a particular hot-spot area with higher capacity demand. We assume that the hot-spot area is served by an access point (AP). The AP can establish parallel FSO-RF links with the satellite and serve ground users in its coverage with a broadband WiFi or cellular network. No additional wired terrestrial infrastructure is required. The ground users can achieve high data transmission over the mixed FSO-RF link through the AP when inside its coverage. However, users have to rely on a direct RF link to the satellite when they are outside the coverage area of the AP. To highlight the significant potential of the proposed SatCom system, we analytically derive the sum capacity outage probability for the transmission to the AP. Note that he proposed system is ideal for providing coverage to a remote community where a traditional terrestrial solution

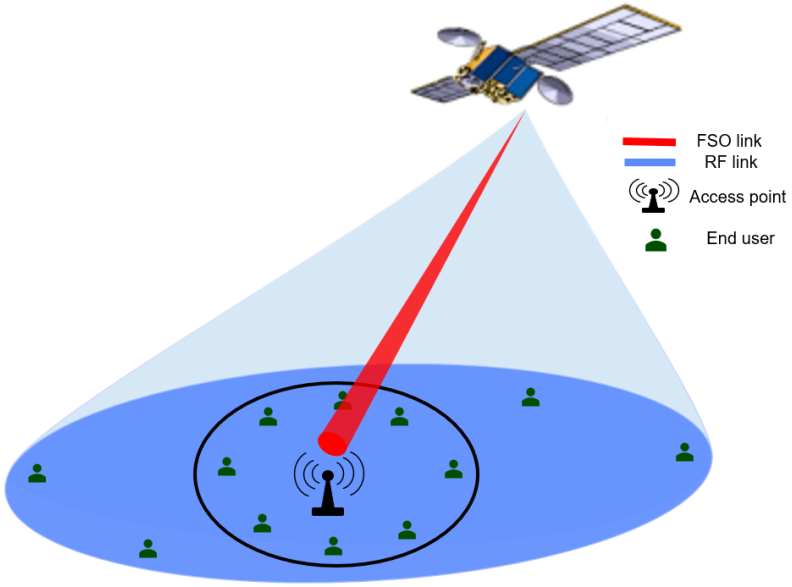

Figure 4.1: Parallel FSO-RF SatCom transmission scheme.

is prohibitively expensive. Low-density populations in remote communities present an economic challenge for a relatively large investment in communication infrastructure [4]. Besides, the diversity of geographical nature, such as hills, mountains, and valleys, poses a physical barrier that increases the cost of installing fiber-optic cables.

4.1 Related Work

As FSO and RF links are vulnerable to non-overlapping weather conditions, i.e., rain affects RF link quality and fog limits FSO transmissions, most previous work adopted a hybrid implementation strategy [27, 31, 37, 41, 59, 82]. The high-rate FSO link enjoyed higher priority, while the RF link was employed as a backup. The system will switch to the RF link if the FSO link fails to support the desired data rate. This approach will, however, require frequent hardware switching between the RF and FSO links, which may lead to service disruption due to the required setup time. In [33, 80, 83], an adaptive-combining-based solution was proposed to

reduce the on-off switching of the FSO link. The RF link will be activated when the FSO-link performance deteriorates, and identical data will be transmitted over both links, enabling maximal ratio combining at the receiver. In [32, 63], rate adaptive transmission was proposed to minimize the frequency of switching between RF and FSO links. Despite improving the system's error rate and outage performance [27, 31–33, 37, 41, 59, 63, 80, 82, 83], switching back or combining with the RF link reduces the overall system throughput. Note that with hybrid implementation, the RF resource is reserved but not utilized continuously, which may lead to certain resource wastage.

Typically, there is a hot-spot area with high-capacity demand, e.g., hospital, school, and community center in the remote community. Users are dispersed over a wide geographical area inside or outside the hot-spot area. We prioritize the service to the hot-spot area, assuming there are more users with critical demand. With the proposed parallel FSO and RF transmissions, we can better utilize both links to improve the throughput and reliability of the hot-spot area while supporting ubiquitous coverage. Independent data streams are adaptively sent over both links to satisfy capacity and availability requirements. While the switching-based system uses full transmit power on either link, the parallel FSO-RF transmission system adaptively allocates power among the two links according to the weather conditions. Due to its wider beamwidth, the satellite will use the RF link to transmit information essential to all ground users, regardless of location. The FSO link, on the other hand, can be used to enhance the reception of this essential information and provide a value-added service to users in the hot-spot area through the AP. Another implementation of parallel FSO and RF transmission is the soft-switching strategy [84, 85]. While incurring higher decoding complexity, soft switching is not applicable to our proposed design as data from both links needs to be jointly decoded. Note that the quality of service experienced by users in the coverage of the AP is limited by the capacity outage probability of the parallel FSO-RF links. As

such, we present a sum capacity outage analysis for parallel FSO-RF transmissions. To the best knowledge of the authors, this is the first attempt at this challenging problem. The results also establish the capacity bound for parallel FSO and RF transmissions with soft-switching strategy.

4.2 System and Channel Models

In this work, we consider a SatCom system for connecting a remote community, as illustrated in Figure 4.1. We assume both the satellite and the AP host RF and FSO payload. As such, satellite can establish a parallel FSO-RF link to the AP. Users in the coverage of the AP can enjoy reliable high throughput transmission through the AP, whereas users outside the coverage of the AP rely on a direct RF link to the satellite.

4.2.1 Signalling Schemes

The baseband signal at the optical receiver can be expressed as

$$y_f = \left(\eta \, \frac{P_f \, G_f^{tx} \, G_f^{rx}}{FL_f} \, I \right)^{\frac{b}{2}} \, x_f + n_f, \tag{4.1}$$

where b defines the detection type at the optical receiver (i.e. $b = 2$ for IM/DD and $b = 1$ for HD), x_f is the transmitted signal over FSO link, n_f denotes the AWGN at the optical receiver with variance $\sigma_{n_f}^2$, P_f indicates the transmit power over the FSO link, η represents the efficiency of the optical-to-electrical conversion, G_f^{tx} defines the transmit gain of the telescope, and G_f^{rx} defines the receive gain of the telescope. The free-space loss is given by $FL_f = \frac{4\pi L_{\mathrm{SG}}}{\lambda_f}$, where λ_f indicates the optical wavelength and $L_{\mathrm{SG}} = (H_{\mathrm{S}} - H_{\mathrm{G}}) \sec(\theta_{\mathrm{SG}})$ denotes the slant range to satellite with H_{S}, H_{G}, and θ_{SG} being the satellite altitude, the aperture height of the AP, and the satellite zenith angle, respectively. The irradiance of the FSO channel

is represented by $I = I^l I^a I^p$, where I^l denotes the atmospheric attenuation, I^a denotes the atmospheric turbulence, and I^p denotes the pointing errors. The FSO link attenuation due to weather conditions is modeled using the Beer-Lambert law as $I^l = \exp(-\varphi_f d_w)$ [23], where φ_f is the attenuation coefficient (in dB/km) and d_w indicates the distance over which the weather impact takes place. According to (4.1), the instantaneous received SNR can be obtained as [31, eq. (6)]

$$\gamma_f = \frac{\left(\eta\ P_f\, G_f^{tx}\ G_f^{rx}\right)^b}{FL_f^b\ \sigma_{n_f}^2}\ I^b, \tag{4.2}$$

The baseband signal of the RF link at the receiver is given by

$$y_r = \left(\frac{P_r\ G_r^{tx}\ G_r^{rx}}{FL_r\ L_w}\right)^{\frac{1}{2}}\ h\ x_r + n_r, \tag{4.3}$$

where P_r defines the RF transmit power, the receive and transmit antenna gains are denoted by G_r^{rx} and G_r^{tx}, respectively, x_r denotes the transmitted signal over RF link, h is the channel coefficient that follows Rician fading, and n_r denotes the thermal noise at the RF receiver that is represented by AWGN. The free-space loss of the RF link is given by $FL_r = \left(\frac{4\pi L_{\mathrm{SG}}}{\lambda_r}\right)^2$, where λ_r denotes the RF signal wavelength. The RF link attenuation due to weather conditions is given by $L_w = \varphi_r d_w$, where φ_r is the corresponding attenuation coefficient (in dB/km) [64]. Based on (4.3), the instantaneous SNR of the RF link can be written as [30, eq. (12)]

$$\gamma_r = \frac{P_r\ G_r^{tx}\ G_r^{rx}}{FL_r\ L_w\ \sigma_{n_r}^2}\ h_r^2, \tag{4.4}$$

where $\sigma_{n_r}^2$ represents the thermal noise variance, which is given by $\sigma_{n_r}^2 = P_{n_r} N_r$, where P_{n_r} is the noise power and N_r is the noise figure of the RF receiver.

4.2.2 Channel Model

We conduct our analysis assuming that FSO transmission encounters G-G fading with weather attenuation and pointing error effects. The unified expression of the pdf of the instantaneous SNR, $\gamma_{_f}$, is given by [86, eq. (2)]

$$f_{\gamma_{_f}}(\gamma) = \frac{\xi^2\ \gamma^{-1}}{b\ \Gamma(\alpha)\ \Gamma(\beta)} G_{1,3}^{3,0}\left(\alpha\beta k \left(\frac{\gamma}{\mu_{_b}}\right)^{\frac{1}{b}} \middle| \begin{matrix} \xi^2+1 \\ \\ \xi^2, \alpha, \beta \end{matrix} \right), \tag{4.5}$$

where $\mu_{_b}$ denotes the average receive electrical SNR, which is a function of the average receive SNR at the optical receiver, $\bar{\gamma}_{_f}$, as [31, eq. (10)]

$$\mu_{_1} = \bar{\gamma}_{_f},$$

and

$$\mu_{_2} = \frac{\alpha\ \beta\ \xi^2\ (\xi^2+2)}{(\alpha+1)(\beta+1)(\xi^2+1)^2}\ \bar{\gamma}_{_f}.$$

In a SatCom environment, RF transmissions encounter less reflection and scattering due to a strong line-of-sight between the AP and satellite. As a result, the Rician fading can accurately model the RF link [33,34]. The pdf of the instantaneous receive SNR is expressed as [57, eq. (2.16)]

$$f_{\gamma_{_r}}(\gamma) = \frac{K+1}{\bar{\gamma}_r}\ \exp\left(-(K+1)\ \frac{\gamma}{\bar{\gamma}_r} - K\right) I_0\left(2\ \sqrt{K(K+1)\ \frac{\gamma}{\bar{\gamma}_r}}\right), \tag{4.6}$$

With the application of series expansion to the modified Bessel function using [52, eq. (8.447.1)] and the exponential function using [52, eq. (1.211.1)], the pdf of the RF instantaneous receive SNR in (4.6) can be expressed as

$$f_{\gamma_{_r}}(\gamma) = \mathcal{F} \exp(-K) \sum_{i=0}^{\infty} \frac{(-\mathcal{F})^i}{i!}\ \sum_{j=0}^{\infty} \frac{(K\mathcal{F})^j}{(j!)^2}\ \gamma^{\,i+j}. \tag{4.7}$$

Table 4.1: List of notations

$\mathcal{F} = \frac{K+1}{\bar{\gamma}_r}$
$\mathcal{X} = \frac{b^{\alpha+\beta-2}\ \xi^2}{(2\pi)^{b-1}\ \Gamma(\alpha)\Gamma(\beta)}$
$\mathcal{E} = \left(\frac{\alpha\beta k}{b^2}\right)^b$
$\mathcal{B}^1 = \{\frac{\xi^2+1}{b}, \ldots, \frac{\xi^2+b}{b}\}$ includes b terms.
$\mathcal{B}^2 = \{\frac{\xi^2}{b}, \ldots, \frac{\xi^2+b-1}{b}, \frac{\alpha}{b}, \ldots, \frac{\alpha+b-1}{b}, \frac{\beta}{b}, \ldots, \frac{\beta+b-1}{b}\}$ includes $3b$ terms.
$\mathcal{A}_1 = \sum_{z=1}^{\infty} \frac{(n-v)!}{(1+a_1)^z(n-v-z)!}(\ln(a_1+1))^{n-v-z}\ \sum_{d=0}^{z} \binom{z}{d} \frac{(-a_1)^{z-d}}{z!}$
$\mathcal{A}_2 = \frac{\ln(2)\mathcal{F}\exp(-K)}{BW_r} \sum_{i=0}^{\infty} \frac{(-\mathcal{F})^i}{i!} \sum_{j=0}^{\infty} \frac{(K\mathcal{F})^j}{(j!)^2} \sum_{m=0}^{i+j} \binom{i+j}{m} (-1)^{i+j-m}$ $\sum_{n=0}^{\infty} \frac{\left(\frac{(m+1)\ln(2)}{BW_r}\right)^n}{n!} \sum_{v=0}^{n} \binom{n}{v} (-1)^{n-v}$
$\mathcal{A}_3 = \sum_{u=1}^{\infty} \frac{(v+h)!}{(1+a_2)^u(v+h-u)!} (\ln(a_2+1))^{v+h-u}\ \sum_{g=0}^{u} \binom{u}{g} \frac{(-a_2)^{u-g}}{u!}$

4.3 Exact Sum Capacity Outage Analysis

In this section, we analyze the sum capacity outage probability of parallel FSO-RF transmissions over the satellite-to-AP hop. The outage capacity threshold C_{o} of parallel FSO-RF transmissions is defined as the capacity guaranteed for $(1 - P_{\mathrm{o}})\%$ of channel realizations. Here, P_{o} is the outage probability, calculated as

$$P_{\mathrm{o}} = \Pr\left[C_f\ +\ C_r < C_{\mathrm{o}}\right] = \int_0^{C_{\mathrm{o}}} f_{C_f\ +\ C_r}(c)\ dc, \tag{4.8}$$

where $f_{C_f\ +\ C_r}(c)$ is the pdf of the instantaneous sum capacity of parallel FSO-RF transmission. Given that the satellite-to-AP RF and FSO links are statistically

independent, $f_{C_f\,+\,C_r}(c)$ can be evaluated as

$$f_{C_f\,+\,C_r}(c) = \int_0^c f_{C_f}(x)\; f_{C_r}(c-x)\; dx. \tag{4.9}$$

With the application of (4.5), the capacity definition for FSO communications [87]

$$C_f = BW_f\; \log_2(1+\epsilon\;\gamma_f), \tag{4.10}$$

and the power transformation of random variables, the pdf of the instantaneous capacity of the FSO link is derived after some algebraic manipulations, as [88, eq. (14)]

$$f_{C_f}(c) = \frac{\ln(2)\;\;\xi^2\;2^{c/BW_f}}{BW_f\, b\;\Gamma(\alpha)\;\Gamma(\beta)}\left(2^{c/BW_f}-1\right)^{-1} \times G_{1,3}^{3,0}\left(\alpha\beta k\left(\frac{2^{c/BW_f}-1}{\epsilon\;\mu_b}\right)^{\frac{1}{b}}\middle|\begin{matrix}\xi^2+1\\ \\ \xi^2,\alpha,\beta\end{matrix}\right), \tag{4.11}$$

where BW_f indicates the FSO link bandwidth and ϵ is a constant, which is defined as $\epsilon = e/(2\pi)$ for IM/DD and $\epsilon = 1$ for HD. The pdf of the instantaneous capacity of the RF link is similarly derived using (4.7) as

$$f_{C_r}(c) = \frac{\ln 2\;\mathcal{F}\;\exp(-K)\;2^{c/BW_r}}{BW_r}\sum_{i=0}^{\infty}\frac{(-\mathcal{F})^i}{i!}\;\sum_{j=0}^{\infty}\frac{(K\mathcal{F})^j}{(j!)^2}\;\left(2^{c/BW_r}-1\right)^{i+j}, \tag{4.12}$$

where BW_r denotes the RF link bandwidth. The pdf of the instantaneous sum capacity is analytically expressed, after some algebraic manipulations, as given by (4.13) (see Appendix A for derivation details). Note that $\mathcal{X}$, $\mathcal{E}$, $\mathcal{B}^1$, and $\mathcal{B}^2$ are defined in Table 4.1.

$$f_{C_{f^+}\ C_r}(c) = \frac{\ln(2)\mathcal{X}(K+1)\exp(-K)}{BW_r\ \ \bar{\gamma}_r}\sum_{i=0}^{\infty}\frac{(-\mathcal{F})^i}{i!}\sum_{j=0}^{\infty}\frac{(K\mathcal{F})^j}{(j!)^2}\sum_{m=0}^{i+j}\binom{i+j}{m}\Big(-1\Big)^{i+j-m}$$

$$\sum_{n=0}^{\infty}\frac{\left(\frac{(m+1)\ln(2)}{BW_r}\right)^n}{n!}\sum_{v=0}^{n}\binom{n}{v}(-1)^{n-v}\Bigg[\ \left(\frac{BW_f}{\ln(2)}\ln(a_1+1)\right)^{n-v}C^v$$

$$G_{b+1,3b+1}^{3b,1}\left(\mathcal{E}\ \frac{2^{C/BW_f}-1}{\epsilon\ \mu_{_b}}\middle|\begin{matrix}1,\mathcal{B}^1\\ \\ \mathcal{B}^2,0\end{matrix}\right)+\mathcal{A}_1\left(\frac{BW_f}{\ln(2)}\right)^{n-v}C^v\left(2^{C/BW_f}-1\right)^d$$

$$G_{b+1,3b+1}^{3b,1}\left(\mathcal{E}\ \frac{2^{C/BW_f}-1}{\epsilon\ \mu_{_b}}\middle|\begin{matrix}1-d,\mathcal{B}^1\\ \\ \mathcal{B}^2,-d\end{matrix}\right)\Bigg]. \quad (4.13)$$

Substituting (4.13) in (4.8), changing variable $y = 2^{c/BW_f} - 1$, adjusting integral limits, and applying series expansion to $2^{-y/BW_f}$ using [52, eq. (1.211.2)], the capacity outage probability of the parallel FSO-RF SatCom can be written in the form

$$P_{\mathrm{o}}\ =\ I_{_1}\ +\ I_{_2}, \quad (4.14)$$

where

$$I_{_1} = \int_0^{2^{C_{\mathrm{o}}/BW_f}-1}\mathcal{X}\mathcal{A}_2\left(\frac{BW_f}{\ln 2}\ln(a_1+1)\right)^{n-v}\sum_{h=0}^{\infty}\frac{\left(\frac{-\ln(2)}{BW_f}\right)^h}{h!}\left(\frac{BW_f}{\ln(2)}\right)^{v+h+1}$$

$$\Big(\ln(y+1)\Big)^{v+h}G_{b+1,3b+1}^{3b,1}\left(\mathcal{E}\ \frac{y}{\epsilon\mu_{_b}}\middle|\begin{matrix}1,\mathcal{B}^1\\ \\ \mathcal{B}^2,0\end{matrix}\right)dy, \quad (4.15)$$

and

$$I_2 = \int_0^{2^{C_o/BW_f}-1} \mathcal{X}\mathcal{A}_1\mathcal{A}_2\left(\frac{BW_f}{\ln 2}\right)^{n-v} \sum_{h=0}^{\infty} \frac{\left(\frac{-\ln(2)}{BW_f}\right)^h}{h!} \left(\frac{BW_f}{\ln(2)}\right)^{v+h+1} y^d \left(\ln(y+1)\right)^{v+h} G_{b+1,3b+1}^{3b,1}\left(\mathcal{E}\,\frac{y}{\epsilon\mu}\,\middle|\, \begin{matrix} 1-d, \mathcal{B}^1 \\ \mathcal{B}^2, -d \end{matrix}\right) dy, \quad (4.16)$$

respectively. The analytical expressions of I_1 and I_2 are obtained, using [55, eq. (07.34.21.0084.01)] and Taylor series expansion of $(\ln(y+1))^{v+h}$ about a constant a_2 (see Appendix B), and some algebraic manipulations, as in (4.17) and (4.18), respectively. According to (4.35), we set $a_2 = 0.788$ to ensure the convergence of the Taylor series, assuming a capacity threshold of 1.5 Gbps. Note that the infinite summations in (4.17) and (4.18) are convergent since their terms are decreasing at

the rate of $\frac{1}{i!}$, $\frac{1}{j!}$, $\frac{1}{n!}$, and $\frac{1}{h!}$.

$$I_{_1} = \frac{\ln(2)\mathcal{X}\ (K+1)\exp(-K)}{BW_r\ \ \bar{\gamma}_r}\ \sum_{i=0}^{\infty}\frac{(-\mathcal{F})^i}{i!}\sum_{j=0}^{\infty}\frac{(K\mathcal{F})^j}{(j!)^2}\sum_{m=0}^{i+j}\binom{i+j}{m}\Big(-1\Big)^{i+j-m}$$

$$\sum_{n=0}^{\infty}\frac{\left(\frac{(m+1)\ln(2)}{BW_r}\right)^n}{n!}\sum_{v=0}^{n}\binom{n}{v}(-1)^{n-v}\sum_{h=0}^{\infty}\frac{(-1)^h}{h!}\left(\frac{BW_f}{\ln(2)}\right)^{v+1}\left[\left(\frac{BW_f}{\ln(2)}\ln(a_1+1)\right)^{n-v}\right.$$

$$\Big(\ln(a_2+1)\Big)^{v+h}\Big(2^{C_{\mathrm{O}}/BW_f}-1\Big)\,G^{3b,2}_{b+2,3b+2}\left(\mathcal{E}\ \frac{2^{C_{\mathrm{O}}/BW_f}-1}{\epsilon\ \mu_{_b}}\middle|\begin{matrix}0,1,\mathcal{B}^1\\ \\ \mathcal{B}^2,0,-1\end{matrix}\right)$$

$$\left.+\mathcal{A}_3\Big(2^{C_{\mathrm{O}}/BW_f}-1\Big)^{1+g}\,G^{3b,2}_{b+2,3b+2}\left(\mathcal{E}\ \frac{2^{C_{\mathrm{O}}/BW_f}-1}{\epsilon\ \mu_{_b}}\middle|\begin{matrix}-g,1,\mathcal{B}^1\\ \\ \mathcal{B}^2,0,-1-g\end{matrix}\right)\ \right]. \quad (4.17)$$

$$I_{_2} = \frac{\ln(2)\mathcal{X}\mathcal{A}_1(K+1)\exp(-K)}{BW_r\ \ \bar{\gamma}_r}\sum_{i=0}^{\infty}\frac{(-\mathcal{F})^i}{i!}\sum_{j=0}^{\infty}\frac{(K\mathcal{F})^j}{(j!)^2}\sum_{m=0}^{i+j}\binom{i+j}{m}\Big(-1\Big)^{i+j-m}$$
$$\sum_{n=0}^{\infty}\frac{\left(\frac{(m+1)\ln(2)}{BW_r}\right)^n}{n!}\sum_{v=0}^{n}\binom{n}{v}\sum_{h=0}^{\infty}\frac{(-1)^{n-v+h}}{h!}\left(\frac{BW_f}{\ln(2)}\right)^{n+1}\Bigg[\Big(\ln(a_2+1)\Big)^{v+h}$$
$$\Big(2^{C_{\rm o}/BW_f}-1\Big)^{1+d}\,G^{3b,2}_{b+2,3b+2}\left(\mathcal{E}\,\frac{2^{C_{\rm o}/BW_f}-1}{\epsilon\ \mu_{_b}}\,\middle|\,\begin{matrix}-d,1-d,\mathcal{B}^1\\ \mathcal{B}^2,-d,-1-d\end{matrix}\right)$$
$$+\ \mathcal{A}_3\ \Big(2^{C_{\rm o}/BW_f}-1\Big)^{1+d+g}\,G^{3b,2}_{b+2,\ 3b+2}\left(\mathcal{E}\,\frac{2^{C_{\rm o}/BW_f}-1}{\epsilon\ \mu_{_b}}\,\middle|\,\begin{matrix}-d-g,1-d,\mathcal{B}^1\\ \mathcal{B}^2,-d,-1-d-g\end{matrix}\right)\Bigg]. \tag{4.18}$$

4.4 Asymptotic Sum Capacity Outage Analysis

We derive a simplified asymptotic expression for the sum capacity outage probability in this section to gain better insights into the behavior of parallel transmission system at higher SNRs. After applying asymptotic expansion of the Meijer G-function [52, eq. (9.303)], the asymptotic capacity outage probability can be written, by removing the high-order terms, as

$$P_{{\rm o},a} = \sum_{k=1}^{3b}\frac{4\ \mathcal{X}\ (K+1)\ \exp(-K)\ BW_f\ \Big(2^{C_{\rm o}/BW_f}-1\Big)}{BW_r\ \bar{\gamma}_r}$$
$$\times\ \frac{\mathcal{A}_4}{\mathcal{B}^{2,k}\ (1+\mathcal{B}^{2,k})}\left(\mathcal{E}\frac{2^{C_{\rm o}/BW_f}-1}{\epsilon\ \mu_{_b}}\right)^{\mathcal{B}^{2,k}}, \tag{4.19}$$

where $\mathcal{A}_4 = \frac{\prod_{J=1;J\neq k}^{3b}\Gamma\left(\mathcal{B}^{2,J}-\mathcal{B}^{2,k}\right)}{\prod_{J=1}^{b}\Gamma\left(\mathcal{B}^{1,J}-\mathcal{B}^{2,k}\right)}$. We can conclude from (4.19) that $P_{\mathrm{o},a} \propto \left(\bar{\gamma}_r\right)^{-1}\left(\mu_b\right)^{\mathcal{B}^2}$. Therefore, the diversity gain of the SatCom system is given by

$$\mathcal{D} = \min\left(\frac{\xi^2}{b}, \frac{\alpha}{b}, \frac{\beta}{b}\right) \ + \ 1. \tag{4.20}$$

4.5 Numerical Results

We now present selected numerical examples to demonstrate the performance of parallel FSO and RF transmissions for SatCom systems. We set the system parameters as given in Table 4.2 while assuming an IM/DD receiver. Note that the infinite summations in (4.17) and (4.18) require 10 terms to converge with a convergence error of 5×10^{-9}.

In Figure 4.2, we study the impact of power allocation by plotting the outage probability as a function of the power allocation ratio to the FSO link under different weather conditions. The attenuation coefficients due to weather effects are given in Table 4.2 [64]. We assume a 45$^{\mathrm{o}}$ satellite zenith angle and a total transmit power of 12 dBW. As we can see, there is an optimal value of the ratio at which the system achieves minimum outage probability for target transmission rate. In addition, the optimal value, ρ^*, decreases as the weather becomes more severe, i.e., ρ^* equals 0.8 and 0.7 for clear air and light rain, respectively. In heavy fog, the FSO link is unavailable, and the transmission system should allocate all transmit power to the RF link, leading to $\rho^* = 0$. Notably, even under clear weather conditions, allocating a portion of the total power to the RF link can achieve better outage performance than the scenario with the total power allocated to the FSO link, as the FSO transmission is susceptible to turbulence, scintillation, and pointing errors. Furthermore, while varying with the weather conditions, the optimal value for the power ratio, ρ^*, is insensitive to the value of the target transmission rate.

Table 4.2: Simulation parameters

Parameter	Value
Satellite altitude	620 km
Access point aperture height	2 m
Satellite zenith angle	45°
FSO subsystem	
FSO wavelength	1550 nm
FSO link bandwidth	1 GHz
Telescope aperture diameter	20 cm
Transmit telescope gain	75 dB
Receive telescope gain	75 dB
Variance of background noise	250μ W [63]
Beam radius at transmitter	2 cm
Optical-to-electrical efficiency	0.8
Pointing error coefficient	5.2
Wind speed	21 m/s
Ground level turbulence	$1.7 \times 10^{-14}\mathrm{m}^{\frac{-2}{3}}$
RF subsystem [64]	
RF carrier frequency	30 GHz
RF link bandwidth	300 MHz
Rician factor	6
Receive antenna gain	52 dB
Transmit antenna gain	52 dB
Noise figure	5 dB
Noise power spectral density	-114 dBW/MHz
Weather dependent variables [64]	
Ligh rain:	
- Ground level turbulence	$0.6 \times 10^{-14}m^{\frac{-2}{3}}$
- FSO attenuation	1.98 dB/km
- RF attenuation	1.50 dB/km
- Effective distance	1 km
Heavy fog:	
- Ground level turbulence	$0.1 \times 10^{-14}m^{\frac{-2}{3}}$
- FSO attenuation	113.2 dB/km
- RF attenuation	0 dB/km
- Effective distance	1 km

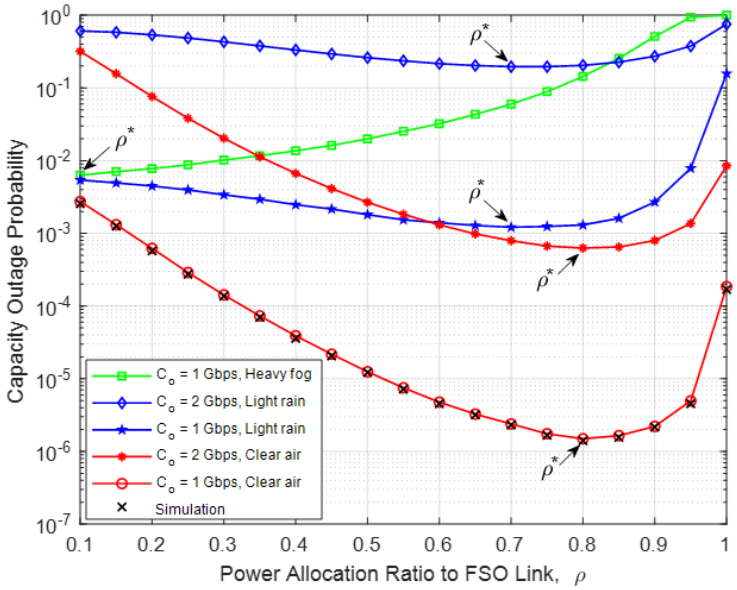

Figure 4.2: Optimum ratio of total power assigned for FSO link.

The strength of atmospheric turbulence depends mainly on the distribution of aerosol particles and is usually measured by the ground level turbulence $C_n^2(0)$ [47]. In Figure 4.3, we investigate the effect of strong turbulence ($C_n^2(0) = 9.64 \times 10^{-13}\mathrm{m}^{\frac{-2}{3}}$, $\alpha = 2.21$, $\beta = 3.48$) and moderate turbulence ($C_n^2(0) = 4.69 \times 10^{-13}\mathrm{m}^{\frac{-2}{3}}$, $\alpha = 4.28$, $\beta = 5.62$) on the proposed parallel transmission system. We also compare IM/DD and HD detection schemes, assuming a capacity threshold of 1.5 Gbps, a wind speed of 41 m/s, a 45° satellite zenith angle, and the optimal ratio ρ^* of 0.8 under clear air conditions. The asymptotic expression is presented to verify its accuracy. As we can see, the increase in $C_n^2(0)$ value has a negative impact on the outage probability. The transmission system with HD scheme suffers a performance loss of about 5 dB when $C_n^2(0)$ increases from $4.69 \times 10^{-13}\mathrm{m}^{\frac{-2}{3}}$ to $9.64 \times 10^{-13}\mathrm{m}^{\frac{-2}{3}}$, at an outage probability of 10^{-6}. Also, the HD scheme suffers a larger outage probability penalty when compared to the IM/DD scheme. Nevertheless, HD scheme maintains a performance advantage over IM/DD scheme, because of its coherent detection nature. From Figure 4.3, we also calculate the diversity gain by taking the logarithm of the outage probabilities obtained at the related transmit power levels. We obtain

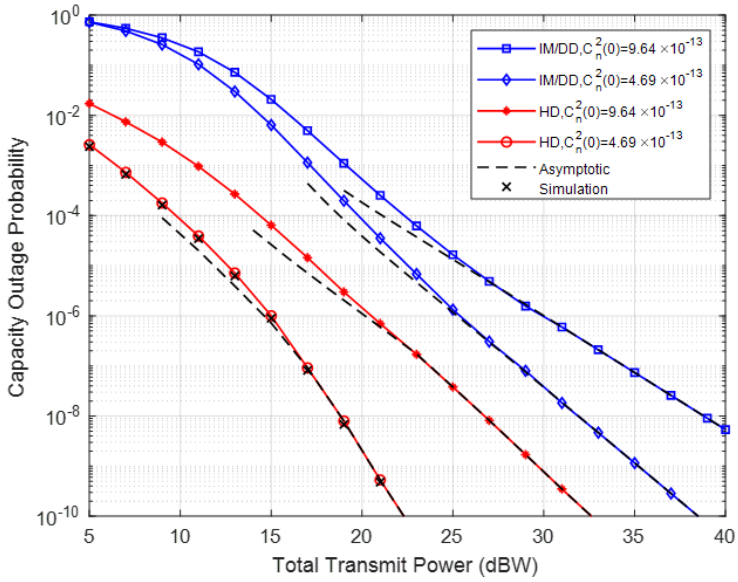

Figure 4.3: Effect of ground level turbulence.

7.8×10^{-8} and 1.2×10^{-5} for the IM/DD scheme under strong turbulence effects at 35 dBW and 25 dBW, respectively. This leads to a diversity gain of $2.18 \approx \mathcal{D} = 2.11$. The diversity gain increases to $3.09 \approx \mathcal{D} = 3.14$ under moderate turbulence effects. Similarly, we obtain a diversity gain of $3.23 \approx \mathcal{D} = 3.21$ and $5.34 \approx \mathcal{D} = 5.28$ for the HD scheme under strong and moderate turbulence effects, respectively.

Note that the level of laser radiation to which a person may be exposed without any hazardous effect is a few tens of watts per square meter for about 15 min, i.e., $50\,W/m^2$. This power level decreases with an increase in the duration of exposure [38, 89]. Figure 4.4 plots the capacity outage probability as a function of the total transmit power. We assume a 45° satellite zenith angle, an outage capacity threshold of 1.5 Gbps, a power allocation ratio of 0.8, and atmospheric turbulence parameters of $\alpha = 15.67$ and $\beta = 17.49$. For comparison purposes, the results of hybrid FSO/RF, FSO-only, and RF-only systems are also plotted. Note that hybrid FSO/RF and parallel FSO-RF transmission systems host FSO and RF transceivers at the satellite and access point, which increases the system cost when compared to FSO-only transmission system. On the other hand, the parallel FSO-RF trans-

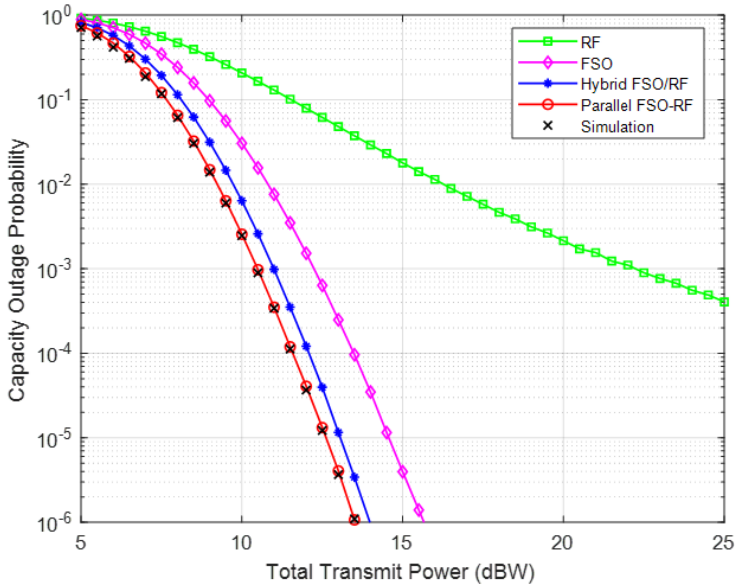

Figure 4.4: Comparison of various SatCom systems.

mission scheme outperforms the FSO transmission [25] by about 2 dB and hybrid FSO/RF transmission by about 0.5 dB for a target transmission rate of 1.5 Gbps at an outage probability of 10^{-5}. The performance advantage of parallel transmission over hybrid FSO/RF transmission is because that hybrid FSO/RF transmission has to use full transmit power on either the FSO or RF link. In addition, the RF link in the proposed scheme can serve the users over a wide geographical area to maintain ubiquitous coverage. From Figure 4.4, a diversity gain of $9 \approx \mathcal{D} = 8.83$ is also obtained under weaker turbulence effects. Furthermore, the analytical results match the Monte Carlo simulation results well.

As another numerical example, in Figure 4.5, the outage performance of parallel transmission is plotted as a function of capacity threshold values, assuming a 45° satellite zenith angle, a total transmit power of 12 dBW, and an FSO link power allocation ratio of 0.8. From this figure, we see that multiplexing traffics through the RF link will improve the system's reliability when the capacity threshold is large. At a capacity threshold of 2.2 Gbps, the parallel FSO-RF transmission achieves an outage probability of 1.6×10^{-3} compared to 1.4×10^{-2} for both hybrid FSO/RF

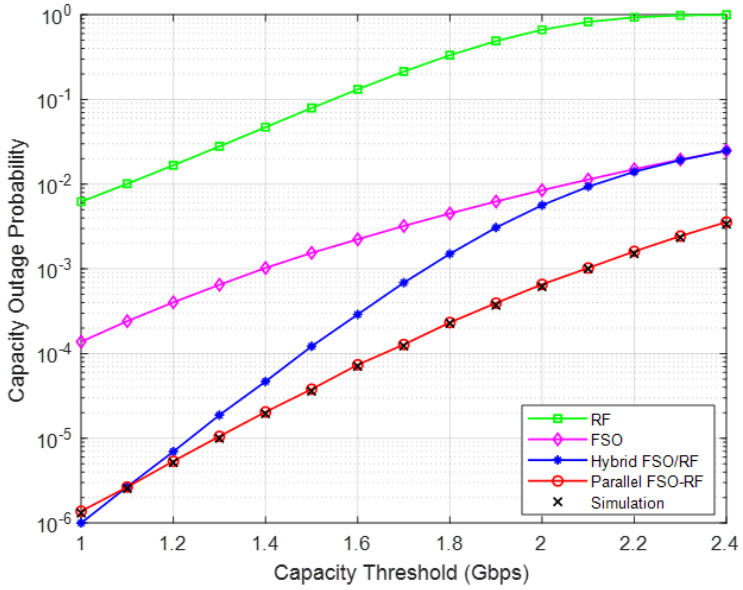

Figure 4.5: Effect of capacity threshold values.

and FSO transmissions. This is because the RF link alone cannot support such a high data rate due to its limited bandwidth. Therefore, switching back to the RF link leads to a marginal improvement in outage probability over FSO transmission. On the other hand, hybrid FSO/RF transmission with hard switching can achieve better performance than parallel FSO-RF transmission when the capacity threshold is very small, say less than 1 Gbps. The hybrid FSO/RF transmission can support such a small data rate with full transmit power on either the FSO or RF link. As such, we can conduct that parallel transmission is more desirable where the capacity demand is high, i.e., hot-spot areas.

Appendix A: Pdf of the Sum Received Capacity with Parallel FSO-RF Transmissions

This appendix derives the pdf of the instantaneous sum capacity $f_{C_f + C_r}(c)$. After applying the binomial expansion [52, eq. (1.111)], we can rewrite $f_{C_r}(c)$ in (4.12) as

$$f_{C_r}(c) = \frac{\ln 2 \ \mathcal{F} \ \exp(-K)}{BW_r} \ \sum_{i=0}^{\infty} \frac{(-\mathcal{F})^i}{i!} \sum_{j=0}^{\infty} \frac{(K\mathcal{F})^j}{(j!)^2} \sum_{m=0}^{i+j} \binom{i+j}{m} \Big(-1\Big)^{i+j-m} \Big(2^{c/BW_r}\Big)^{m+1}. \quad (4.21)$$

Applying series expansion to $\Big(2^{c/BW_r}\Big)^{m+1}$ using [52, eq. (1.211.2)], the pdf in (4.21) can be rewritten after some algebraic manipulations as

$$f_{C_r}(c) = \frac{\ln 2 \ \mathcal{F} \ \exp(-K)}{BW_r} \ \sum_{i=0}^{\infty} \frac{(-\mathcal{F})^i}{i!} \sum_{j=0}^{\infty} \frac{(K\mathcal{F})^j}{(j!)^2} \sum_{m=0}^{i+j} \binom{i+j}{m} \Big(-1\Big)^{i+j-m} \sum_{n=0}^{\infty} \frac{\Big(\frac{(m+1)\ln 2}{BW_r}\Big)^n}{n!} \ c^n. \quad (4.22)$$

After substituting (4.11) and (4.22) in (4.9), using the binomial expansion given by [52, eq. (1.111)] to $(c-x)^n$, along with changing variable $t = 2^{x/BW_f} - 1$ and adjusting integral limits, $f_{C_f \ + \ C_r}(c)$ will have the form

$$f_{C_f \ + \ C_r}(c) = \int_0^{2^{c/BW_f}-1} \mathcal{A}_2 \ c^v \ \left(\frac{BW_f}{\ln 2}\ln(t+1)\right)^{n-v} \frac{\xi^2 \ t^{-1}}{b\Gamma(\alpha)\Gamma(\beta)} \ G_{1,3}^{3,0}\left(\alpha\beta k\left(\frac{t}{\epsilon\mu_b}\right)^{\frac{1}{b}} \middle| \begin{matrix} \xi^2+1 \\ \xi^2, \alpha, \beta \end{matrix}\right) dt, \quad (4.23)$$

where $\mathcal{A}_2$ denotes the summation operation as

$$\mathcal{A}_2 = \frac{\ln 2\ \mathcal{F}\ \exp(-K)}{BW_r}\ \sum_{i=0}^{\infty}\frac{(-\mathcal{F})^i}{i!}\sum_{j=0}^{\infty}\frac{(K\mathcal{F})^j}{(j!)^2}\sum_{m=0}^{i+j}\binom{i+j}{m}$$
$$\Big(-1\Big)^{i+j-m}\ \sum_{n=0}^{\infty}\frac{\left(\frac{(m+1)\ln 2}{BW_r}\right)^n}{n!}\sum_{v=0}^{n}\binom{n}{v}(-1)^{n-v}. \quad (4.24)$$

To evaluate the integral in (4.23), $\Big(\ln(t+1)\Big)^{n-v}$ is replaced by its Taylor series given in Appendix B of this chapter. Now, the integral in (4.23) can be expressed in the form $f_{C_f\ +\ C_r}(c) = I_3 + I_4$, where

$$I_3 = \int_0^{2^{c/BW_f}-1}\mathcal{A}_1\ c^v\ \left(\frac{BW_f}{\ln 2}\ln(a_1+1)\right)^{n-v}\frac{\xi^2\ t^{-1}}{b\Gamma(\alpha)\Gamma(\beta)}$$
$$G_{1,3}^{3,0}\left(\alpha\beta k\left(\frac{t}{\epsilon\ \mu_b}\right)^{\frac{1}{b}}\middle|\begin{matrix}\xi^2+1\\ \xi^2,\alpha,\beta\end{matrix}\right)\ dt \quad (4.25)$$

and

$$I_4 = \int_0^{2^{c/BW_f}-1}\mathcal{A}_1\ \mathcal{A}_2\ c^v\ \left(\frac{BW_f}{\ln 2}\right)^{n-v}\frac{\xi^2\ t^{d-1}}{b\Gamma(\alpha)\Gamma(\beta)}$$
$$G_{1,3}^{3,0}\left(\alpha\beta k\left(\frac{t}{\epsilon\ \mu_b}\right)^{\frac{1}{b}}\middle|\begin{matrix}\xi^2+1\\ \xi^2,\alpha,\beta\end{matrix}\right)\ dt, \quad (4.26)$$

respectively. The analytical expression of I_3 and I_4 are obtained after some algebraic

manipulations, using [55, eq. (07.34.21.0084.01)] as

$$I_{_3} = \mathcal{X}\ \mathcal{A}_2 \left(\frac{BW_f}{\ln 2}\ln(a_1+1)\right)^{n-v}\ c^v\ \ G^{\ 3b,\ \ 1}_{b+1,\ 3b+1}\left(\mathcal{E}\ \frac{2^{c/BW_f}-1}{\epsilon\ \mu_{_b}}\ \middle|\ \begin{matrix} 1 & , & \mathcal{B}^1 \\ \mathcal{B}^2 & , & 0 \end{matrix}\right) \tag{4.27}$$

and

$$I_{_4} = \mathcal{X}\ \mathcal{A}_1\ \mathcal{A}_2 \left(\frac{BW_f}{\ln 2}\right)^{n-v}\ c^v\ \left(2^{c/BW_f}-1\right)^d \ G^{\ 3b,\ \ 1}_{b+1,\ 3b+1}\left(\mathcal{E}\ \frac{2^{c/BW_f}-1}{\epsilon\ \mu_{_b}}\ \middle|\ \begin{matrix} 1-d & , & \mathcal{B}^1 \\ \mathcal{B}^2 & , & -d \end{matrix}\right). \tag{4.28}$$

Note that a_1 is a constant satisfying (4.35) of Appendix B. We set $a_1 = 0.788$ to ensure the convergence of the Taylor series.

Appendix B: Taylor Series Expansion of $(\ln(t+1))^n$

Applying Taylor series expansion around a defined as

$$f(t) = \sum_{u=0}^{\infty}\ f^{(u)}(a)\frac{(t-a)^u}{u!}, \tag{4.29}$$

$\Big(\ln(t+1)\Big)^n$ is written as

$$\begin{aligned}\Big(\ln(t+1)\Big)^n &= \Big(\ln(a+1)\Big)^n \\ &+ \frac{(n)}{(a+1)}\Big(\ln(a+1)\Big)^{n-1}\frac{(t-a)}{1!} \\ &+ \frac{(n)(n-1)}{(a+1)^2}\Big(\ln(a+1)\Big)^{n-2}\ \frac{(t-a)^2}{2!} \\ &+ \frac{(n)(n-1)(n-2)}{(a+1)^3}\Big(\ln(a+1)\Big)^{n-3}\ \frac{(t-a)^3}{3!}+\ldots \end{aligned} \tag{4.30}$$

After some algebraic manipulations, $\Big(\ln(t+1)\Big)^n$ can be written as

$$\begin{aligned}\Big(\ln(t+1)\Big)^n &= \Big(\ln(a+1)\Big)^n \\ &+ \sum_{z=1}^{\infty}\frac{(n)!}{(a+1)^z(n-z)!}\Big(\ln(a+1)\Big)^{n-z}\ \Big(t-a\Big)^z, \end{aligned} \tag{4.31}$$

Applying binomial expansion using [52, eq. (1.111)], $(t-a)^z$ can be written as

$$\Big(t-a\Big)^z = \sum_{d=0}^{z}\binom{z}{d}\ \Big(-a\Big)^{z-d}\ t^d. \tag{4.32}$$

Then, $\Big(\ln(t+1)\Big)^n$ is given by

$$\Big(\ln(t+1)\Big)^n = \Big(\ln(a+1)\Big)^n\ +\ \mathcal{A}_1\ t^d, \tag{4.33}$$

where $\mathcal{A}_1$ denotes the double summation operation as

$$\mathcal{A}_1 = \sum_{z=1}^{\infty} \frac{(n)!}{(1+a)^z (n-z)!} \Big(\ln(a+1) \Big)^{n-z} \sum_{d=0}^{z} \binom{z}{d} \frac{(-a)^{z-d}}{z!}. \tag{4.34}$$

The interval of convergence, satisfying the ratio test, is given by [41, eq. (33)]

$$-1 < \frac{t-a}{(1+a)\ln(1+a)} < 1. \tag{4.35}$$

The value of a depends on the range of t, which varies from 0 to $2^{c/BW_f} - 1$. For C_o up to 3 Gbps and an FSO link bandwidth of 1 GHz, the value of $t \in [0, 7]$, and therefore we select the corresponding value of $a \in [0, 2.5]$ satisfies the ratio test in (4.35).

Chapter 5

Conclusions and Future Work

In this chapter, we conclude the thesis by summarizing the accomplished work and suggesting further potential research topics.

5.1 Conclusions

In this thesis, we first present a novel space-air-ground FSO transmission strategy for SatCom systems. In particular, by dispatching a HAP relay above the ground station, we can significantly mitigate the atmospheric turbulence effects and achieve high-performance FSO transmission, regardless of the zenith angle of a satellite. We also propose a novel integrated FSO transmission network to improve FSO-link usability for SatCom. We demonstrated, using selected numerical examples, that integrating space-air-ground and single-hop FSO transmissions to a satellite can remarkably decrease the frequency of switching to a low-throughput RF link, maximally benefiting the higher transmission rate of FSO links. The probability of RF-link usage is decreased from 5×10^{-3} for SAG-FSO/RF transmission [31] to 7×10^{-6} for our proposed SAG-FSO/SH-FSO/RF transmission system. Despite its vulnerability to atmospheric turbulence, the SH-FSO transmission contributes to improved system performance.

Taking advantage of the superior performance of SAG-FSO transmission, we propose to combine SAG-FSO transmission with site diversity to mitigate weather effects and increase the reliability of SAG-FSO networks even further. To achieve a similar diversity benefit with reduced cost and lower complexity, we also propose a hybrid SAG-FSO/RF transmission system with multiple HAP relays. Meanwhile, the ground–HAP links may experience correlated atmospheric turbulence. The obtained results illustrate that, despite the correlation adversely affecting performance, the transmission system still maintains a considerable gain over hybrid FSO/RF and single HAP systems. In addition, the analysis revealed that changing the correlation coefficient value doesn't affect the transmission system's diversity gain but degrades the SEP performance. Compared to the non-correlated case, the transmission system suffers a performance loss of about 2.5 dB when the correlation coefficient increases from 0 to 0.8 for the HD scheme, at an average SEP of 1×10^{-10}. Furthermore, the correlation effect is more noticeable for weak turbulence scenarios than for strong turbulence environments.

To satisfy capacity and availability requirements for remote access, we proposed parallel FSO and RF transmissions for non-terrestrial networks. In particular, the FSO link is used for high-rate transmission to the access point, whereas the RF link is used to support all users inside or outside the coverage of the access point. The proposed scheme with parallel transmission can achieve a target transmission rate of 2.2 Gbps with an outage probability of 1.6×10^{-3} compared to 1.4×10^{-2} for hybrid FSO/RF transmission. From these results, we conclude that SatCom systems with parallel FSO-RF transmissions can increase the throughput to hot-spot regions with high traffic demand while maintaining ubiquitous coverage via RF links.

5.2 Future Work

The ideas proposed in this thesis can be expanded in the future in different directions as follows:

5.2.1 HAP-Based Networks for Broadband Internet Access in Remote Communities

There is a pressing need to provide reliable broadband Internet access to rural and remote communities and achieve Internet access equality. HAPs network can provide an effective solution [90, 91]. In this research direction, we propose a novel network architecture to deliver reliable broadband Internet access for rural and remote areas using HAP-based multi-hop transmission. The key is to exploit hybrid FSO/RF transmission and switching-based FSO transmission via multiple HAP relays. The proposed network design can support high-speed connections to access points in densely populated regions via FSO links. To maintain ubiquitous coverage, the RF link is used to serve lower-demand users outside the coverage of access points due to its wider beamwidth.

It is worth noting that the global HAPs market is expected to reach US$6.5 billion by 2030 [92], which helps reduce the manufacturing and operation costs of HAPs. The proposed HAP-based solution will serve as an attractive alternative to LEO satellite systems for connectivity provision in remote areas.

5.2.2 Hybrid Space-Air-Ground-Underwater FSO/RF Transmission for Future Wireless Connectivity

We have considered hybrid SAG-FSO/RF transmission in the design of advanced SatCom systems. To provide trustworthy support for future global connectivity, our proposed system designs can be extended to include underwater communications.

RF links are a good complement to FSO links when propagating through the atmosphere. Only FSO transmissions, on the other hand, could propagate through the water. Innovative solutions are required to solidify the FSO link for underwater communications and increase end-to-end system throughput. Many open research topics in this field, including channel modelling, performance limitations, and trade-off studies such as data rate and communication range, can be considered in future work [93–96].

5.2.3 Development of Advanced Deep Reinforcement Learning Algorithms for Optimal HAP Hovering Location

In this research direction, we will apply and develop advanced machine learning tools to dynamically determine the HAP position to mitigate beam wandering, turbulence, and weather effects such as clouds. Flying HAP is more likely to establish a line-of-sight link with a ground station by adjusting its hovering location in 3D space, thus providing favorable link conditions with the ground station. We propose using deep reinforcement learning (DRL) algorithms to train a smart agent that can determine optimal HAP hovering locations with minimal computation based on environmental observation.

Most existing works only study the deployment of HAPs to maximize their coverage on the ground and improve the spectrum and energy efficiency [97–99]. Based on the user clustering, the HAPs were first deployed at the centroids of the clusters, and then the altitudes of the HAPs were optimized under ideal transmission scenarios. In the proposed research direction, we will address transmission system design in a practical operating environment of atmospheric turbulence and weather effects.

Bibliography

[1] I. T. Union, "Measuring Digital Development. Facts and Figures 2022," *Technical Report International Telecommunication Union (ITU)*, Geneva, Switzerland, 2022.

[2] G. Geraci, D. Lopez-Perez, M. Benzaghta, and S. Chatzinotas, "Integrating terrestrial and non-terrestrial networks: 3D opportunities and challenges," *IEEE Communications Magazine*, vol. 61, no. 4, pp. 42–48, 2022.

[3] M. M. Azari, S. Solanki, S. Chatzinotas, O. Kodheli, H. Sallouha, A. Colpaert, J. F. M. Montoya, S. Pollin, A. Haqiqatnejad, A. Mostaani, E. Lagunas, and B. Ottersten, "Evolution of non-terrestrial networks from 5G to 6G: A survey," *IEEE Communications Surveys & Tutorials*, vol. 24, no. 4, pp. 2633–2672, 2022.

[4] T. Ahmmed, A. Alidadi, Z. Zhang, A. U. Chaudhry, and H. Yanikomeroglu, "The digital divide in Canada and the role of LEO satellites in bridging the gap," *IEEE Communications Magazine*, vol. 60, no. 6, pp. 24–30, 2022.

[5] B. Al Homssi, A. Al-Hourani, K. Wang, P. Conder, S. Kandeepan, J. Choi, B. Allen, and B. Moores, "Next generation mega satellite networks for access equality: Opportunities, challenges, and performance," *IEEE Communications Magazine*, vol. 60, no. 4, pp. 18–24, 2022.

[6] X. Lin, S. Rommer, S. Euler, E. A. Yavuz, and R. S. Karlsson, "5G from space: An overview of 3GPP non-terrestrial networks," *IEEE Communications Standards Magazine*, vol. 5, no. 4, pp. 147–153, 2021.

[7] G. Araniti, A. Iera, S. Pizzi, and F. Rinaldi, "Toward 6G non-terrestrial networks," *IEEE Network*, vol. 36, no. 1, pp. 113–120, 2021.

[8] G. M. Capez, S. Henn, J. A. Fraire, and R. Garello, "Sparse satellite constellation design for global and regional direct-to-satellite IoT services," *IEEE Transactions on Aerospace and Electronic Systems*, vol. 58, no. 5, pp. 3786–3801, 2022.

[9] M. Höyhtyä, S. Boumard, A. Yastrebova, P. Järvensivu, M. Kiviranta, and A. Anttonen, "Sustainable satellite communications in the 6G era: A european view for multi-layer systems and space safety," *IEEE Access*, vol. 10, pp. 99 973–100 005, 2022.

[10] K. Liolis, A. Geurtz, R. Sperber, D. Schulz, S. Watts, G. Poziopoulou, B. Evans, N. Wang, O. Vidal, B. Tiomela Jou *et al.*, "Use cases and scenarios of 5G integrated satellite-terrestrial networks for enhanced mobile broadband: The SaT5G approach," *International Journal of Satellite Communications and Networking*, vol. 37, no. 2, pp. 91–112, 2019.

[11] H. Al-Hraishawi, H. Chougrani, S. Kisseleff, E. Lagunas, and S. Chatzinotas, "A survey on non-geostationary satellite systems: The communication perspective," *IEEE Communications Surveys & Tutorials*, vol. 25, no. 1, pp. 101–132, 2022.

[12] M. Y. Abdelsadek, A. U. Chaudhry, T. Darwish, E. Erdogan, G. Karabulut-Kurt, P. G. Madoery, O. B. Yahia, and H. Yanikomeroglu, "Future space networks: Toward the next giant leap for humankind," *IEEE Transactions on Communications*, vol. 71, no. 2, pp. 949–1007, 2022.

[13] S. Liu, Z. Gao, Y. Wu, D. W. K. Ng, X. Gao, K.-K. Wong, S. Chatzinotas, and B. Ottersten, "LEO satellite constellations for 5G and beyond: How will they reshape vertical domains?" *IEEE Communications Magazine*, vol. 59, no. 7, pp. 30–36, 2021.

[14] O. Kodheli, E. Lagunas, N. Maturo, S. K. Sharma, B. Shankar, J. F. M. Montoya, J. C. M. Duncan, D. Spano, S. Chatzinotas, S. Kisseleff, J. Querol, L. Lei, T. X. Vu, and G. Goussetis, "Satellite communications in the new space era: A survey and future challenges," *IEEE Communications Surveys & Tutorials*, vol. 23, no. 1, pp. 70–109, 2020.

[15] E. Lutz, "Towards the terabit/s satellite–interference issues in the user link," *International Journal of Satellite Communications and Networking*, vol. 34, no. 4, pp. 461–482, 2016.

[16] E. Zedini, A. Kammoun, and M.-S. Alouini, "Performance of multibeam very high throughput satellite systems based on FSO feeder links with HPA nonlinearity," *IEEE Transactions on Wireless Communications*, vol. 19, no. 9, pp. 5908–5923, 2020.

[17] G. K. Kurt, M. G. Khoshkholgh, S. Alfattani, A. Ibrahim, T. S. Darwish, M. S. Alam, H. Yanikomeroglu, and A. Yongacoglu, "A vision and framework for the high altitude platform station (HAPS) networks of the future," *IEEE Communications Surveys & Tutorials*, vol. 23, no. 2, pp. 729–779, 2021.

[18] G. K. Kurt and H. Yanikomeroglu, "Communication, computing, caching, and sensing for next-generation aerial delivery networks: Using a high-altitude platform station as an enabling technology," *IEEE Vehicular Technology Magazine*, vol. 16, no. 3, pp. 108–117, 2021.

[19] S. C. Arum, D. Grace, and P. D. Mitchell, "A review of wireless communication using high-altitude platforms for extended coverage and capacity," *Computer Communications*, vol. 157, pp. 232–256, 2020.

[20] M. S. Alam, G. K. Kurt, H. Yanikomeroglu, P. Zhu, and N.-D. Dao, "High altitude platform station based super macro base station constellations," *IEEE Communications Magazine*, vol. 59, no. 1, pp. 103–109, 2021.

[21] A. Dochhan, J. Poliak, J. Surof, M. Richerzhagen, H. F. Kelemu, and R. M. Calvo, "13.16 Tbit/s free-space optical transmission over 10.45 km for geostationary satellite feeder-links," in *Photonic Networks; 20th ITG-Symposium*, 2019, pp. 1–3.

[22] C. M. Schieler, K. M. Riesing, A. J. Horvath, B. C. Bilyeu, J. S. Chang, A. S. Garg, J. P. Wang, and B. S. Robinson, "200 Gbps TBIRD CubeSat downlink: Pre-flight test results," in *Free-Space Laser Communications XXXIV*, vol. 11993. SPIE, 2022, pp. 200–206.

[23] A. Trichili, M. A. Cox, B. S. Ooi, and M.-S. Alouini, "Roadmap to free space optics," *JOSA B*, vol. 37, no. 11, pp. A184–A201, 2020.

[24] N. Maharjan, N. Devkota, and B. W. Kim, "Atmospheric effects on satellite–ground free space uplink and downlink optical transmissions," *Applied Sciences*, vol. 12, no. 21, p. 10944, 2022.

[25] A. Viswanath, V. K. Jain, and S. Kar, "Analysis of Earth-to-Satellite Free-Space Optical Link Performance in the Presence of Turbulence, Beam-Wander Induced Pointing Error and Weather Conditions for Different Intensity Modulation Schemes," *IET Communications*, vol. 9, no. 18, pp. 2253–2258, 2015.

[26] M. Z. Chowdhury, M. K. Hasan, M. Shahjalal, M. T. Hossan, and Y. M. Jang, "Optical wireless hybrid networks: Trends, opportunities, challenges, and research directions," *IEEE Communications Surveys & Tutorials*, vol. 22, no. 2, pp. 930–966, 2020.

[27] O. B. Yahia, E. Erdogan, G. K. Kurt, I. Altunbas, and H. Yanikomeroglu, "A weather-dependent hybrid RF/FSO satellite communication for improved power efficiency," *IEEE Wireless Communications Letters*, vol. 11, no. 3, pp. 573–577, 2021.

[28] S. Sharma, A. Madhukumar, and R. Swaminathan, "Capacity analysis for hybrid FSO/RF networks," *Proc. IEEE Int. Symp. Inf. Theory Appl.*, vol. 55, no. 11, p. 501, 2018.

[29] N. Vishwakarma and R. Swaminathan, "Capacity analysis of adaptive combining for hybrid FSO/RF satellite communication system," in *2021 National Conference on Communications (NCC)*, 2021, pp. 1–6.

[30] N. D. Chatzidiamantis, G. K. Karagiannidis, E. E. Kriezis, and M. Matthaiou, "Diversity combining in hybrid RF/FSO systems with PSK modulation," in *2011 IEEE International Conference on Communications (ICC)*, 2011, pp. 1–6.

[31] R. Swaminathan, S. Sharma, N. Vishwakarma, and A. Madhukumar, "HAPS-based relaying for integrated space-air-ground networks with hybrid FSO/RF communication: A performance analysis," *IEEE Transactions on Aerospace and Electronic Systems*, vol. 57, no. 3, pp. 1581–1599, 2021.

[32] T. V. Nguyen, H. D. Le, N. T. Dang, and A. T. Pham, "On the design of rate adaptation for relay-assisted satellite hybrid FSO/RF systems," *IEEE Photonics Journal*, vol. 14, no. 1, pp. 1–11, 2021.

[33] S. Shah, M. Siddharth, N. Vishwakarma, R. Swaminathan, and A. Madhukumar, "Adaptive-combining-based hybrid FSO/RF satellite communication with and without HAPS," *IEEE Access*, vol. 9, pp. 81 492–81 511, 2021.

[34] R. Swaminathan, S. Sharma, and A. MadhuKumar, "Performance analysis of HAPS-based relaying for hybrid FSO/RF downlink satellite communication," in *2020 IEEE 91st Vehicular Technology Conference (VTC2020-Spring)*, 2020, pp. 1–5.

[35] J. Liu, Y. Shi, Z. M. Fadlullah, and N. Kato, "Space-Air-Ground Integrated Network: A Survey," *IEEE Communications Surveys & Tutorials*, vol. 20, no. 4, pp. 2714–2741, 2018.

[36] R. Samy, H.-C. Yang, T. Rakia, and M.-S. Alouini, "Hybrid SAG-FSO/SH-FSO/RF transmission for next-generation satellite communication systems," *IEEE Transactions on Vehicular Technology*, early access, 2023.

[37] ——, "Symbol error rate analysis of satellite communication systems with SAG-FSO/SH-FSO/RF transmission," in *2022 IEEE Global Communications Conference*, 2022, pp. 431–436.

[38] H. Kaushal and G. Kaddoum, "Optical Communication in Space: Challenges and Mitigation Techniques," *IEEE Communications Surveys & Tutorials*, vol. 19, no. 1, pp. 57–96, 2017.

[39] D. Singh and R. Swaminathan, "Comprehensive performance analysis of hybrid FSO/RF space–air–ground integrated network," *Optics Communications*, vol. 527, 2023, Art. no. 128964.

[40] D. Vasylyev, W. Vogel, and F. Moll, "Satellite-Mediated Quantum Atmospheric Links," *Physical Review A*, vol. 99, no. 5, p. 053830, 2019.

[41] R. Samy, H.-C. Yang, T. Rakia, and M.-S. Alouini, "Ergodic capacity analysis of satellite communication systems with SAG-FSO/SH-FSO/RF transmission," *IEEE Photonics Journal*, vol. 14, no. 5, pp. 1–9, 2022.

[42] H. Kaushal, V. Jain, and S. Kar, "Ground-to-satellite optical communication link performance with spatial diversity in weak atmospheric turbulence," *Fiber and Integrated Optics*, vol. 29, no. 4, pp. 315–340, 2010.

[43] H. Kaushal, S. Kar, and V. Jain, *Free Space Optical Communication*. Springer, 2017.

[44] Z. Ghassemlooy, W. Popoola, and S. Rajbhandari, *Optical Wireless Communications: System and Channel Modelling with Matlab®*. CRC press, 2019.

[45] B. Kumbhani and R. Kshetrimayum, "Error performance of two-hop decode and forward relaying systems with source and relay transmit antenna selection," *Electronics Letters*, vol. 51, no. 6, pp. 530–532, 2015.

[46] ——, "Error performance of two-hop decode and forward relaying systems with source and relay transmit antenna selection," *Electronics Letters*, vol. 51, no. 6, pp. 530–532, 2015.

[47] R. Samy, H.-C. Yang, T. Rakia, and M.-S. Alouini, "Performance analysis of hybrid SAG-FSO/RF satellite communication system," *TechRxiv. Preprint. https://doi.org/10.36227/techrxiv.19623849.v1*, 2022.

[48] I. T. Union, "Attenuation due to Clouds and Fog," Int. Telecommun. Union, Geneva, Switzerland, Tech. Rep. ITU-R P.840-8, 2019.

[49] R. Priyadarshani, M. R. Bhatnagar, Z. Ghassemlooy, and S. Zvanovec, "Effect of correlation on BER performance of the FSO-MISO system with repetition coding over gamma–gamma turbulence," *IEEE Photonics Journal*, vol. 9, no. 5, pp. 1–15, 2017.

[50] G. T. Djordjevic, M. I. Petkovic, J. A. Anastasov, P. N. Ivanis, and Z. M. Marjanovic, "On the effects of correlation on outage performance of FSO-unbalanced multibranch SC receiver," *IEEE Photonics Technology Letters*, vol. 28, no. 12, pp. 1348–1351, 2016.

[51] I. S. Ansari, F. Yilmaz, and M.-S. Alouini, "Performance analysis of FSO links over unified Gamma-Gamma turbulence channels," in *2015 IEEE 81st Vehicular Technology Conference (VTC Spring)*, 2015, pp. 1–5.

[52] D. Zwillinger and A. Jeffrey, *Table of Integrals, Series, and Products*. Elsevier, 2007.

[53] J. Ma, K. Li, L. Tan, S. Yu, and Y. Cao, "Performance analysis of satellite-to-ground downlink coherent optical communications with spatial diversity over Gamma–Gamma atmospheric turbulence," *Applied optics*, vol. 54, no. 25, pp. 7575–7585, 2015.

[54] E. Zedini, H. Soury, and M.-S. Alouini, "Dual-hop FSO transmission systems over Gamma–Gamma turbulence with pointing errors," *IEEE Transactions on Wireless Communications*, vol. 16, no. 2, pp. 784–796, 2016.

[55] "The Wolfram research Meijer G-function document. acessed. Aug. 1, 2023. [online]. available: https://functions.wolfram.com/pdf/meijerg.pdf," 2023.

[56] G. Maral, M. Bousquet, and Z. Sun, *Satellite Communications Systems: Systems, Techniques and Technology*. John Wiley & Sons, 2020.

[57] M. K. Simon and M.-S. Alouini, *Digital Communication over Fading Channels*. John Wiley & Sons, 2005.

[58] V. Adamchik and O. Marichev, "The algorithm for calculating integrals of hypergeometric type functions and its realization in REDUCE system," in *Proceedings of the International Symposium on Symbolic and Algebraic Computation*, 1990, pp. 212–224.

[59] M. Usman, H.-C. Yang, and M.-S. Alouini, "Practical switching-based hybrid FSO/RF transmission and its performance analysis," *IEEE Photonics Journal*, vol. 6, no. 5, pp. 1–13, 2014.

[60] M. Selvaraj and R. K. Mallik, "Error analysis of the decode and forward protocol with selection combining," *IEEE transactions on wireless communications*, vol. 8, no. 6, pp. 3086–3094, 2009.

[61] W. A. Alathwary and E. S. Altubaishi, "On the performance analysis of decode-and-forward multi-hop hybrid FSO/RF systems with hard-switching configuration," *IEEE Photonics Journal*, vol. 11, no. 6, pp. 1–12, 2019.

[62] Z. Wang and G. B. Giannakis, "A Simple and General Parameterization Quantifying Performance in Fading Channels," *IEEE Transactions on Communications*, vol. 51, no. 8, pp. 1389–1398, 2003.

[63] T. V. Nguyen, H. D. Le, N. T. Dang, and A. T. Pham, "Average transmission rate and outage performance of relay-assisted satellite hybrid FSO/RF ssystems," in *2021 International Conference on Advanced Technologies for Communications (ATC)*, 2021, pp. 1–6.

[64] H. Kazemi, M. Uysal, and F. Touati, "Outage analysis of hybrid FSO/RF systems based on finite-state markov chain modeling," in *2014 IEEE 3rd International Workshop in Optical Wireless Communications (IWOW)*, 2014, pp. 11–15.

[65] B. L. Edwards and D. J. Israel, "Update on NASA's laser communications relay demonstration project," in *2018 SpaceOps Conference*, 2018, p. 2395.

[66] R. Samy, H.-C. Yang, T. Rakia, and M.-S. Alouini, "Reliable terabits feeder link for very high-throughput satellite systems with SAG-FSO transmission," *IEEE Wireless Communications*, early access, 2023.

[67] E. Erdogan, I. Altunbas, G. K. Kurt, M. Bellemare, G. Lamontagne, and H. Yanikomeroglu, "Site diversity in downlink optical satellite networks through ground station selection," *IEEE Access*, vol. 9, pp. 31 179–31 190, 2021.

[68] Z. Katona, F. Clazzer, K. Shortt, S. Watts, H. P. Lexow, and R. Winduratna, "Performance, cost analysis, and ground segment design of ultra high throughput multi-spot beam satellite networks applying different capacity enhancing techniques," *International Journal of Satellite Communications and Networking*, vol. 34, no. 4, pp. 547–573, 2016.

[69] E. Erdogan, G. K. Kurt, I. Altunbas, and H. Yanikomeroglu, "HAPS selection for hybrid RF/FSO satellite networks," *IEEE Transactions on Aerospace and Electronic Systems*, vol. 58, no. 4, pp. 2855–2867, 2022.

[70] Y. Fu, X. Li, J. Ma, and H. Wang, "BER analysis of coherent FSO systems with SC receive diversity over correlated turbulence channels," in *Eighth Symposium on Novel Photoelectronic Detection Technology and Applications*, vol. 12169. SPIE, 2022, pp. 505–511.

[71] K. Peppas, G. Alexandropoulos, C. Datsikas, and F. Lazarakis, "Multivariate gamma–gamma distribution with exponential correlation and its applications in radio frequency and optical wireless communications," *IET microwaves, antennas & propagation*, vol. 5, no. 3, pp. 364–371, 2011.

[72] R. Priyadarshani, A. Jaiswal, M. R. Bhatnagar, Z. Ghassemlooy, and S. Zvanovec, "Performance of space shift keying over a correlated gamma-gamma FSO-MISO channel," in *IEEE 11th International Symposium on Communication Systems, Networks & Digital Signal Processing (CSNDSP)*, 2018, pp. 1–6.

[73] R. Samy, H.-C. Yang, T. Rakia, and M.-S. Alouini, "Space-air-ground FSO networks for high-throughput satellite communications," *IEEE Communications Magazine*, vol. 61, no. 3, pp. 82–87, 2023.

[74] B. Ashrafzadeh, E. Soleimani-Nasab, M. Kamandar, and M. Uysal, "A framework on the performance analysis of dual-hop mixed FSO-RF cooperative systems," *IEEE Transactions on Communications*, vol. 67, no. 7, pp. 4939–4954, 2019.

[75] S. Sharma, J. Tan, A. Madhukumar, and R. Swaminathan, "Switching-based transmit antenna/aperture selection in a MISO hybrid FSO/RF system," in *GLOBECOM 2018 IEEE Global Communications Conferenc*, 2018, pp. 1–6.

[76] I. A. Alimi, A. O. Mufutau, A. L. Teixeira, and P. P. Monteiro, "Performance analysis of space-air-ground integrated network (SAGIN) over an arbitrarily correlated multivariate FSO channel," *Wireless Personal Communications*, vol. 100, no. 1, pp. 47–66, 2018.

[77] A. Mukherjee, S. Kar, and V. Kumar Jain, "Analysis of beam wander effect in high turbulence for FSO communication link," *IET Communications*, vol. 12, no. 20, pp. 2533–2537, 2018.

[78] G. Yang, M.-A. Khalighi, Z. Ghassemlooy, and S. Bourennane, "Performance evaluation of receive-diversity free-space optical communications over correlated gamma–gamma fading channels," *Applied optics*, vol. 52, no. 24, pp. 5903–5911, 2013.

[79] G. Yang, M.-A. Khalighi, S. Bourennane, and Z. Ghassemlooy, "Fading correlation and analytical performance evaluation of the space-diversity free-space optical communications system," *Journal of Optics*, vol. 16, no. 3, p. 035403, 2014.

[80] D. Singh and R. Swaminathan, "Comprehensive performance analysis of hybrid FSO/RF space-air-ground integrated network," *Optics Communications*, p. 128964, 2022.

[81] G. V. Damme, "Bivariate Gamma Distribution CDF, PDF, samples," in *MATLAB Central File Exchange*, October, 2022. [Online]. Available: https://www.mathworks.com/matlabcentral/fileexchange/26682-bivariate-gamma-distribution-cdf-pdf-samples.

[82] N. Vishwakarma and R. Swaminathan, "Performance analysis of hybrid FSO/RF communication over generalized fading models," *Optics Communications*, vol. 487, p. 126796, 2021.

[83] T. Rakia, H.-C. Yang, M.-S. Alouini, and F. Gebali, "Outage analysis of practical FSO/RF hybrid system with adaptive combining," *IEEE Communications Letters*, vol. 19, no. 8, pp. 1366–1369, 2015.

[84] W. Zhang, S. Hranilovic, and C. Shi, "Soft-switching hybrid FSO/RF links using short-length raptor codes: Design and implementation," *IEEE Journal on Selected Areas in Communications*, vol. 27, no. 9, pp. 1698–1708, 2009.

[85] B. He and R. Schober, "Bit-interleaved coded modulation for hybrid RF/FSO systems," *IEEE Transactions on Communications*, vol. 57, no. 12, pp. 3753–3763, 2009.

[86] L. Huang, S. Liu, P. Dai, M. Li, G.-K. Chang, Y. Shi, and X. Chen, "Unified performance analysis of hybrid FSO/RF system with diversity combining," *Journal of Lightwave Technology*, vol. 38, no. 24, pp. 6788–6800, 2020.

[87] A. Lapidoth, S. M. Moser, and M. A. Wigger, "On the capacity of free-space optical intensity channels," *IEEE Transactions on Information Theory*, vol. 55, no. 10, pp. 4449–4461, 2009.

[88] G. T. Djordjevic, M. I. Petkovic, M. Spasic, and D. S. Antic, "Outage capacity of FSO link with pointing errors and link blockage," *Optics express*, vol. 24, no. 1, pp. 219–230, 2016.

[89] M. Toyoshima, T. Jono, T. Yamawaki, K. Nakagawa, and A. Yamamoto, "Assessment of eye hazard associated with an optical downlink in free-space laser communications," in *Free-Space Laser Communication Technologies XIII*, vol. 4272. SPIE, 2001, pp. 219–226.

[90] P. K. Singya and M.-S. Alouini, "Mixed FSO/RF based multiple HAPs assisted multiuser multiantenna terrestrial communication," *Frontiers in Communications and Networks*, vol. 3, p. 746201, 2022.

[91] O. B. Yahia, E. Erdogan, and G. K. Kurt, "HAPS-assisted hybrid RF-FSO multicast communications: Error and outage analysis," *IEEE Transactions on Aerospace and Electronic Systems*, vol. 59, no. 1, pp. 140–152, 2022.

[92] G. I. A. Inc, "High Altitude Platforms: Global Strategic Business Report," *Research and Markets*, California, USA, Jan. 2023.

[93] J. Xu, M. A. Kishk, Q. Zhang, and M.-S. Alouini, "Three-hop underwater wireless communications: A novel relay deployment technique," *IEEE Internet of Things Journal*, vol. 10, no. 15, pp. 13 354–13 369, 2023.

[94] S. Li, L. Yang, D. B. da Costa, and S. Yu, "Performance analysis of UAV-based mixed RF-UWOC transmission systems," *IEEE Transactions on Communications*, vol. 69, no. 8, pp. 5559–5572, 2021.

[95] L. Yang, Q. Zhu, S. Li, I. S. Ansari, and S. Yu, "On the performance of mixed FSO-UWOC dual-hop transmission systems," *IEEE wireless communications letters*, vol. 10, no. 9, pp. 2041–2045, 2021.

[96] E. Zedini, H. M. Oubei, A. Kammoun, M. Hamdi, B. S. Ooi, and M.-S. Alouini, "Unified statistical channel model for turbulence-induced fading in underwater wireless optical communication systems," *IEEE Transactions on Communications*, vol. 67, no. 4, pp. 2893–2907, 2019.

[97] M. Zhang, S. Fu, and Q. Fan, "Joint 3D deployment and power allocation for uav-bs: A deep reinforcement learning approach," *IEEE Wireless Communications Letters*, vol. 10, no. 10, pp. 2309–2312, 2021.

[98] J.-H. Lee, J. Park, M. Bennis, and Y.-C. Ko, "Integrating LEO satellites and multi-UAV reinforcement learning for hybrid FSO/RF non-terrestrial networks," *IEEE Transactions on Vehicular Technology*, vol. 72, no. 3, pp. 3647–3662, 2022.

[99] L. Li, Q. Cheng, K. Xue, C. Yang, and Z. Han, "Downlink transmit power control in ultra-dense UAV network based on mean field game and deep reinforcement learning," *IEEE Transactions on Vehicular Technology*, vol. 69, no. 12, pp. 15 594–15 605, 2020.